TU/e EINDHOVEN UNIVERSITY OF TECHNOLOGY

Organic electronic ratchets

Document status and date:
Published: 01/01/2011

Document Version:
Publisher's PDF, also known as Version of Record (includes final page, issue and volume numbers)

Please check the document version of this publication:

Download date: 04. Oct. 2023

Organic electronic ratchets

Erik Roeling

Organic electronic ratchets

PROEFSCHRIFT

ter verkrijging van de graad van doctor aan de
Technische Universiteit Eindhoven, op gezag van de
rector magnificus, prof.dr.ir. C.J. van Duijn, voor een
commissie aangewezen door het College voor
Promoties in het openbaar te verdedigen
op woensdag 11 mei 2011 om 16.00 uur

door

Erik Maria Roeling

geboren te Ammerzoden

Dit proefschrift is goedgekeurd door de promotor:

prof.dr.ir. R.A.J. Janssen

Copromotor:
dr.ir. M. Kemerink

Contents

Chapter 1

Introduction

Ratchets are intriguing and counterintuitive devices. A *Gedankenexperiment* conceived by Marian Smoluchowski in 1912 and extended by Richard Feynman in 1963 showed how asymmetry can be used to rectify the undirected (Brownian) motion of particles. Using the example of the flashing ratchet —where an asymmetric time–dependent potential is used to direct particles— the subject of ratchets and more specifically organic electronic ratchets is introduced. These ratchets are created by modifying organic field effect transistors. Inside the gate dielectric of the transistor, asymmetrically spaced interdigitated electrodes are placed. Applying a specific oscillating potential on these finger electrodes will induce a ratchet effect; charge can move between source and drain contacts with zero source–drain bias. At the end of this chapter the scope and outline of the thesis is presented.

1.1   Introduction

The possibility to extract work from undirected forces has intrigued scientists for over a century. Particularly intriguing is the rectification of undirected motion of particles by ratchet potentials, which are periodic but asymmetric functions. In 1912, in a *Gedankenexperiment* closely related to Maxwell's demon [1], Marian Smoluchowski described a small machine surrounded by a gas, which at first sight seems to be able to extract useful work out of heat in a system at thermal equilibrium [2]. The machine —the Feynman–Smoluchowski ratchet [2–3]— consists of a paddle wheel, which is connected to a ratchet shaped wheel via a thin axis. The rotation direction of the machine is controlled by a light and thin pawl so that it can rotate frictionless, but in only one direction. Gas molecules collide with the machine and due to its size, the thermal energy is large enough to rotate the wheel. *Prima facie* this device should work. It can rotate in only one direction and a small weight, e.g. a flea hanging on a very thin string would be lifted and work would be performed, even when in equilibrium with the surrounding gas $(T_1 = T_2)$.
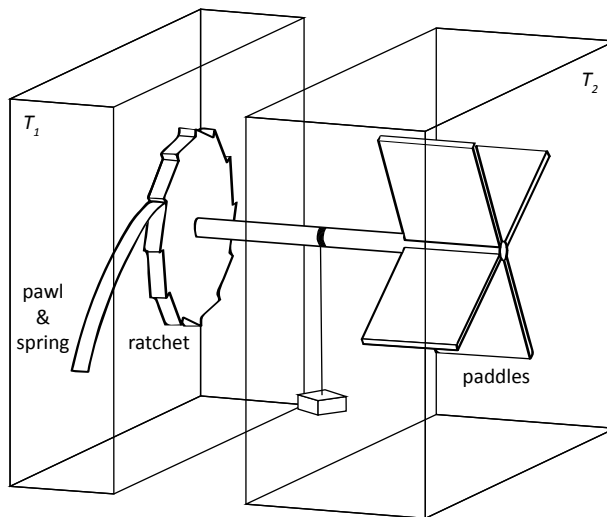
Figure 1.1 | The Feynman–Smoluchowski ratchet. The rotation direction of a ratchet shaped wheel is controlled by a pawl and spring. The ratchet wheel is connected to a paddle wheel by a thin axis. When $T_1 = T_2$ the total system is at thermal equilibrium with the surrounding environment and no net rotation will take place, opposite to the case in which $T_1 \neq T_2$.

Despite the cleverly designed system it cannot work. The total entropy of the system —i.e. of the machine and surrounding gas molecules— would reduce which is a violation of the second law of thermodynamics. The catch is in the pawl and spring of the system. They are subjected to the same thermal fluctuations as the paddle wheel. As the pawl

should be light and thin it can be lifted up by the same collisions with gas molecules that move the paddle wheel, giving the machine the possibility to rotate in the counter–clockwise direction. On average this machine will perform no net work.

Despite the fact that the Feynman–Smoluchowski ratchet does not work, Smoluchowski's *Gedankenexperiment* was popularized in 1963 in the famous *Feynman lectures on physics*. Richard Feynman not only repeated but also extended Smoluchowski's thought experiment to find the Feynman–ratchet, showing that by placing the paddle wheel in a different heat bath than the pawl and ratchet shaped wheel (Figure 1.1, $T_1 \neq T_2$) —i.e. removing the Feynman–Smoluchowski ratchet from thermal equilibrium— the machine is able to perform work [2]. This is not in violation with the second law of thermodynamics as the system is removed from thermal equilibrium, meaning that a constant energy supply is necessary to keep the device operating. The rotation direction of the Feynman–ratchet can also be controlled by the temperature difference between the two heat baths. The behavior of a sudden rotation inversion upon a small parameter change is found in (almost) every type of ratchet in the form of current inversion. Experimentally, the thought experiments of Smoluchowski and Feynman have been realized at the molecular level in 1998 using specially designed molecules [4–5] and in a granular gas in 2010 by Eshuis *et al.* [6] —decades after Feynman and almost a century after Smoluchowski.

Thermal fluctuations are often regarded as a burden as they disturb processes and generate losses. Interestingly enough, Brownian ratchets like the Feynman ratchet actually benefit from thermal fluctuations as is further shown by examples in the next sections. This property alone already makes it worth studying Brownian ratchets, despite the fact that also they cannot evade the second law of thermodynamics.

1.2   The flashing ratchet

A clearer and more abstract example of a ratchet can be found when looking at randomly moving particles being subjected to a periodic time–dependent ratchet–shaped potential. In Figure 1.2, the principle behind the flashing ratchet is explained [7–8]. Particles are trapped in an asymmetric potential well. When the potential is turned off, the (non–interacting) particles will spread due to diffusion. Turning the potential on again will trap them in the in energy nearest potential minimum. Due to the asymmetry of the potential, this is not necessarily the spatially nearest potential minimum. When repeating this process, a particle current can emerge. As energy is brought into the

system by the time–dependent potential, this device is not in violation with the second law of thermodynamics.

As one can expect, the frequency at which this potential is turned on and off influences the particle current [8–10]. When oscillating too fast, the particles have hardly time to react on the applied potential and no net particle movement will take place. However, the frequency can also be too low. This will give the particles ample time to spread evenly across the device which also results in no net particle movement.

The ideal on–time is chosen such that all particles can drift back to a potential minimum. With ν the drag coefficient which is inversely proportional to the mobility and U the amplitude, the ideal on–time t_{on} (i.e. the transit time) of a particle to move over the long distance $(1-\alpha)L$ is:

$$t_{on} = \nu (1-\alpha)^2 L^2 \big/ U \,, \tag{1.1}$$

where it is assumed that drift dominates over diffusion. L is the total length of one asymmetric period and $\alpha = s/L$ represents the degree of asymmetry, with s the short length of the asymmetric period. During the off–stage particles diffuse in both directions. The off–time must therefore be long enough to diffuse over the short distance αL, but short enough to prevent particles to diffuse over the long distance $(1-\alpha)L$;

$$t_{off} \approx \alpha^2 L^2 \big/ 2D \ll (1-\alpha)^2 L^2 \big/ 2D \,, \tag{1.2}$$

with D the diffusion coefficient. Note that the on– as well as the off–time scales with
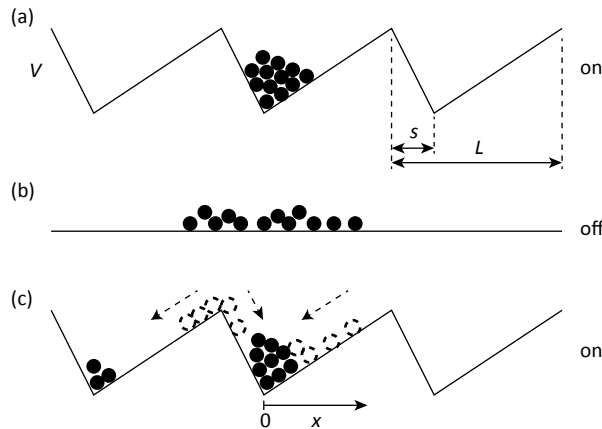
Figure 1.2 | Principle of the flashing ratchet. **(a)** The asymmetric potential is turned on, particles are trapped in potential minima. **(b)** The asymmetric potential is turned off, particles will spread due to diffusion. **(c)** The asymmetric potential is turned on again, particles will move to the potential minimum that is *nearest in energy*. Due to the asymmetry some particles will therefore be trapped above a next potential well, resulting in a net displacement.

L^2, a scaling factor that is also found for the organic electronic ratchets as will be shown in Chapter 4.

Using these ideal on– and off–times, the fraction of particles that is moved during one on–off sequence γ_t can be calculated. The probability distribution for particles undergoing one–dimensional diffusion is given by [8–10]:

$$P\left(x;t_{off}\right) = \exp\left(-x^2\big/4Dt_{off}\right)\big/\sqrt{4\pi Dt_{off}}\ . \tag{1.3}$$

Integrating the probability distribution from $-\alpha L$ to $-\infty$, with $t_{off} = \alpha^2 L^2\big/2D$ chosen well below the upper limit, it is found that γ_t can in theory be as high as 16% [8]. In Chapter 5 we show that the calculated value of γ_t for an organic electronic ratchet is not far removed from the 16% found for the flashing ratchet, despite the fact that the transport mechanism in the organic electronic ratchets is fundamentally different.

1.3 General ratchets and Brownian motors

Guidelines have been proposed to verify if a certain device is a genuine Brownian ratchet [11]. (1) Random forces (of thermal, non thermal, or even deterministic (chaotic) origin) should play a prominent role; (2) Use of spatial (and/or cyclic) periodicity; (3) All acting forces and gradients vanish after averaging over space, time and statistical ensembles, with the exception of an applied load; (4) The system is removed from thermal equilibrium; (5) Symmetry breaking. Often a Brownian motor is referred to as a ratchet. This term is however also used to describe devices that are not majorly influenced by thermal noise, but that do function by the use of spatially asymmetric periodic potentials [8]. In this thesis, the word *ratchet* is used in the broader context, not only referring to devices that function by the use of Brownian motion.

In spite of the —at first sight— logic example of the flashing ratchet, ratchet operation is in reality intricate and counterintuitive [7, 12–13]. A century after Smoluchowski, the study of such devices is still an active field as is shown by the diversity of examples which are briefly touched below.

In nature, ratchets are e.g. found in bipedal motors [14] and in the beak of certain shorebirds [15]. Prakash *et al.* [15] showed that Phalaropes and other shorebirds with long thin beaks use a capillary ratchet mechanism for foraging. These shorebirds drink water by opening and closing their thin beaks in a tweezering motion as is shown in Figure 1.3e. This capillary ratchet motion is strong enough to transport water and submerged prey against the direction of the gravitational force.
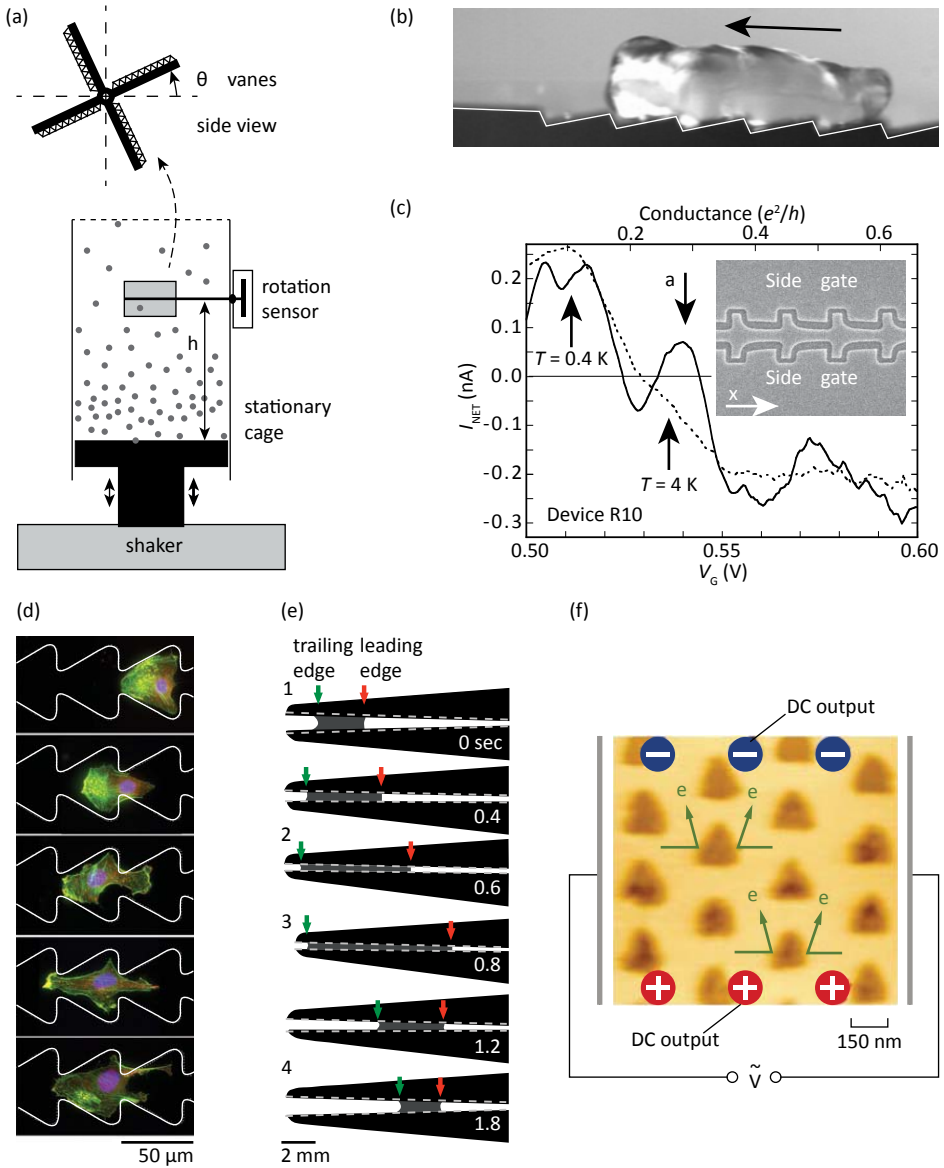
Figure 1.3 | (a) Rotational ratchet in a granular gas [6]. **(b)** Self–propelled Leidenfrost droplet moving uphill against the direction of the gravitational force [17]. **(c)** Experimental tunneling ratchets. Visible is the net transported current I_{NET} as a function of gate voltage V_G [21]. **(d)** Snapshots of a motile cell moving through a ratchet shaped trench [19]. **(e)** Principle of the capillary ratchet which is used by shorebirds to move prey [15]. **(f)** Two–dimensional electron gas in a InGaAsP/InP quantum well structure in which triangular areas are etched away, functioning as a two–dimensional ratchet [25]. Note: for quality reasons the images are digitally remastered from their originals.

Man–made geometrical ratchets have been used for the directed transport of charged phospholipids [16], Leidenfrost droplets [17], granular media [6], liquid cells [18] and even motile cells [19]. Linke *et al.* [17] showed how droplets of liquid can be self–propelled when in the Leidenfrost regime. In this regime, droplets of liquid are placed on a relatively hot surface making the droplets float on a lubricating vapor film (film–boiling regime). In case of a flat surface the droplets will move randomly, while in case of a ratchet–patterned surface the droplets get self–propelled. Figure 1.3b shows a liquid droplet floating on a vapor layer above a ratchet shaped solid plate. The droplet is moving uphill against the direction of the gravitational force.

The Feynman–Smoluchowski ratchet introduced at the beginning of this chapter is realized in granular media by Eshuis *et al.* [6]. In Figure 1.3a a schematic picture of the experimental setup is shown. Glass beads are shaken by a vibrating table bringing them in a gaslike state. A box, disconnected from the vibrating table, prevents the beads from escaping. Attached to the container is the paddle wheel from the Feynman–Smoluchowski ratchet. They showed that with symmetrically coated vanes the paddle wheel has no preferential direction when rotating, which is in agreement with the *Gedankenexperiment* from Feynman and Smoluchowski. The system was turned into a ratchet by adding rubber tape on one specific side of each of the paddle blades, creating an asymmetry in the system. In agreement with Feynman´s results a preferential direction for the paddle wheel was found.

Mahmud *et al.* used 35 nm deep ratchet–shaped trenches with which the random motion of motile cells can be directed [19]. Depending on the geometry, different cell types can move through the trenches in different directions, enabling (partial) cell sorting. A principle which according to Mahmud *et al.* might be used in future cancer treatment. In Figure 1.3d snapshots are shown for different stages of the migration of a motile cell.

The above described experiments show a wide range of areas in which ratchet effects are studied. The ratchets are mainly of mechanical nature, in the sense that e.g. liquid droplets or particles are transported. Also electric ratchet potentials can be used for transporting particles. They have for instance been used to rectify colloidal particle motion [20] and to transport DNA [9]. In this thesis on organic electronic ratchets we are interested in moving charge, which has been studied before in tunneling ratchets where quantum effects play a major role [21–23].

Linke *et al.* created a quantum ratchet by confining electrons to an asymmetric conducting channel [21]. Asymmetrically shaped periodically etched trenches in a GaAs/AlGaAs heterostructure confine a two–dimensional sheet of electrons. The width of these trenches is in the order of the electron wavelength. The variations in width induce a variation in the electron confinement energy, creating asymmetric energy barriers at the constrictions. In Figure 1.3c a scanning electron microscopy (SEM) image is showing the channel, with the darker regions the etched trenches. Source and drain contacts are located at the beginning and end of the conducting channel. The ratchet is operated in a rocking ratchet mode in which a square–wave source–drain potential is applied. In Figure 1.3c the net generated current as a function of gate voltage is shown, with generated currents below 1 nA. Note the current inversions at different temperatures and gate voltages.

Song *et al.* created a two–dimensional electron gas in an InGaAs/InP quantum well structure, in which triangular areas are etched away [25]. In Figure 1.3f an atomic force microscopy (AFM) image shows the height profile of the structure. Contacts are present at all sides of the structure (left, right, upper, lower). The triangles act as scattering sites as the distance between the triangles is smaller than the electron mean free path. An AC voltage applied to the left– and right–contacts can result in a DC voltage (~1 mV) between the upper and lower contacts as electrons accumulate at the upper contact. The structure has an intrinsic nonlinear rectifying property, also found in photogalvanic materials [7,25] and also functions at room temperature.

The above described examples show the diversity in which ratchet effects can occur. However, the overview is far from complete. For an extensive overview we refer the reader to Reimann [7], Hänggi and Marchesoni [12], and to Linke *et al.* in a special edition of *Applied Physics A* [13].

1.4   Organic electronic ratchets

So far, electronic ratchets [21–23] have been of limited use, as they typically operate at cryogenic temperatures and generate sub–nA currents and sub–mV voltages [21–25]. In this thesis a new design for electronic ratchets is presented. The ratchets are based on organic field effect transistors (OFETs) [26–28] in which pentacene, an organic semiconductor, is in contact with source (S) and drain (D) electrodes and separated by a dielectric (silicon dioxide) from a bottom gate (G) contact. In the gate dielectric of
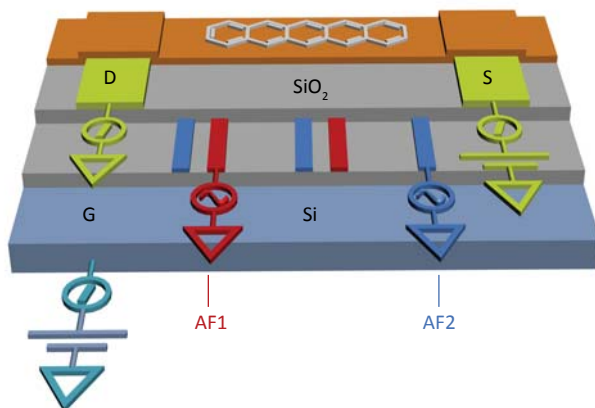
Figure 1.4 | Drawing of the organic electronic ratchet. Visible are the source (S) and drain (D) contacts, which are separated from the silicon (Si) gate (G) contact by the silicon dioxide (SiO$_2$) gate dielectric. Asymmetrically spaced interdigitated finger electrodes denoted by AF1 and AF2 are placed inside the gate dielectric. Note the color coding of the finger electrodes; fingers with like colors are electrically connected. Pentacene is used as a semiconductor (layer with structural formula on top of it).

the OFET asymmetrically spaced interdigitated finger electrodes are embedded (Figure 1.4). Although an organic material is used as semiconductor, inorganic semiconductors should give very similar behavior. Sinusoidal potentials, applied on the two sets of fingers (AF1, AF2) create the typical time dependent asymmetric potential, almost similar to the operation of the flashing ratchet discussed above. The gate electrode of the OFET is used to accumulate charges right above the organic–dielectric interface. As a result, a net, ratchet propelled current can flow between the source and drain contacts at zero source–drain bias.

1.5   Thesis scope

The ratchet devices presented in this thesis are conceptually new in design. The work is primarily performed out of scientific curiosity but with a clear idea of possible applications, such as a wireless current source, in mind. The ratchet devices as shown in Figure 1.4 were therefore designed to deliver a ´quick´ proof–of–principle before the research would continue to smaller length scales and to ´all–organic´ ratchet devices in which specially tailored molecules would be used. However, the complexity and the richness of these proof–of–principle devices turned out to be so large that it lead to the thesis in front of you, which focuses entirely on these devices. In this work, these proof–of–principle ratchets are thoroughly analyzed, giving an understanding of how

they work, and how their properties can be tuned and optimized. The results can be used as a starting point to investigate smaller, faster, more efficient ratchet devices, employing different driving schemes. Eventually this may lead to ratchets with the right specifications to be used in actual applications.

Measurement results from ratchets that differ in length scale and asymmetry are combined with results from numerical device models. Several contributions are made to the rich and diverse research field on (Brownian) ratchets. As will be shown, the charge transport mechanism differs from previously reported ratchets, as the present device functions by the grace of the Coulomb interactions between charges [29–30]. For functional electronic ratchet devices contacts are necessary. As will be discussed, these contacts break the spatial periodicity of the ratchet potential which can lead to major differences in charge transport.

In Chapter 2 *Methods* the design and the fabrication procedure of the electronic ratchets is presented. Furthermore, the (quasi) two–dimensional drift–diffusion models, used to model the ratchets are presented.

The proof of principle of the electronic ratchets is presented in Chapter 3 *Organic electronic ratchets doing work*. It is shown that significant currents and voltages can be generated when the ratchets are operated as a (quasi–)flashing ratchet. This is illustrated by demonstrating the operation of low–end logic, powered by a ratchet. Model results indicate that the ratchets basically function by the grace of many–particle interactions, which is different from other ratchet systems.

Chapter 4 *Scaling of characteristic frequencies of organic electronic ratchets* describes the influence of length scales and characteristic potentials on the optimal frequency for current transport. Drift–diffusion simulations of infinitely long ratchets are compared with measurement results on —necessarily— finite ratchets.

The power efficiency —the output power divided by the input power— is an important benchmark in view of possible applications. In Chapter 5 *Performance of organic electronic ratchets*, it is investigated how the power efficiency of the electronic ratchets can be optimized, by tuning the characteristics of the asymmetric potential.

Measurement results show that charge transport in the ratchets is influenced by the presence of the source and drain contact, which break the spatial periodicity of the ratchet potential. In Chapter 6 *Finite size effects on organic electronic ratchets*, the drift–

diffusion model used in the previous chapters is modified. Source and drain contacts are added to the model, giving the ability to compare simulation results of infinite long ratchets with finite ratchets. Furthermore, the influence of two–dimensional charge transport is addressed.

1.6 References

[1] Maxwell, J.C., *Theory of Heat.* (Longmans, Green and Co., London, 1871).

[2] Smoluchowski, M. v. Experimentell nachweisbare, der üblichen Thermodynamik widersprechende Molekularphänomene. *Physikalische Zeitschrift* **13**, 1069–1080 (1912).

[3] Feynman, R. P., Sands, M. L. & Leighton, R. B. *The Feynman lectures on physics*. (Addison–Wesley, 1989).

[4] Kelly, T. R., Sestelo, J. P. & Tellitu, I. New molecular devices: In search of a molecular ratchet. *J Org Chem* **63**, 3655–3665, (1998).

[5] Davis, A. P. Tilting at windmills? The second law survives. *Angew Chem Int Edit* **37**, 909–910, (1998).

[6] Eshuis, P., van der Weele, K., Lohse, D. & van der Meer, D. Experimental Realization of a Rotational Ratchet in a Granular Gas. *Phys Rev Lett* **104**, 248001, (2010).

[7] Reimann, P. Brownian motors: noisy transport far from equilibrium. *Physics Reports–Review Section of Physics Letters* **361**, 57–265, (2002).

[8] Linke, H., Downton, M. T. & Zuckermann, M. J. Performance characteristics of Brownian motors. *Chaos* **15**, 026111, (2005).

[9] Bader, J. S. *et al.* DNA transport by a micromachined Brownian ratchet device. *P Natl Acad Sci USA* **96**, 13165–13169, (1999).

[10] Astumian, R. D. Thermodynamics and kinetics of a Brownian motor. *Science* **276**, 917–922, (1997).

[11] Reimann, P. & Hänggi, P. Introduction to the physics of Brownian motors. *Appl Phys A–Mater* **75**, 169–178, (2002).

[12] Hänggi, P. & Marchesoni, F. Artificial Brownian motors: Controlling transport on the nanoscale. *Rev Mod Phys* **81**, 387–442, (2009).

[13] Linke, H. Ratchets and Brownian motors: Basics, experiments and applications. *Appl Phys A–Mater* **75**, 167–167, (2002).

[14] Svoboda, K., Schmidt, C. F., Schnapp, B. J. & Block, S. M. Direct Observation of Kinesin Stepping by Optical Trapping Interferometry. *Nature* **365**, 721–727, (1993).

[15] Prakash, M., Quere, D. & Bush, J. W. M. Surface tension transport of prey by feeding shorebirds: The capillary ratchet. *Science* **320**, 931–934, (2008).

[16] van Oudenaarden, A. & Boxer, S. G. Brownian ratchets: Molecular separations in lipid bilayers supported on patterned arrays. *Science* **285**, 1046–1048, (1999).

[17] Linke, H. *et al.* Self–propelled Leidenfrost droplets. *Phys Rev Lett* **96**, 154502, (2006).

[18] Loutherback, K., Puchalla, J., Austin, R. H. & Sturm, J. C. Deterministic Microfluidic Ratchet. *Phys Rev Lett* **102**, 045301, (2009).

[19] Mahmud, G. *et al.* Directing cell motions on micropatterned ratchets. *Nature Physics* **5**, 606–612, (2009).

[20] Rousselet, J., Salome, L., Ajdari, A. & Prost, J. Directional Motion of Brownian Particles Induced by a Periodic Asymmetric Potential. *Nature* **370**, 446–448, (1994).

[21]   Linke, H. *et al.* Experimental tunneling ratchets. *Science* **286**, 2314–2317, (1999).

[22]   Linke, H. *et al.* Asymmetric nonlinear conductance of quantum dots with broken inversion symmetry. *Phys Rev B* **61**, 15914–15926, (2000).

[23]   Khrapai, V. S., Ludwig, S., Kotthaus, J. P., Tranitz, H. P. & Wegscheider, W. Double–Dot Quantum Ratchet Driven by an Independently Biased Quantum Point Contact. *Phys Rev Lett* **97**, 176803, (2006).

[24]   Majer, J. B., Peguiron, J., Grifoni, M., Tusveld, M. & Mooij, J. E. Quantum ratchet effect for vortices. *Phys Rev Lett* **90**, 056802, (2003).

[25]   Song, A. M. *et al.* Room–temperature and 50 GHz operation of a functional nanomaterial. *Appl Phys Lett* **79**, 1357–1359, (2001).

[26]   Dimitrakopoulos, C. D. & Malenfant, P. R. L. Organic thin film transistors for large area electronics. *Adv Mater* **14**, 99–117, (2002).

[27]   Braga, D. & Horowitz, G. High–Performance Organic Field–Effect Transistors. *Adv Mater* **21**, 1473–1486, (2009).

[28]   Sirringhaus, H. Device physics of Solution–processed organic field–effect transistors. *Adv Mater* **17**, 2411–2425, (2005).

[29]   Roeling, E. M. *et al.* Organic electronic ratchets doing work. *Nat Mater* **10**, 51–55, (2011).

[30]   Hänggi, P. Organic Electronics Harvesting Randomness. *Nat Mater* **10**, 6–7, (2011).

Chapter 2

Methods

In this chapter the design and fabrication of the ratchets introduced in Chapter 1 are presented. The important steps in the cleanroom fabrication are highlighted. It is shown that patterning of the semiconducting layer is important to fabricate functioning ratchets. The measurement set–up and techniques are discussed. Furthermore the details of the drift–diffusion models which are used to describe the operation of the ratchet devices are discussed.

2.1   Introduction

In Figure 2.1 a top view and cross section of a ratchet are shown. There are five contacts: source (S), drain (D) and gate (G) contact and two asymmetric interdigitated finger electrode contacts, denoted by AF1 and AF2. The finger electrodes extent the source and drain contacts on both ends, creating a homogenous potential in the direction parallel to the source and drain contact, also at the edges of the channel. To reduce parasitic currents in the device, the organic semiconducting layer is patterned. Currents can therefore only flow in the channel area and between the contact pads and underlying gate.
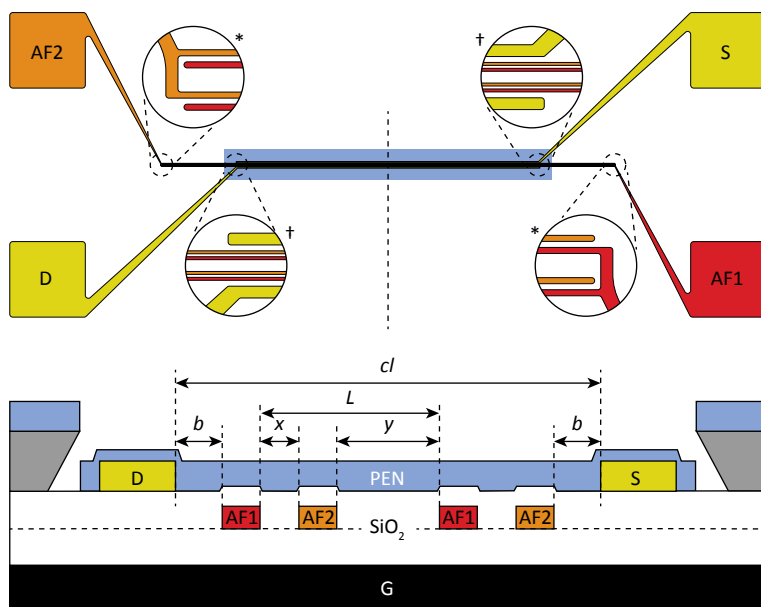
Figure 2.1 | Top view and cross section of a ratchet, with b the distance between the source and drain contacts and the asymmetric finger electrodes, x the short spacing, y the long spacing, L the repeat unit length and cl the channel length. In this example AF1 and AF2 consists of 2 finger electrodes. Hence, this is an Lx–yP2 device. PEN stands for pentacene. *No pentacene, †pentacene present on top of the structure.

Fabricated ratchets differ in asymmetry and number of repetitions of the potential. The short distance x between a finger and its nearest neighbor is 1 μm; the long distance y varies from 1 to 16 μm. These parameters are incorporated in the ratchet notation. An Lx–yPa ratchet has a pairs of interdigitated fingers, with a ranging from 1 to 32 and a short and long spacing between the fingers of x and y micrometer, respectively. In the notation L stands for length and P stands for pairs. The distance b (Figure 2.1) between source or drain contact and the nearest finger electrode equals $y/2$ unless $y<4$ μm in which case b=2 μm. Charge is collected at the source and drain contacts, which necessarily break the spatial periodicity of the asymmetric potential, thereby superimposing

macroscopic (a)symmetries on the potential. To investigate this effect, there are ratchets with a non–integer number of pairs (Lx–yPa.5) of interdigitated finger electrodes and with an integer number (Lx–yPa).

In this chapter the measurement method and set–up are introduced and the drift–diffusion models that are used to model the ratchets is presented. First an overview of the device fabrication is given.

2.2   Fabrication process

The ratchets are fabricated on highly boron–doped (p–type) silicon wafers that serve as substrate and gate contact. The wafer is covered with a 100 nm thick thermally grown silicon dioxide (SiO$_2$) layer (Figure 2.2a). Asymmetrically spaced interdigitated finger electrodes (5 nm Ti/20 nm Au/5 nm Ti), 1 μm wide and 1.5 mm long are placed on top of the SiO$_2$ layer via a lift–off process. First, a layer of negative photoresist is spin coated on top of the SiO$_2$ layer (Figure 2.2b). The finger electrode pattern is then transferred into the photoresist layer via ultraviolet (UV) contact photolithography, after which the titanium–gold–titanium layer stack is evaporated on top of the wafer (Figure 2.2c). A characteristic feature of negative photoresist is the overhanging sidewalls after development (Figure 2.4). The photoresist layer and redundant metal layer stack can therefore be lifted off the sample in an acetone bath, leaving the asymmetric finger electrodes on top of the wafer (Figure 2.2d).

The finger electrodes are covered with an approximately 100 nm thick SiO$_2$ layer using plasma enhanced chemical vapor deposition (PECVD) (Figure 2.2e). Two 4 μm wide, 1 mm long (10 nm Ti/40 nm Au) contacts are positioned symmetrically with respect to the interdigitated fingers on top of the PECVD SiO$_2$ layer, again using UV photolithography and a lift–off process (Figure 2.2f–h).

A thick layer of negative photoresist, serving as a permanent shadow mask, is spincoated and subsequently patterned via UV photolithography. A monolayer of hexamethyldisilazane (HMDS) is applied at room temperature after which a 50 nm thick pentacene layer —a p–type organic semiconductor— is deposited by thermal evaporation in ultra high vacuum (Figure 2.2i–j). Figure 2.3 shows scanning electron microscopy (SEM) images of a cross section of a part of a ratchet. Visible are a drain contact and four interdigitated fingers, embedded in SiO$_2$. The precise process parameters and steps for the ratchet fabrication are listed in Appendix I. In the remainder of this section two fabrication steps are discussed in more detail; the use of metal ion free developers and the patterning of the semiconducting layer.
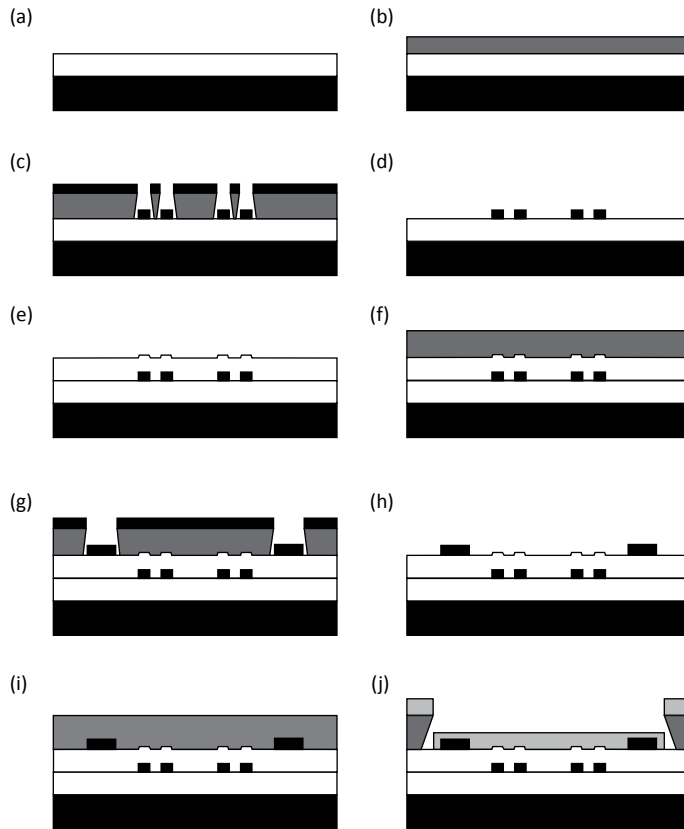
Figure 2.2 | Schematic overview of the major fabrication steps. Black: contacts (source, drain, gate, and interdigitated finger electrodes). White: SiO_2, light grey: pentacene, dark grey: photoresist. See main text for further explanation.
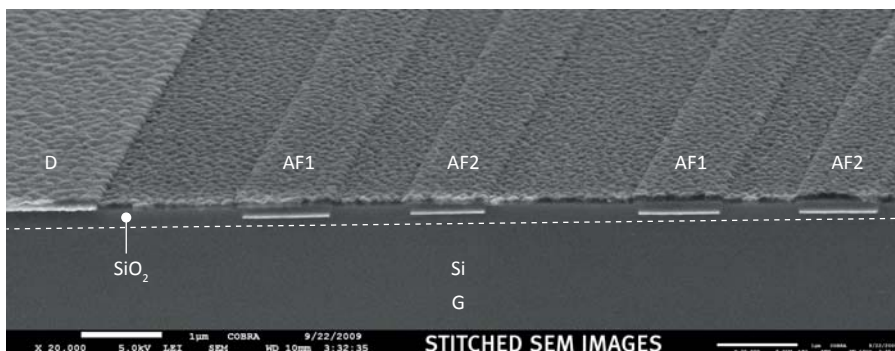
Figure 2.3 | Cross section of a ratchet. A Ti/Au drain (D) contact is shown on the left side. Four interdigitated fingers (AF1, AF2), embedded in SiO_2, are visible. Steps in the PECVD SiO_2 layer are present above the interdigitated fingers. Below the SiO_2 layer the silicon (Si) gate (G) contact is visible. Small pentacene crystals cover the Au contact and SiO_2. The image consists of two scanning electron microscopy images stitched together. The scale bar is 1 µm.

2.3   Photoresist development

The asymmetric finger electrodes and source and drain contacts are fabricated with conventional UV photolithography. After illumination of the photoresist layer the photoresist is developed. Two types of developers are investigated; a sodium hydroxide (NaOH) and a tetramethylammonium hydroxide (TMAH) developer. The latter one is a metal ion free developer. The performance of NaOH and TMAH as developers was evaluated by studying the fabrication yield of organic field effect transistors (OFETs), with a channel width of 1 µm. The gate dielectric was 50 nm thick. OFETs fabricated with NaOH as developer showed 22 structures out of 120 tested structures working well. In most cases of malfunctioning, a significant current was flowing between the gate contact and the source and/or drain contact. When TMAH was used as developer 50 out of 88 tested OFETs were functioning. Of the broken structures, only 10 showed current leakages between gate and source and/or drain contact(s). Due to these results only metal ion free developers are used. We speculate that sodium ions associated with the NaOH–developer are creating a conducting path between source and drain contacts and the gate contact when the transistor is operated.

2.4   Semiconductor patterning

Performance of OFETs can be undermined by leakage currents, i.e. all currents other than the channel current flowing between the source and drain electrodes. By patterning of the semiconducting layer these currents can often be reduced, resulting in increased device performances [1]. In the final fabrication step of the ratchets, a semiconducting layer is applied on top of the SiO_2 layer. When this layer is covering the complete structure, conducting paths are created between the source and drain electrodes and the finger electrode contact pads. It is observed that the resulting leakage currents can be in the same order of magnitude as the current generated by the ratchet effect ($\sim 10^{-8}$ A). Therefore, the semiconductor layer is patterned.

In time, several methods have been developed. Shadow masks are commonly used, but unfortunately of no use when the device scale is too small or the demanded precision too high. Conventional UV photolithography is difficult to deploy due to the incompatibility between the chemicals in photoresists and developers and the organic material(s). This problem can be overcome by using paryleneC as a protective layer between photoresists or developers and the organic layer(s) [2], or by using photoresists and developers

based on hydrofluoroethers [3–4]. Other methods include inkjet printing [5], imprint lithography [6] and microcontact printing [7]. In the ratchet system a negative photoresist layer is used as a patterning mask for the deposition of pentacene [8]. This method is suitable for the deposition of small molecules by evaporation.

A characteristic feature of negative photoresists is the overhanging side walls after development. Because of the under etch, pentacene deposited on top of the photoresist layer is disconnected from the pentacene deposited on top of the channel area, as is shown in Figure 2.4. This is the same principle as used in the lift–off process for electrode fabrication. However, after applying the pentacene layer the photoresist is not removed, preventing contact between the organic semiconductor and solvents.

The disadvantage of using negative photoresist layers is the tendency of the photoresist to reflow at elevated temperatures, preventing deposition of the HMDS layer at 140 ˚C substrate temperature prior to the pentacene evaporation. The HMDS layer is therefore applied at room temperature. It is experimentally observed that this method leads to less reduction in gate bias stress in the ratchets.

In Figure 2.5 typical current versus gate voltage characteristics of field effect transistors without (a) and with (b) a patterning layer are shown. Without patterning of the organic semiconductor the gate current increases several orders of magnitude with increasing gate voltage. If the patterning layer is applied, the gate current is almost independent of the gate voltage. The graphs clearly show that patterning of the semiconductor reduces leakage currents.

2.5   Measurement methods

Measurements are conducted at 40 °C inside a high vacuum probe station equipped with triaxial probe arms (ST–500, Janis Research Company Inc.). Prior to the measurements, samples are heated inside the probe station for over one hour at 110 °C to remove water present at the silicon dioxide–pentacene interface. A KE4200–SCS parameter analyzer (Keithley Instruments Inc.) equipped with pre–amplifiers is used to source voltage and measure current at source, drain and gate contact. The source contact is always placed at zero bias. An Agilent 81150 dual channel arbitrary waveform generator is used for applying the potentials on the asymmetric finger electrodes AF1 and AF2. The measurements are automated using Keithley User Library Tool and Keithley Interactive Test Environment software.
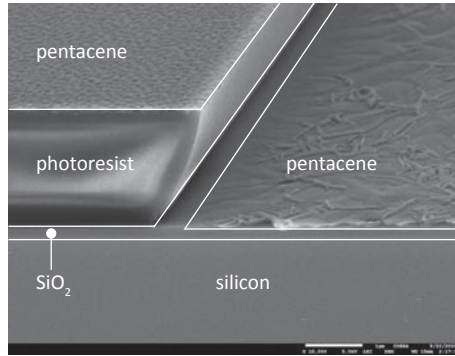
Figure 2.4 | The patterned pentacene layer is shown. At the location where the pentacene layer is deposited on top of the silicon dioxide layer large pentacene crystals and dendrites are shown. Small pentacene crystals are visible on top of the photoresist layer. Note the difference in pentacene crystal structure between Figure 2.3 and Figure 2.4. This is attributed to the surface roughness of the different substrates [13] (PECVD SiO_2 versus thermally grown SiO_2). The scale bar is 1 μm.
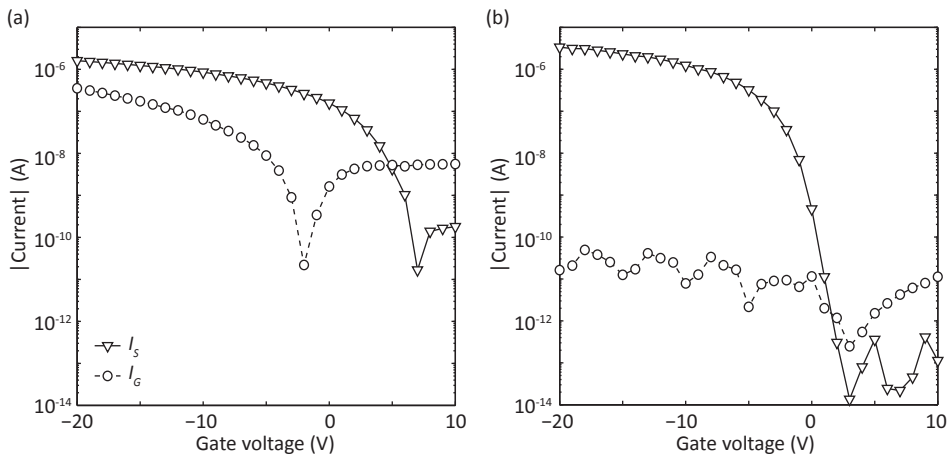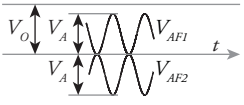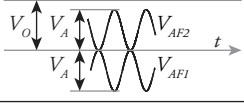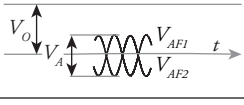
Figure 2.5 | Source (I_s) and gate (I_G) current versus gate voltage plot for a transistor without **(a)** and with **(b)** patterning of the semiconducting layer. Both transistors have a channel length of 11 μm and a channel width of 1 mm. The thermal SiO_2 layer is 200 nm thick. The graph clearly shows the reduction in gate current when patterning is applied. The applied source–drain bias V_{SD} is −2 V.

Measurement data is used when the source and drain current are of opposite sign and equal magnitude and the gate current is orders of magnitude lower. Furthermore, because of Kirchoff's sum law, the sum of the source, drain and gate current equals the current flowing to or from the asymmetric fingers. Also this current was checked to be orders of magnitude lower than the source and drain currents.

Four driving schemes are used for the device characterization: forward, reversed, symmetric and transistor drive. Table 2.1 shows the time–dependent potentials applied on AF1 and AF2. The sinusoidal signals applied on AF1 and AF2 have a phase difference of 180 degrees.

Transfer characteristics (transistor drive, Table 2.1) of the ratchets are measured in a similar fashion as those of OFETs without embedded asymmetric fingers. By applying a DC voltage equal to half the applied gate voltage on AF1 and AF2, the charge density in the channel will be homogenous as the asymmetric fingers are placed halfway the gate dielectric. The ratchet is subsequently operated as a conventional OFET.

Table 2.1 | Overview of the applied potentials on AF1 and AF2 for the four driving schemes. A graphical representation is shown in the right column. V_G is the applied gate voltage, V_O is a central offset voltage, V_A is the amplitude of the ratchet potential (i.e. peak–peak voltage of the sinusoidal potentials applied on AF1 and AF2), ω the angular frequency and t the time.

Drive	$V_{AF1}(t)$	$V_{AF2}(t)$	
Forward (AC)	$V_O + \dfrac{V_A}{2}\left(1+\sin\left(\omega t\right)\right)$	$V_O - \dfrac{V_A}{2}\left(1+\sin\left(\omega t\right)\right)$	
Reversed (AC)	$V_O - \dfrac{V_A}{2}\left(1+\sin\left(\omega t\right)\right)$	$V_O + \dfrac{V_A}{2}\left(1+\sin\left(\omega t\right)\right)$	
Symmetric (AC)	$V_O + \dfrac{V_A}{2}\sin\left(\omega t\right)$	$V_O + \dfrac{V_A}{2}\sin\left(\omega t + \pi\right)$	
Transistor (DC)	$\dfrac{V_G}{2}$	$\dfrac{V_G}{2}$	

2.6   Simulation methods

A drift–diffusion model has been developed to investigate the microscopic mechanism behind the charge transport. In the model, an infinitely long ratchet is simulated in a transistor–like geometry, similar to the investigated structures. Below the model will be described in more detail.

In the drift–diffusion equation the first term on the right–hand side describes the drift and the second term diffusion of particles:

$$\overline{j}_p = q\mu_p p\overline{E} - qD_p\overline{\nabla}p \,, \tag{2.1}$$

with p the free hole concentration, j_p the hole current density, D_p the hole diffusion coefficient, $\overline{E}$ the electric field, q the elementary charge, and μ_p the hole mobility. Charge conservation is implemented via the continuity equation (2.2):

$$\overline{\nabla}\cdot\overline{j}_p = -q\partial_t p \,. \tag{2.2}$$

The Coulomb interaction between charged particles in the semiconducting layer is incorporated in the model via Poisson's equation (2.3):

$$\overline{\nabla}\cdot\left(\varepsilon\overline{\nabla}\phi\right) = -qp \,. \tag{2.3}$$

Here ϕ denotes the electrostatic potential and, $\varepsilon = \varepsilon_0\varepsilon_r$ with ε_0 the permittivity of vacuum and ε_r the relative permittivity that is assumed constant. Displacement currents are included in the calculation as time–dependent electric fields are present:

$$\overline{j}_{dis} = \varepsilon_0\varepsilon_r\partial_t\overline{E} \,. \tag{2.4}$$

To keep the model as transparent as possible, a constant mobility is assumed even though the mobility in organic semiconductors is known to be density and/or field dependent [9]. Furthermore, we assume that the system is in local thermal equilibrium. The Einstein–Smoluchowski relation is therefore used to describe the relation between the mobility of the organic semiconductor and the diffusion constant as:

$$D_p = \mu_p k_b T / q \,. \tag{2.5}$$

Here, k_b is the Boltzmann constant, and T the system temperature. The drift–diffusion equations are linearized and solved via forward integration in time using Matlab. After each time step new current densities and charge densities are calculated for each grid point in the semiconducting layer, followed by the potential and electric field at each grid point.

In Figure 2.6 a schematic overview of the simulation space is shown. As the ratchets are translational invariant in the direction parallel to the source–drain contacts and finger electrodes, only a two–dimensional (2D) cross section of the device is simulated. Furthermore, charge transport in the organic semiconductor layer is confined to the first few nanometers above the semiconductor–dielectric interface [10–11]. In the model, the semiconducting layer is therefore taken to be only one grid cell thick, turning the charge transport equations (2.1) and (2.2) one–dimensional (1D). The dielectric layer below and the vacuum above consist of multiple grid cells in the vertical direction; hence Poisson's equation (2.3) is solved in 2D. Therefore equation (2.3) is linearized which gives:

$$\overline{\overline{M}} \cdot \overline{V} = \overline{\rho}\big/\varepsilon \, , \tag{2.6}$$

where $\overline{\overline{M}}$ is a square matrix with (number of horizontal grid cells x number of vertical grid cells)² elements and $\overline{V}$ and $\overline{\rho}$ are column vectors of corresponding size, containing respectively the electrostatic potential and charge density in each gridpoint.

The gate contact and the asymmetric interdigitated electrodes are incorporated in the bottom grid layer. On each grid point in the bottom layer, a grid cell specific, time–dependent voltage is applied. In the experimental situation, the dielectric layer between the gate and the active layer has twice the thickness of that between the asymmetric fingers and the active layer. For simplicity the gate and interdigitated fingers are collapsed on a single layer in the calculations. The simulated gate dielectric thickness is taken equal to the dielectric layer thickness above the fingers in the experiment, which is half
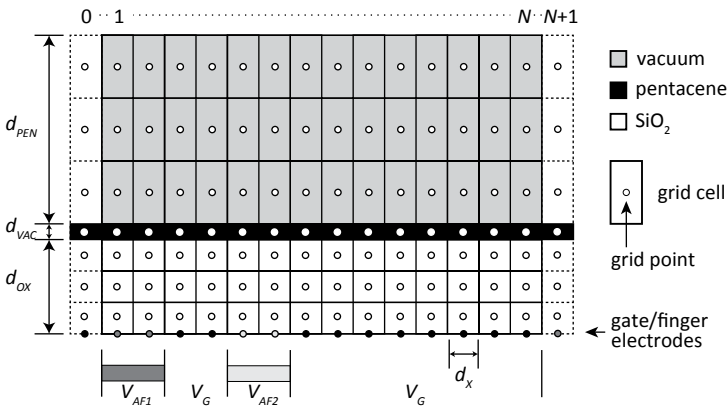
Figure 2.6 | Schematic overview of the simulation space (not on scale). For all simulation results d_x is 62.5 nm, d_{VAC} 1000 nm, d_{PEN} 3 nm and d_{OX} 100 nm, unless mentioned otherwise. The device ranges from column 1 to N. Columns 0 and $N+1$ are only present in the model when modeling the efficiency as explained in Section 2.6.1.

the thickness of the total dielectric layer above the 'experimental' gate; hence the applied 'numerical' gate voltage is half the experimental one[1]. A zero vertical electric field is assumed for the top grid cell layer. Periodic boundary conditions are applied at the left and right edges of the simulation space.

Infinite long ratchets are modeled. Therefore no contacts are present and as a result the channel must be filled with charges prior to running the simulation. A fixed amount of charge is placed inside the semiconducting layer at time $t = 0$, calculated from the equation for a parallel plate capacitor $C = \varepsilon A/d = Q/V$ in which the time–averaged gate potential at each grid point is used as the voltage V applied over the capacitor plates. Here C is the capacitance, A the area of the capacitor plates, d the thickness of the gate dielectric, and Q the total amount of charge. The total amount of charge is constant, but it may, and will, redistribute in time because of the oscillating finger potentials. The amount of charge placed inside the device is slightly overestimated compared to the actual situation. It is verified that this has a negligible influence on the simulation results.

2.6.1   Efficiency modeling

The power efficiency of the ratchets is defined as:

$$\eta_p = P_{out}/P_{in} , \tag{2.7}$$

with P_{out} the maximum output power and P_{in} the power put into the device via the finger electrodes.

When no load is applied, the output power is zero by definition. Therefore, the maximum output power is modeled by applying a potential V_{tilt} across the simulation grid, simulating an applied load. The output power is the current at maximum power point multiplied by the applied potential V_{tilt}.

The model is adjusted to accommodate for the load. V_{tilt} is added as a linear, constant slope to the (time–varying) potentials applied on the bottom grid layer (gate and finger electrodes). On left and right hand sides of the simulation grid, an extra grid cell column is added to modify the periodic boundary conditions for the applied load. For a simulation with $N+2$ grid columns (the term +2 accounts for the added columns with the columns ranging from 0 through $N+1$, the actual device ranges from 1 through N), the potentials of the cells in column number $N+1$ are set to $V_{N+1} = V_1 + V_{tilt}$, and similarly

---

[1] The gate voltage values mentioned in this thesis for all modeling results are the 'experimental' gate voltages instead of the 'numerical' gate voltages.

in column number 0 to $V_0 = V_N - V_{tilt}$. The charge carrier densities in columns 0 and $N+1$ are omitted from (numerical) solving equations (2.1) and (2.2). Instead charge leaving from column 1 is flowing to column N or 2 and charge from column N is flowing to column 1 or $N-1$. Before the tilt potential is applied, a fixed amount of charge is placed inside the channel as described in the previous paragraph.

Energy enters the ratchet via the finger electrodes. The input power is calculated as the sum over space and time of one oscillation period of the local channel potential V_i multiplied by the local particle current I_i averaged over time:

$$P_{in} = f \sum_{t=0}^{1/f} \sum_{i=1}^{N} I_i(t) V_i(t), \qquad (2.8)$$

with $f \left(= \omega/2\pi \right)$ the applied frequency.

Neglected in the calculation for the power efficiency are the losses due to coupling of the finger electrodes to the bottom gate contact. At the end of chapter 5 it is explained why these losses are merely a technology issue and can be ignored.

2.6.2   Drift–diffusion model for finite devices

In Chapter 6 a modified version of the above–described model is used to model finite ratchets as shown in Figure 2.1. Source–drain contacts are added on left and right sides of the simulation grid. Charge is injected via the contacts. The hole density p at the electrode–semiconductor interface is calculated via the Boltzmann equation $p = N_0 \exp\left(-\varphi/kT\right)$ with N_0 the density of states and φ the injection barrier. In the previously described model, the accumulation layer was assumed to be one grid cell thick. To investigate the role of vertical charge transport in the accumulation layer, equations (2.1) and (2.2) are solved in 2D. The last major modification is the location of the finger electrodes. Instead of incorporating the finger electrodes in the same layer as the gate electrode (Figure 2.6), the finger electrodes are located inside the gate dielectric, as in the actual devices (Figure 2.1).

2.6.3   Fast Ratchet Analysis Tool

For frequency regions where drift dominates over diffusion the Fast Ratchet Analysis Tool (FRAT) can be used (Chapter 6). In this model the drift equation (i.e. equation (2.1) without the diffusion term) and continuity equation (2.2) are solved in 1D by forward time integration.
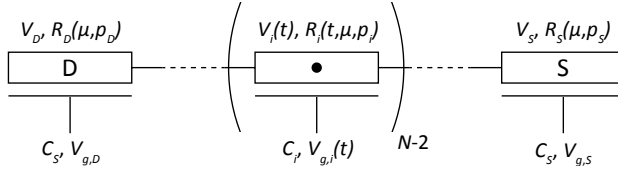
Figure 2.7 | Fast Ratchet Analysis Tool. The ratchet is considered to be an RC–network. D is the drain and S is the source contact. Each grid cell has a position–specific capacitance C_i and gate voltage $V_{g,i}(t)$. $V_i(t)$ and $R_i(t,\mu,p_i)$ are respectively the channel potential and resistance at time t, p_i is the local time–dependent hole density.

The ratchet is implemented in a resistor–capacitor (RC) circuit as shown in Figure 2.7, where it is assumed that the transverse field is much larger than the longitudinal field (i.e. the gradual channel approximation) [12]. A constant charge mobility μ is assumed although the mobility of organic semiconductors is density dependent as mentioned before. The channel–gate capacitor is regarded as an ideal parallel plate capacitor. Each grid cell has a specific capacitance C_i in which the placement of the finger electrodes halfway the gate dielectric is taken into account if applicable. Locally applied gate voltages $V_{g,i}(t)$ can vary in time like the sinusoidal potentials applied on the asymmetric finger electrodes. In the calculation of the local channel potential, charges screen the gate potential. After each time step, the channel potential is calculated as:

$$V_i(t) = Q_i(t)/C_i + V_{g,i}(t),\qquad(2.9)$$

with $Q_i(t)$ the charge at grid cell i. The presence of source (S) and drain (D) contacts is imbedded in the boundary conditions, in which the hole densities p_D and p_S at respectively the drain and source contact are kept constant in time. At frequencies where diffusion indeed can be ignored, this approach yields identical results as the full drift–diffusion model discussed before, at about a hundredfold higher speed.

2.7 References

[1] Balocco, C., Majewski, L. A. & Song, A. M. Non–destructive patterning of conducting–polymer devices using subtractive photolithography. *Org Electron* **7**, 500–507, (2006).

[2] DeFranco, J. A., Schmidt, B. S., Lipson, M. & Malliaras, G. G. Photolithographic patterning of organic electronic materials. *Org Electron* **7**, 22–28, (2006).

[3] Zakhidov, A. A. *et al.* Hydrofluoroethers as orthogonal solvents for the chemical processing of organic electronic materials. *Adv Mater* **20**, 3481–3484, (2008).

[4] Lee, J. K. *et al.* Orthogonal Processing: A Novel Photolithographic Patterning Method for Organic Electronics. *J Photopolym Sci Tec* **22**, 565–569, (2009).

[5] Forrest, S. R. The path to ubiquitous and low–cost organic electronic appliances on plastic. *Nature* **428**, 911–918, (2004).

[6] Behl, M. *et al.* Towards plastic electronics: Patterning semiconducting polymers by nanoimprint lithography. *Adv Mater* **14**, 588–591, (2002).

[7] Zschieschang, U., Klauk, H., Halik, M., Schmid, G. & Dehm, C. Flexible organic circuits with printed gate electrodes. *Adv Mater* **15**, 1147–1151, (2003).

[8] De Vusser, S., Steudel, S., Myny, K., Genoe, J. & Heremans, P. Integrated shadow mask method for patterning small molecule organic semiconductors. *Appl Phys Lett* **88**, 103501, (2006).

[9] Coehoorn, R., Pasveer, W. F., Bobbert, P. A. & Michels, M. A. J. Charge–carrier concentration dependence of the hopping mobility in organic materials with Gaussian disorder. *Phys Rev B* **72**, 155206, (2005).

[10] Horowitz, G., Hajlaoui, R. & Delannoy, P. Temperature–Dependence of the Field–Effect Mobility of Sexithiophene – Determination of the Density of Traps. *J Phys III* **5**, 355–371, (1995).

[11] Horowitz, G., Hajlaoui, R., Bouchriha, H., Bourguiga, R. & Hajlaoui, M. The concept of "threshold voltage" in organic field–effect transistors. *Adv Mater* **10**, 923–927, (1998).

[12] Sze, S. M. & Ng, K. K. *Physics of semiconductor devices.* 3rd edn, (Wiley–Interscience, 2007).

[13] Knipp, D., Street, R. A., Volkel, A. & Ho, J. Pentacene thin film transistors on inorganic dielectrics: Morphology, structural properties, and electronic transport. *J Appl Phys* **93**, 347–355, (2003).

Chapter 3

Organic electronic ratchets doing work

The possibility to extract work from periodic but undirected forces has intrigued scientists for over a century. In particular, the random motion of particles can be rectified by a ratchet potential. Such potentials are periodic but lack symmetry. Here ratchet devices are presented in which an oscillating asymmetric potential is applied to the channel of an organic field effect transistor. The devices operate up to radio frequencies and deliver sufficient power to drive logic. Moreover, characteristic reversals in the time–averaged current are observed in a multidimensional parameter space formed by the (a)symmetry, frequency, amplitude and offset of the driving ratchet potential. Drift–diffusion simulations show that inter–particle interactions play a major role.

3.1   Introduction

The possibility to extract work from periodic, undirected forces has intrigued scientists for over a century —in particular, the rectification of undirected motion of particles by ratchet potentials— which are periodic but asymmetric functions. Introduced by Smoluchowski and Feynman [1–2] to study the (dis)ability to generate motion from an equilibrium situation, ratchets operate out of equilibrium, where the second law of thermodynamics no longer applies. While ratchet systems have both been identified in nature [3–4] and used in the laboratory for the directed motion of microscopic objects [5–9], electronic ratchets [10–13] have been of limited use, as they typically operate at cryogenic temperatures and generate sub–nA currents and sub–mV voltages [10–14]. Here, organic electronic ratchets are presented that operate up to radio frequencies (RF) at room temperature and generate currents and voltages that are orders of magnitude larger. This enables their use as a direct current (DC) power source. The ratchets are integrated into logic circuits, in which they act as the DC equivalent of the alternating current (AC) transformer, and generate enough power to drive the circuitry. The findings show that electronic ratchets may be of actual use.

Various types of ratchets have been proposed [15–16]; the basic idea behind the ratchet is most easily understood from the flashing ratchet that is depicted in the top part of Figure 3.1a. Particles are trapped in asymmetric potential wells. When the asymmetric potential is turned off, particles will spread due to diffusion and, in the case of charged particles, due to drift. Turning the potential on again will confine particles in the energetically nearest potential well. It is crucial to note that this is not necessarily the spatially nearest potential well. Hence, the asymmetry of the potential leads to the directed transport of particles. In reality, ratchet operation is far more intricate and counterintuitive; a century after Smoluchowski, the study of such devices is still an active field [15–17]. Experimentally the ratchet effect has been studied in such various systems as granular media [18], liquid cells [19], and electronic devices [14,20]. The latter include tunneling ratchets [10–12], where quantum effects play a major role.

The presented ratchets are based on organic field effect transistors (OFETs) in which pentacene, an organic semiconductor, is in contact with source and drain electrodes and separated by a dielectric (SiO_2) from the bottom gate contact. In the gate dielectric of the OFET asymmetrically spaced interdigitated finger electrodes are embedded (Figure 3.1a). Other semiconductors or (top) gate geometries should give very similar behavior,

(a)

(b)

(c)
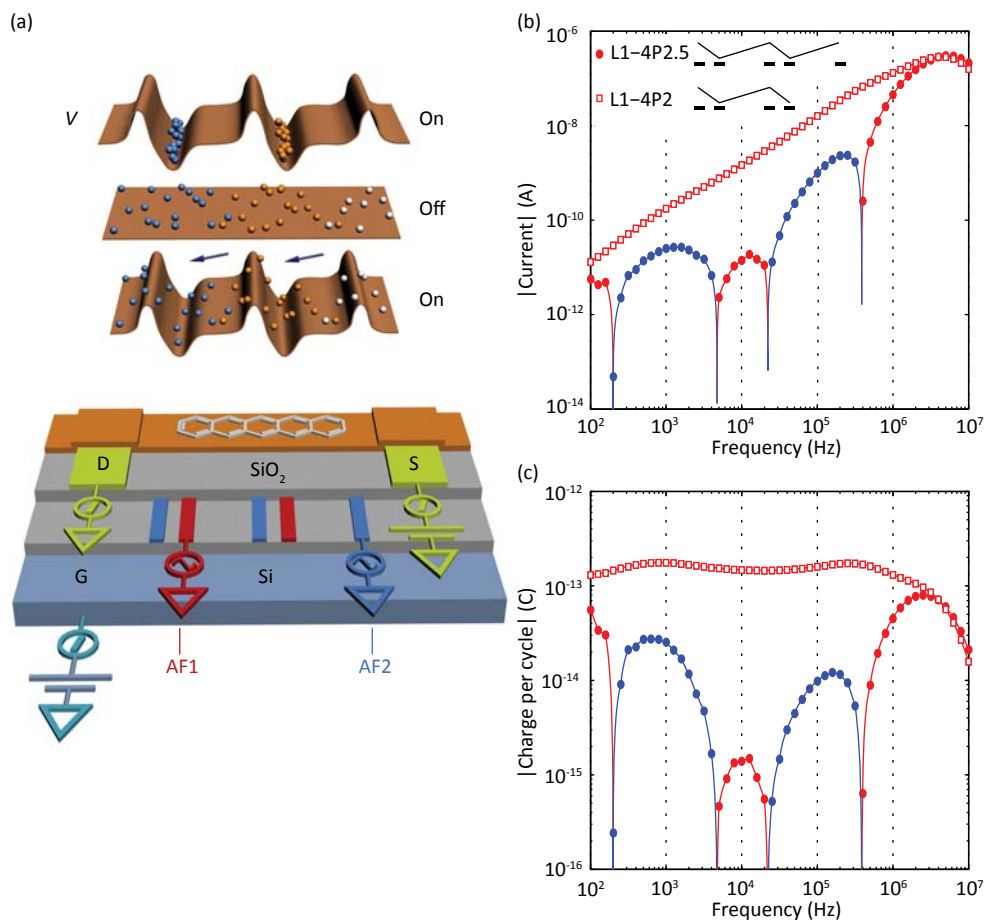
Figure 3.1 | Ratchet mechanism and proof of principle. **(a)** Schematic representation of the flashing ratchet mechanism with a schematic drawing of an investigated ratchet. **(b)** Current[1] versus frequency for an L1–4P2.5 and L1–4P2 ratchet. Red (blue) lines indicate positive (negative) currents (positive current means that holes are leaving the contact). Dashed lines mark the frequencies used in the measurements shown in Figures 3.5 and 3.6. Measurements parameters: $V_A = 8$ V, $V_O = -7$ V, $V_{SD} = 0$ V, and $V_G - V_{TH} = -20$ V (V_G is the gate voltage, V_{TH} is the threshold voltage). **(c)** Charge per cycle versus frequency, with red (blue) indicating a positive (negative) charge value.

apart from a scaling with charge mobility and dimensions. Sinusoidal potentials, applied on the two sets of fingers (AF1, AF2, see Figure 3.1a) create the typical time dependent asymmetric potential. The gate electrode of the OFET is used to accumulate charges at the organic–dielectric interface. As a result, a net, ratchet propelled current can flow between the source and drain contacts at zero source–drain bias ($V_{SD} = 0$ V). These devices, which will be shown below to function by the grace of many–particle interactions, are conceptually new, and outperform previously reported electronic ratchets by orders of magnitude in terms of output voltage, current and power.

---

[1] All measured and modeled currents shown in this thesis are the currents at the source contact.

Fabricated ratchets differ in asymmetry and number of repetitions of the potential. The short distance between a finger and its nearest neighbor is 1 μm; the long distance varies from 1 to 16 μm. Charge is collected at the source and drain contacts, which necessarily breaks the spatial periodicity of the asymmetric potential, thereby superimposing macroscopic (a)symmetries on the potential. To investigate this effect, ratchets with both a non–integer number of pairs of interdigitated finger electrodes (Figure 3.1a) and with an integer number of pairs of finger electrodes have been made.

Time varying potentials are applied on the finger electrodes following $V_{AF1}(t) = V_O + (V_A/2)(1 + \sin(\omega t))$ and $V_{AF2}(t) = V_O - (V_A/2)(1 + \sin(\omega t))$. Here, V_O is a central offset voltage, V_A the peak–peak voltage of each signal, ω the angular frequency and t the time. All voltages are set with respect to the grounded source contact. Note that $V_{AF1}(t)$ and $V_{AF2}(t)$ are opposite in phase.

The current versus frequency f $\left(f = \omega/2\pi\right)$ dependence for two different ratchets denoted by L1–4P2.5 and L1–4P2 is shown in Figure 3.1b. An Lx–yPa ratchet has a pairs of interdigitated fingers and a short and long spacing between the fingers of x and y micrometer, respectively. Note that L stands for length and P stands for pairs. Zero source–drain bias is applied.

For L1–4P2 the time averaged (DC) current increases with increasing frequency until a maximum of 0.28 μA is reached around 5 MHz, after which the current decreases again. The sign of the current is consistent with the naïve picture sketched in Figure 3.1a. In Figure 3.1c the charge per cycle versus frequency is depicted, which is the net amount of charge that is moved in one period and is obtained by dividing the ratchet current by its corresponding frequency. For the L1–4P2 ratchet, the charge per cycle shows two broad maxima around 10^3 and $3 \cdot 10^5$ Hz, after which it decreases to approximately 10^{-14} C at 10 MHz. The results indicate that at low frequencies the generated current is limited by the frequency and that the efficiency with which charge is moved is roughly constant up to a frequency of 1 MHz. At high frequencies (>5 MHz), charges can no longer follow the oscillating potential, causing the observed decrease in current and charge per cycle.

3.2   Drift–diffusion simulations

Drift–diffusion simulations (see Chapter 2) have been performed to elucidate the mechanism of charge transport in the ratchets. The Coulomb interaction between particles is taken into account via Poisson's law, through which the local potential is depending on the charge density in the device. The simulation grid has a transistor–like

geometry with periodic boundary conditions; hence a single period of an infinitely long ratchet without contacts is simulated.

In Figure 3.2, an experimental result performed on an L1–4P32.5 ratchet is compared with the model in a charge per cycle versus frequency graph. A device with 32.5 pairs of asymmetric fingers is used, where it is assumed that this is long enough to resemble the infinite device from the model. For the simulations as well as for the measurement, V_A is 8 V. The offset voltage V_O used in the simulations is slightly higher than during the measurements; –6.1 V compared to –7 V. This is done to account for the threshold voltage V_{TH} in the measured ratchet that is around –1 V. In the simulation the threshold voltage is equal to 0 V. The mobility used in the simulation is 0.35 cm²/Vs. This is similar to the actual device.
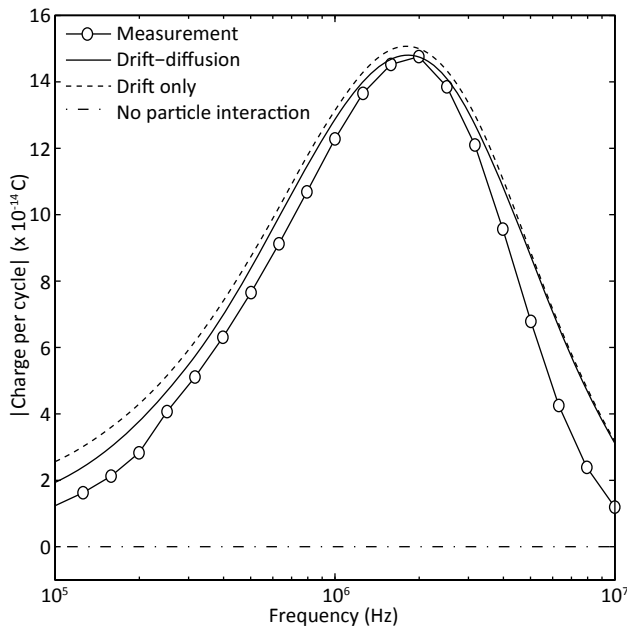
Figure 3.2 | Charge per cycle versus frequency graph for an L1–4 ratchet. Four different cases are shown; (1) measurement on an L1–4P32.5 ratchet, (2) drift–diffusion simulation, (3) drift–only simulation and (4) drift–diffusion simulation without particle–particle interaction. Note that for the modeled curves an L1–4P∞ ratchet is simulated.

Three different situations are modeled. In the first situation the drift and diffusion equations are solved and particle–particle interaction is taken into account. The simulation result matches well with the measurement result. This confirms that the microscopic mechanism underlying the observed DC currents is indeed the intended ratchet mechanism. For the second situation, diffusion of particles is neglected and only drift is taken into account, i.e. the second term on the right–hand side of equation (2.1)

is dropped. When comparing the drift and diffusion simulation with the drift–only simulation only a small difference between these two can be found, especially at lower frequencies ($\sim 10^5$ Hz), indicating that the particles are mainly transported by a drift process. In the third case, drift and diffusion simulations are solved without taking particle–particle interaction into account, i.e. particles feel the applied potential but not each other, which is established by removing the charge density from the Poisson equation, i.e. setting the right hand side of equation (2.3) to zero. An extremely small current is found for all simulated frequencies ($\leq 10^{-17}$ A).

The small current in absence of particle–particle interactions can be understood from the absence of a net drift–based driving force in large parts of the device, in particular in the long leg of the asymmetric potential (Figure 3.3b). Hence, particles have to traverse these regions by diffusion, which is a very slow process as compared to the reciprocal frequency used in the simulation. Therefore the net time averaged current is extremely small. In presence of particle–particle interactions (Figure 3.3a) the long range Coulomb interaction between particles causes significant lateral fields throughout the device, resulting in a significant time–averaged ratchet current. It is checked that when an oscillating saw tooth potential is applied to the channel, i.e. a potential that yields finite fields everywhere, a nonzero net current is produced in the order of 10^{-8} A, even in absence of particle–particle interactions. Taking particle–particle interactions into account a current of approximately 10^{-10} A is found. These results are obtained at a frequency of 10 kHz at which the diffusion contribution, which is necessary for the saw tooth shaped ratchet potential to work in absence of particle–particle interactions, is increased. At a frequency of 10 kHz, the ratchets described in this chapter will generate currents in the order of 10^{-11} A with and 10^{-17} A without particle–particle interactions.

From the simulation results it is therefore concluded that the charge transport at higher frequencies ($\sim 10^5$–10^7 Hz) is dominated by drift currents, with the Coulomb interaction between the particles being of vital importance. When the asymmetric potential changes shape, e.g. because it is switched off in a flashing ratchet, the Coulomb repulsion between charges in the channel will cause the build–up of potential variations that are as large as those just removed.

It should be noted that asymmetric Schottky barriers at the contacts could cause similar behavior as the proposed microscopic mechanism. However, such 'contact rectification effects' should also yield nonzero currents when a symmetric finger pattern or a symmetric driving scheme is used. In the next section it is shown that these currents are
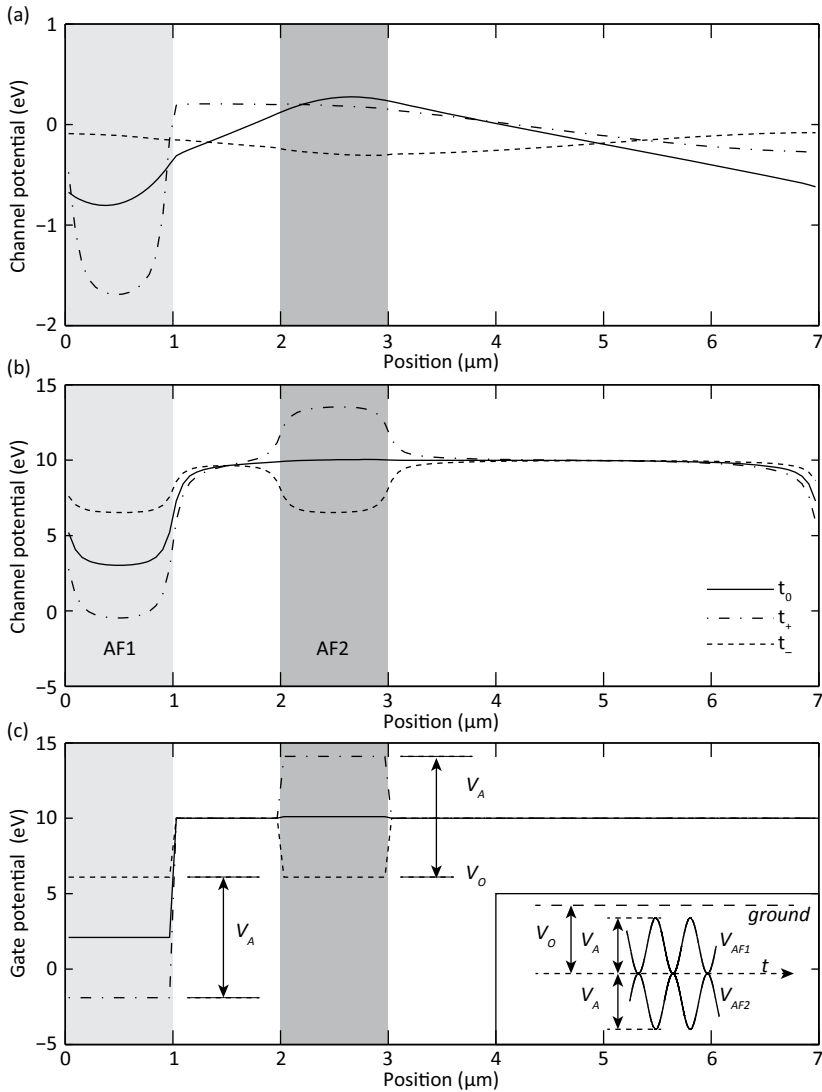
Figure 3.3 | Channel potential at time t_0, t_+, and t_- for a drift–diffusion simulation with **(a)** and without **(b)** particle–particle interactions. The applied gate and finger electrode potentials corresponding with time t_0, t_+, and t_- are shown in **(c)**. The inset in panel (c) show how the voltages applied on the finger electrodes vary in time for the forward drive (see also Table 2.1). The simulations are performed at $f = 2$ MHz, $V_o = -6.1$ V, and $V_A = 8$ V. Note the different potential scales in (a)–(c).

orders of magnitude below those described above. In addition, a misalignment between the finger electrodes and the contacts could yield spurious rectification effects. Also this scenario has been ruled out by fabricating deliberately misaligned devices.

Despite its simplicity, the model describes the behavior of the ratchets at higher frequency strikingly well.

3.3   Current reversals

The current versus frequency behavior of the L1–4P2.5 structure qualitatively differs from that of the L1–4P2 structure (Figure 3.1b). With increasing frequency the net current changes direction at four points. Current reversals are often observed in ratchet systems [10, 15–16, 21]. There, reversals have been attributed to changes in temperature or to particle–particle interactions in the ratchet potential. In our system, the reversals are only observed in ratchets with non–integer number of pairs of interdigitated finger electrodes. Although extreme care should be taken when qualitatively explaining features of these counterintuitive, non–equilibrium systems [16], the origin of the current reversals in the present system is likely related to the breaking of spatial periodicity due to the presence of contacts (Chapter 6). While in theoretical modeling, and in our numerical simulations, the ratchet potential is often treated as infinitely periodic [16], the measurement results show that the presence and the details of contacts, obviously needed in functional devices, drastically alter the ratchet behavior.

The L1–4P2 ratchet is mirror symmetric, opposite to the L1–4P2.5 ratchet. When the L1–4P2 ratchet is driven symmetrically, i.e. $V_{AF1}(t) = V_O + (V_A/2)\sin(\omega t)$ and $V_{AF2}(t) = V_O - (V_A/2)\sin(\omega t)$, the time–averaged current drops by several orders of magnitude (Figure 3.4c–d). The current that is still flowing is attributed to macroscopic asymmetries in the system, e.g. small alignment errors introduced during the fabrication process. When the symmetry of the potential applied to AF1 and AF2 is inverted (reversed drive) the current as expected changes in sign but not in magnitude.

The L1–4P2.5 ratchet has no inversion symmetry between the forward and reversed driving mode, as it consists of five asymmetric interdigitated fingers (Figure 3.1a). In forward drive several current reversals occur. For the reversed drive (Figure 3.4a–b) however, no current reversals are observed and the current direction is in agreement with the naively sketched picture of Figure 3.1. The current generated in symmetric drive is of the same order of magnitude as the current observed in reversed drive, only to drop at higher frequencies (>1 MHz) below the current generated in forward drive. As the ratchet is not mirror symmetric a macroscopic asymmetry, besides potential alignment errors, is inherently present in the system, causing the large currents under symmetric drive.

The net amount of charge moved during one period for the L1–4P2.5 ratchet strongly depends on the frequency due to the current reversals and is overall lower than for the L1–4P2 ratchet. This trend is generally observed when comparing complementary
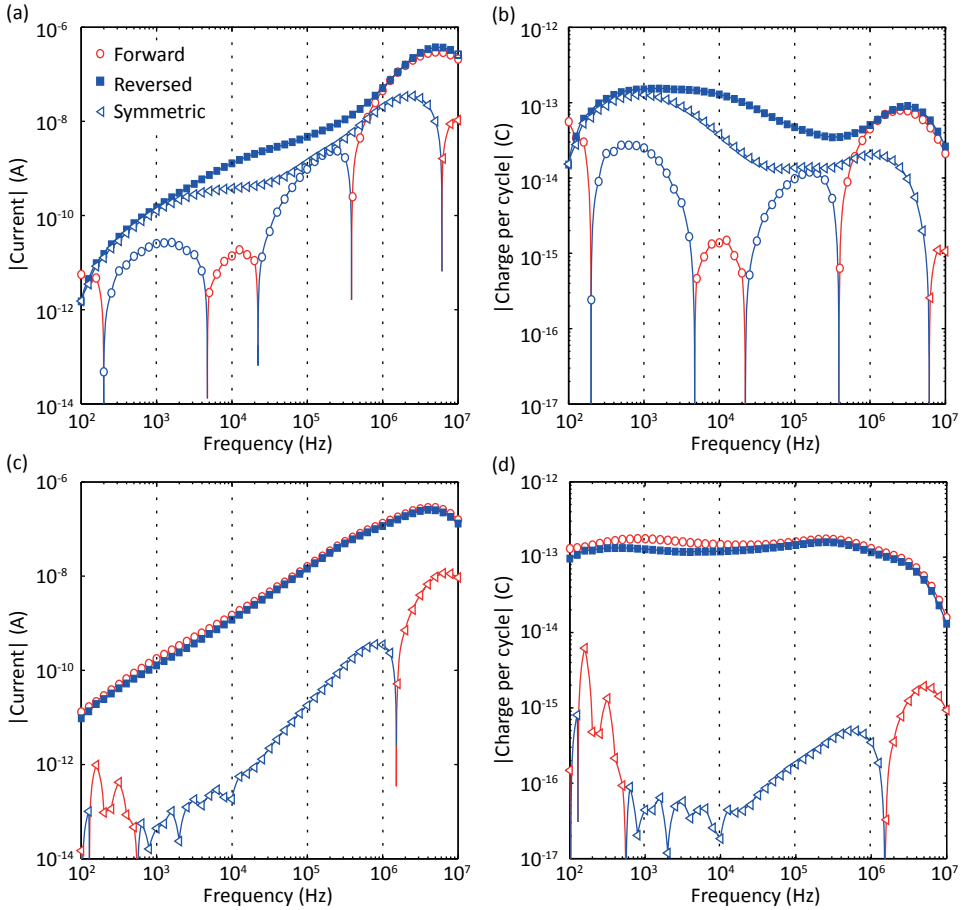
Figure 3.4 | Current and charge per cycle as a function of frequency for the L1–4P2.5 ratchet **(a)**, **(b)** and L1–4P2 ratchet **(c)**, **(d)** for forward, reversed and symmetric drive. Dashed lines mark the frequencies used in the measurements shown in Figures 3.5 and 3.6. The red lines indicate a positive, and the blue lines a negative source current. Measurements are performed for $V_G - V_{TH} = -20$ V, $V_A = 8$ V, $V_O = -7$ V and $V_{SD} = 0$ V.

ratchets with a non–integer and integer number of pairs of asymmetric interdigitated finger electrodes.

More insight in the behavior of these ratchet devices can be obtained by plotting the DC current versus driving amplitude V_A and offset V_O. In Figure 3.5, the influence of V_O and V_A on the ratchet current for L1–4P2.5 is presented for four different frequencies: 1 kHz, 10 kHz, 100 kHz and 1 MHz. The black dots indicate the offset and amplitude at which Figures 3.1b–c and 3.4a–b are taken. The sign changes in Figures 3.1b–c and 3.4a–b can now be seen to reflect the back– and forward shifts of the boundary for current reversal, indicated by the white line. The fact that the sign of the current at the
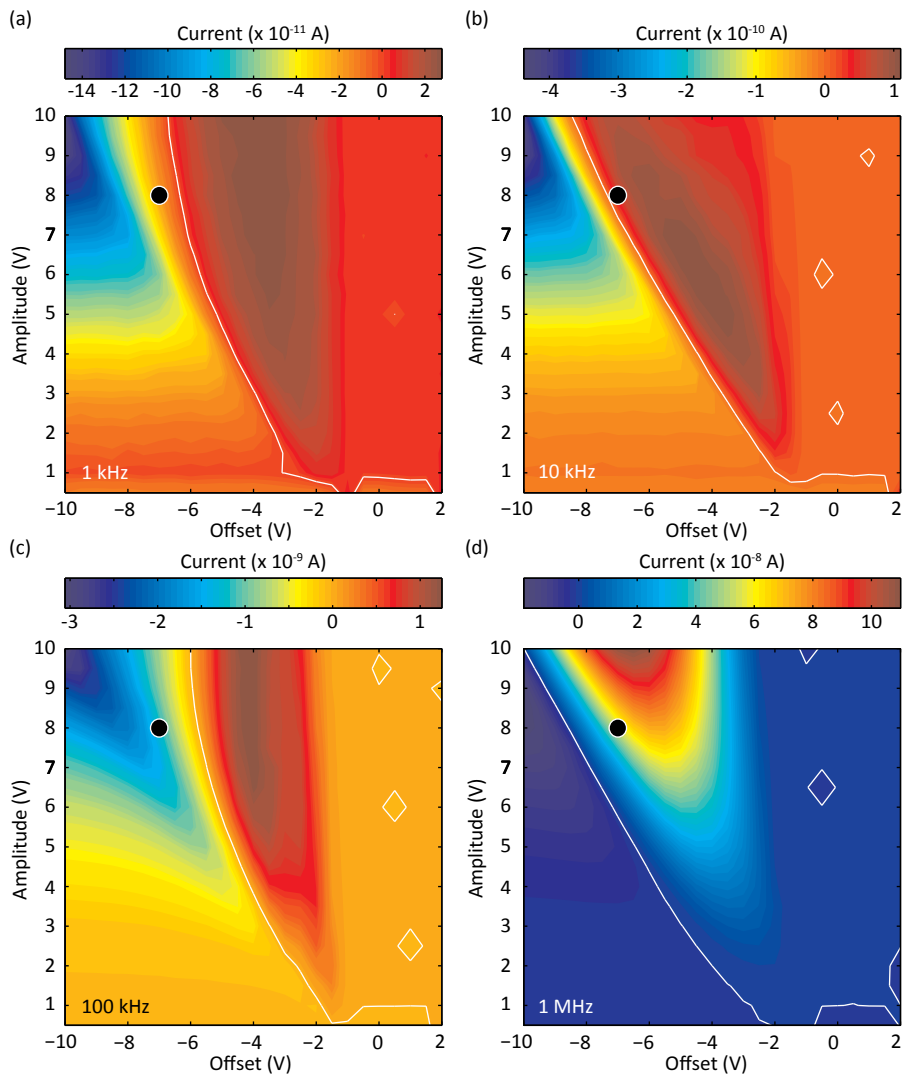
Figure 3.5 | Ratchet generated current in a multi dimensional parameter space. Contour plots for an L1–4P2.5 ratchet for different offsets V_O and amplitudes V_A, measured at frequencies of 1 kHz **(a)**, 10 kHz **(b)**, 100 kHz **(c)**, and 1 MHz **(d)**. The color indicates the ratchet current in the source contact. White lines mark current reversal boundaries, black dots mark the offset and amplitude used for the measurements in Figures 3.1 and 3.4. Measurement parameters: $V_{SD} = 0$ V, and $V_G - V_{TH} = -20$ V.

black dots agrees with the sign at the corresponding frequencies in Figure 3.1b shows the robustness and reproducibility of the sign changes. In general, offset–amplitude–current graphs for structures with a non–integer number of finger pairs show current reversals, while similar graphs for structures with an integer number do not (Figure 3.6).
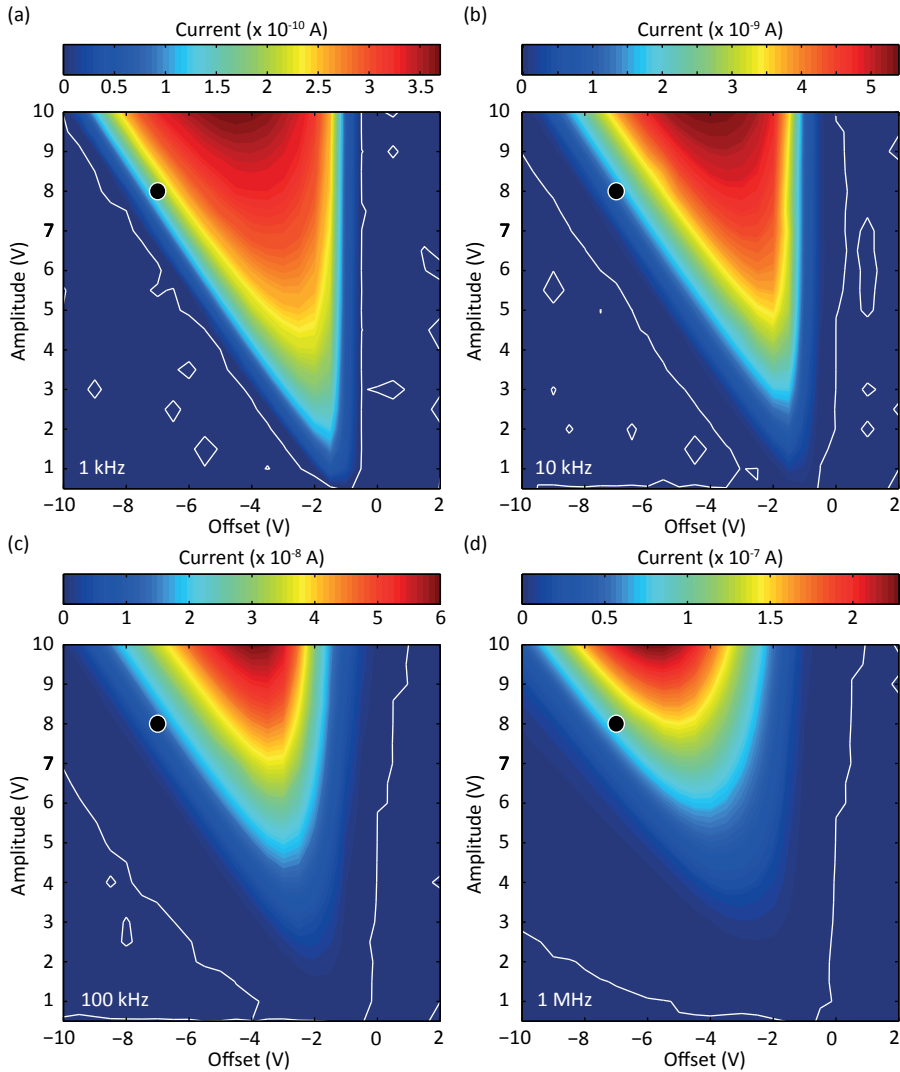
Figure 3.6 | Contour current plots for an L1–4P2 ratchet for different offsets V_O and amplitudes V_A, measured at frequencies of 1 kHz **(a)**, 10 kHz **(b)**, 100 kHz **(c)**, and 1 MHz **(d)**. The color is an indication of the ratchet current in the source contact. The white lines indicate zero current. The black dot marks the offset and amplitude value used for the measurements shown in Figures 3.1 and 3.4. The measurements are performed for V_{SD} = 0 V, and $V_G - V_{TH}$ = −20 V.

The presence and systematic shift of the white lines in Figure 3.6 might suggest current reversal effects like in Figure 3.5. However, the sign and magnitude in these regions are in the noise and leakage limits of the system.

In Figures 3.5–6 it is furthermore visible that for $V_O \geq -1$ V no (change in) current is observed. In this offset region, DC currents are blocked since the accumulation layer is locally depleted, as the applied potential on AF1 is continuously higher than the threshold voltage V_{TH}. The nonlinear nature of these devices is further illustrated by the amplitude dependence of the current in Figure 3.5. The intuitively expected behavior of a current going down with decreasing drive amplitude is only observed at large negative offsets, $V_O \approx -10$ V. At more modest values, the current may not only increase with decreasing V_A, but also reverse direction, see e.g. $V_O \approx -4$ V at 10 kHz.

3.4   Driving logic

Apart from being intriguing devices exhibiting complex electrical responses, these ratchets can also be used to deliver DC power to external devices. When a force is superimposed on an asymmetric ratchet potential, there is a region of force where the particles are moving and performing work against the direction of force [16]. In our ratchet system a force is applied by applying a source–drain bias. In Figure 3.7a the current versus drain voltage dependence for a ratchet is shown. There are three distinct regions. In region *I* and *III* charges move in the direction of the applied drain bias. In region *II*, they move in the direction opposite to the applied force. The ratchet system operates as a power source. It basically acts as the DC equivalent of the well–known AC
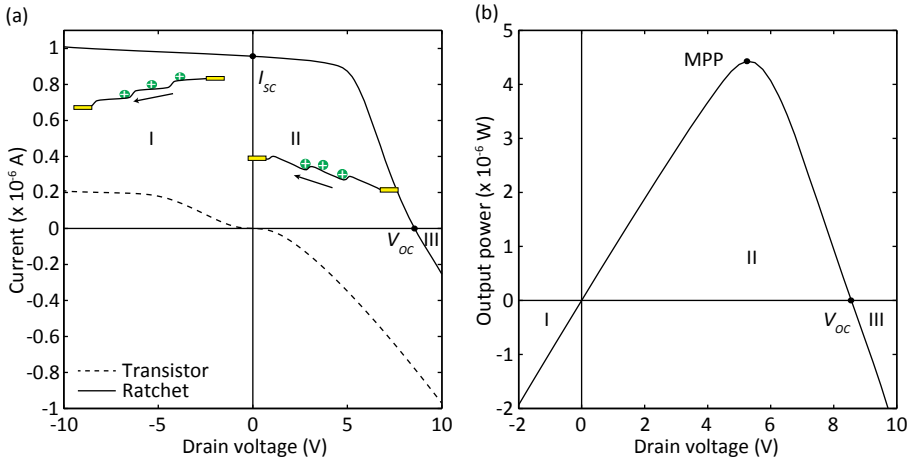
Figure 3.7 | Ratchet as power source. **(a)** Current versus drain voltage for an L1–8P16 ratchet. There are three distinctive regions: (I) the ratchet and the applied V_{SD} move charge in the same direction; (II) the ratchet moves charge against the applied V_{SD}; (III) current runs in the direction of the applied bias. The s–shape of the transistor curve is due to the presence of contact resistances at source and drain [23]. **(b)** Output power versus drain voltage. MPP indicates the maximum power point. Measurement parameters: $V_G - V_{TH} = -30$ V, $V_O = -7$ V, and $V_A = 13$ V.

transformer, as the location where the power is generated —the organic semiconducting layer— is galvanically separated from where the energy is put into the system —the asymmetric fingers. Evidently, with the ratchet potential switched off, region *II* is absent (dashed curve); the output characteristic of a transistor is obtained. The output power of the ratchet is shown in Figure 3.7b. The maximum output power is 4.5 μW, the open circuit voltage (V_{OC}) 8.55 V and the short circuit current (I_{SC}) approximately 1 μA. Drift–diffusion simulations were used to estimate the power efficiency (Section 2.6). For infinitely long L1–4P∞ and L1–8P∞ ratchets a maximum power efficiency of 0.7% and 1.5%, respectively, is found. The modeling settings used in these calculations are representative for the measurement settings used throughout this chapter. Note that optimization of the power efficiency is investigated in Chapter 5.

The output power of these ratchets can be used to drive external logic circuits. As an illustration, a ratchet is used to deliver the supply voltage V_{DD} for an inverter based on two unipolar pentacene OFETs [22]. The input–output characteristics and circuit schematics are shown in Figure 3.8. The normal switching of the inverter from on–state to off–state is observed. In the on–state the output voltage of almost –7 V corresponds to the V_{OC} of the ratchet. A gain of almost 4 is obtained. This is achieved despite a
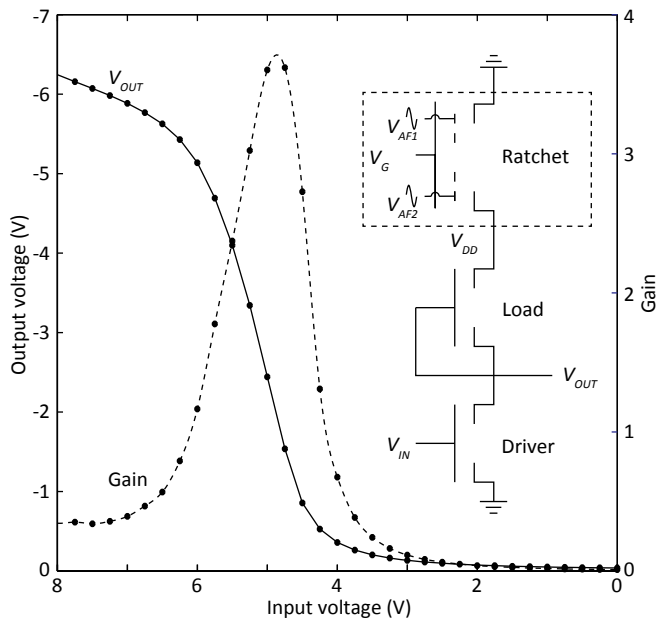
Figure 3.8 | Ratchet powered logic circuit. Input–output characteristics for a pentacene based unipolar inverter for which an L1–8P8 ratchet generated voltage is used as the DC supply voltage V_{DD}. V_{IN} the input voltage; V_{OUT} the output voltage. The load to driver ratio is twenty. Measurement parameters: $V_G - V_{TH} = -30$ V, $V_O = -7$ V, and $V_A = 13$ V.

relatively large drive current $I_{DD} \approx 0.4\ \mu A$ in the off–state that is required due to the positive threshold voltage $V_{TH} = 5$ V of the pentacene OFETs in the inverter that is operated in ambient air.

3.5 Summary

The ratchet devices presented here differ significantly from previous charge–transporting ratchets. Not only are the generated powers orders of magnitude larger and generated at ambient temperatures, also the operational mechanism differs in the sense that it inherently requires a description in terms of many–body effects instead of the more commonly employed single particle picture [2, 15–16]. Like previously reported ratchets, the present devices share the rich behavior of current reversals occurring in a complex multi–parameter space. In terms of practical applications the present work demonstrates that ratchets can deliver enough power to drive simple yet low–end logic. Using CMOS technology, with its far lower off–currents, would already enable substantially more complex circuitry than shown here.

3.6   References

[1]   Smoluchowski, M. v. Experimentell nachweisbare, der üblichen Thermodynamik widersprechende Molekularphänomene. *Physikalische Zeitschrift* **13**, 1069–1080 (1912).

[2]   Feynman, R. P., Sands, M. L. & Leighton, R. B. *The Feynman lectures on physics*. (Addison–Wesley, 1989).

[3]   Prakash, M., Quere, D. & Bush, J. W. M. Surface tension transport of prey by feeding shorebirds: The capillary ratchet. *Science* **320**, 931–934 (2008).

[4]   Svoboda, K., Schmidt, C. F., Schnapp, B. J. & Block, S. M. Direct Observation of Kinesin Stepping by Optical Trapping Interferometry. *Nature* **365**, 721–727 (1993).

[5]   van Oudenaarden, A. & Boxer, S. G. Brownian ratchets: Molecular separations in lipid bilayers supported on patterned arrays. *Science* **285**, 1046–1048 (1999).

[6]   Linke, H. *et al.* Self–propelled Leidenfrost droplets. *Phys Rev Lett* **96**, 154502 (2006).

[7]   Mahmud, G. *et al.* Directing cell motions on micropatterned ratchets. *Nature Physics* **5**, 606–612 (2009).

[8]   Rousselet, J., Salome, L., Ajdari, A. & Prost, J. Directional Motion of Brownian Particles Induced by a Periodic Asymmetric Potential. *Nature* **370**, 446–448 (1994).

[9]   Bader, J. S. *et al.* DNA transport by a micromachined Brownian ratchet device. *P Natl Acad Sci USA* **96**, 13165–13169 (1999).

[10]   Linke, H. *et al.* Experimental tunneling ratchets. *Science* **286**, 2314–2317 (1999).

[11]   Linke, H. *et al.* Asymmetric nonlinear conductance of quantum dots with broken inversion symmetry. *Phys Rev B* **61**, 15914–15926 (2000).

[12]   Khrapai, V. S., Ludwig, S., Kotthaus, J. P., Tranitz, H. P. & Wegscheider, W. Double–Dot Quantum Ratchet Driven by an Independently Biased Quantum Point Contact. *Phys Rev Lett* **97**, 176803 (2006).

[13]   Majer, J. B., Peguiron, J., Grifoni, M., Tusveld, M. & Mooij, J. E. Quantum ratchet effect for vortices. *Phys Rev Lett* **90**, 056802 (2003).

[14]   Song, A. M. *et al.* Room–temperature and 50 GHz operation of a functional nanomaterial. *Appl Phys Lett* **79**, 1357–1359 (2001).

[15]   For a review see: Hänggi, P. & Marchesoni, F. Artificial Brownian motors: Controlling transport on the nanoscale. *Rev Mod Phys* **81**, 387–442 (2009).

[16]   For a review see: Reimann, P. Brownian motors: noisy transport far from equilibrium. *Physics Reports–Review Section of Physics Letters* **361**, 57–265 (2002).

[17]   Linke, H. Ratchets and Brownian motors: Basics, experiments and applications. *Appl Phys A–Mater* **75**, 167–167 (2002).

[18]   Eshuis, P., van der Weele, K., Lohse, D. & van der Meer, D. Experimental Realization of a Rotational Ratchet in a Granular Gas. *Phys Rev Lett* **104**, 248001 (2010).

[19]   Loutherback, K., Puchalla, J., Austin, R. H. & Sturm, J. C. Deterministic Microfluidic Ratchet. *Phys Rev Lett* **102**, 045301 (2009).

[20]   Sassine, S. *et al.* Experimental investigation of the ratchet effect in a two–dimensional electron system with broken spatial inversion symmetry. *Phys Rev B* **78**, 045431 (2008).

[21]   Silva, C. C. D., de Vondel, J. V., Morelle, M. & Moshchalkov, V. V. Controlled multiple reversals of a ratchet effect. *Nature* **440**, 651–654 (2006).

[22]   Cantatore, E., Meijer, E.J. ESSCIRC. *Proceedings 29th Eur. Solid State Ciruits Conf.*, 29–36 (2003).

[23]   Wu, Y. L., Li, Y. N. & Ong, B. S. Printed silver ohmic contacts for high–mobility organic thin–film transistors. *J Am Chem Soc* **128**, 4202–4203 (2006).

Chapter 4

Scaling of characteristic frequencies of organic electronic ratchets

The scaling of the characteristic frequencies for organic electronic ratchets operating in a flashing mode is investigated by performing measurements and numerical simulations. The electronic ratchets are modified organic field effect transistors, having asymmetrically spaced interdigitated finger electrodes placed inside the gate dielectric. Oscillating potentials applied to the finger electrodes create a periodic time–depending asymmetric transistor channel potential. As a result a current can flow between source and drain with zero source–drain bias. It is shown that the frequency at current maximum is linearly dependent on the applied DC gate potential and mobility and is inversely proportional to the squared length of one ratchet period, which can be related to the RC–time of one asymmetric unit. It is furthermore shown that the frequency at current maximum depends on the asymmetry of the ratchet potential. The frequency of maximum charge pumping efficiency is also investigated and turns out not to depend on the asymmetry of the ratchet potential but only on the length of the asymmetric unit.

4.1   Introduction

Taming the random motion of particles has drawn scientific interest for over a century [1–2]. The second law of thermodynamics forbids the extraction of work from a system in thermal equilibrium. However, the random motion of particles can be rectified by subjecting the particles to ratchet potentials in systems that are taken out of thermal equilibrium. These potentials consist of repeating units that lack inversion symmetry. The mechanism behind the flashing ratchet is depicted in Figure 4.1a. Particles are trapped in an asymmetric potential. When the potential is turned off, the particles will spread due to diffusion and in case of charged particles due to drift resulting from the inter–particle interaction. If the potential is turned on again, particles will get trapped and will slide to the in energy nearest potential minimum. This is not necessarily the in space nearest potential minimum. Due to the asymmetry of the repeat unit a net transport of particles into one direction can take place. Both experiments and theoretical work have shown that ratchet systems are complicated systems and show intriguing effects like current reversals [1–2].

Prominent examples of ratchets are the electronic ratchets, which so far have been of limited use due to cryogenic operating temperatures and low output currents and voltages [3–5]. Recently, we reported on electronic ratchet systems that operate at room temperature and generate currents (~0.9 μA) and voltages (~8 V) that are orders of magnitude higher than previously reported systems [6]. Being also effective charge pumps with reported charge displacement efficiencies up to 13%, these systems might lead to interesting applications of electronic ratchet systems [6–7]. In this paper we describe how the optimum frequency for current transport scales with device (operating) parameters such as the shape and size of the ratchet potential and the charge carrier density and mobility by comparing experimental measurements and modeling results.

The ratchets studied in this paper consists of bottom–contact, bottom–gate pentacene based organic field effect transistors (OFETs). Inside the silicon dioxide (SiO_2) gate dielectric, asymmetrically spaced interdigitated finger electrodes are placed, denoted by AF1 and AF2 (Figure 4.1b). The width of these electrodes is 1 μm. By placing alternating potentials on the finger electrodes, according to $V_{AF1}(t) = V_O + (V_A/2)(1 + \sin(\omega t))$ and $V_{AF2}(t) = V_O - (V_A/2)(1 + \sin(\omega t))$, the principle of the flashing ratchet is mimicked. As a result, a current can be induced between the source (S) and drain (D) contact with zero bias $(V_{SD} = 0 \text{ V})$ between the two contacts [6]. V_O is a central offset voltage and V_A is the peak–to–peak voltage of each signal, both set with respect to the grounded source contact. ω is the angular frequency and t is the time.

The investigated ratchets differ in length and asymmetry, which is reflected in the notation. An Lx–yPa ratchet has an asymmetry of x to y, where x and y are respectively the short and long distance in micrometers between the interdigitated finger electrodes from AF1 and AF2. Pa is the number of pairs of finger electrodes that is present in the device. In some cases there is a non–integer number of finger electrode pairs, where AF1 has one finger extra as compared to AF2 (e.g. Figure 4.1b, showing an L1–2P2.5 ratchet). The L in Lx–yPa stands for length and the P stands for pairs.
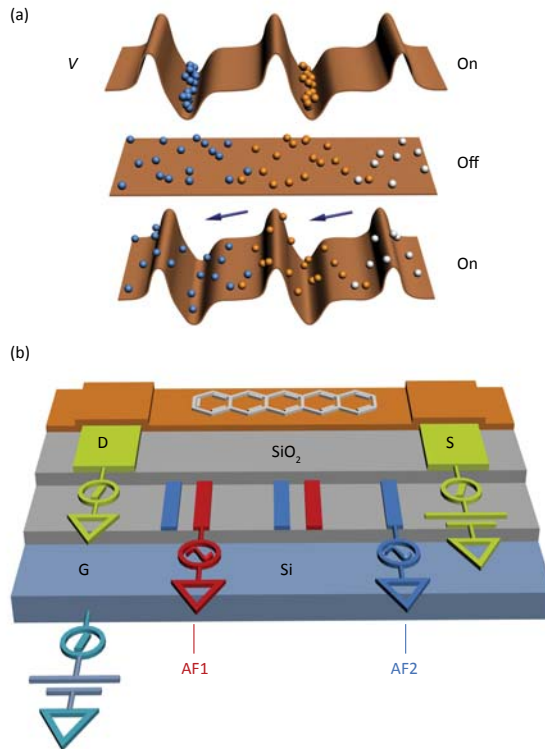
Figure 4.1| (a) On–off–on sequence of the flashing ratchet. **(b)** Drawing of an L1–2P2.5 ratchet. Visible are the source (S) and drain (D) contacts, which are separated from the silicon (Si) gate (G) contact by the silicon dioxide (SiO$_2$) gate dielectric. Asymmetrically spaced interdigitated finger electrodes denoted by AF1 and AF2 are placed inside the gate dielectric. Note the color coding of the finger electrodes; fingers with the same color are electrically connected (not visible in drawing). Pentacene is used as a semiconductor (top layer).

Several parameters might be of influence on the optimum frequency for current transport f_I, e.g. the gate bias, the amplitude V_A, the asymmetry, the temperature of the system and the mobility μ of the semiconductor. At high frequencies (10^5–10^7 Hz), the interesting region for maximum current transport, the influence of diffusion on the charge transport is negligible compared to the influence of charge–charge interactions [6]. Therefore the temperature is not an interesting variable and is kept constant at 40 °C. The offset V_O has only influence on the current I and not on the optimal frequency f_I. Therefore V_O is kept constant at –7 V. Furthermore, all ratchets are operated in short circuit mode (i.e. V_{SD} = 0 V). First the influence of the amplitude is investigated, followed by the mobility and gate voltage V_G. Finally the role of the asymmetry and the repeat unit length on the optimum frequency is addressed.

4.2   Infinite ratchet devices

In Figure 4.2, a modeled current contour plot is shown for an L1–4P∞ ratchet for different frequencies $f\left(f = \omega/2\pi \right)$ and amplitudes V_A. The white lines show for which frequency a maximum current value is reached at the corresponding amplitude values V_A for an L1–2P∞ (dashed line) and an L1–4P∞ (solid line) ratchet. Surprisingly, the results show that the frequency for optimum current transport is independent of the applied amplitude values. In the classical Brownian ratchet, the amplitude of the asymmetric potential plays a major role in the optimum frequency (see Section 1.2) [8]. When a particle is placed in an asymmetric potential landscape, it gets trapped and will slide to the potential minimum. Larger fields (i.e. larger amplitudes with fixed length scale) will decrease the transit time for a particle, i.e. the time it costs for a particle to move from one extreme to the other. As a result, the optimum frequency will increase. Below, in Section 4.4 we will come back to this counterintuitive result.

Modeling is also used to investigate the relationship between the frequency at current maximum and the mobility. The results are depicted in Figure 4.3a. A linear dependence is found between the frequency at current maximum and the mobility for the L1–4P∞ and L1–2P∞ ratchets. This result is not surprising as the Einstein relation is used to couple the diffusion coefficient with the mobility, and hence it can be expected that all transport processes scale linearly with mobility. The influence of the gate voltage on the frequency is shown in Figure 4.3b. The frequency at current maximum is linearly dependent on the gate voltage. As the charge density in the transistor channel is linearly

dependent on the gate voltage this also implies that the frequency at current maximum is linear dependent on the charge density. Also this issue will be further discussed in Section 4.4.

Figure 4.2 | Modeled contour plot for an L1–4P∞ ratchet for different frequencies f and amplitudes V_A. The color indicates the ratchet current I. The white lines show the frequencies at which a maximum current is reached for the corresponding amplitude values for an L1–2P∞ and L1–4P∞ ratchet. Modeling settings: $\mu = 10^{-6}$ m²/Vs, $V_G = -20$ V, $V_O = -7$ V.
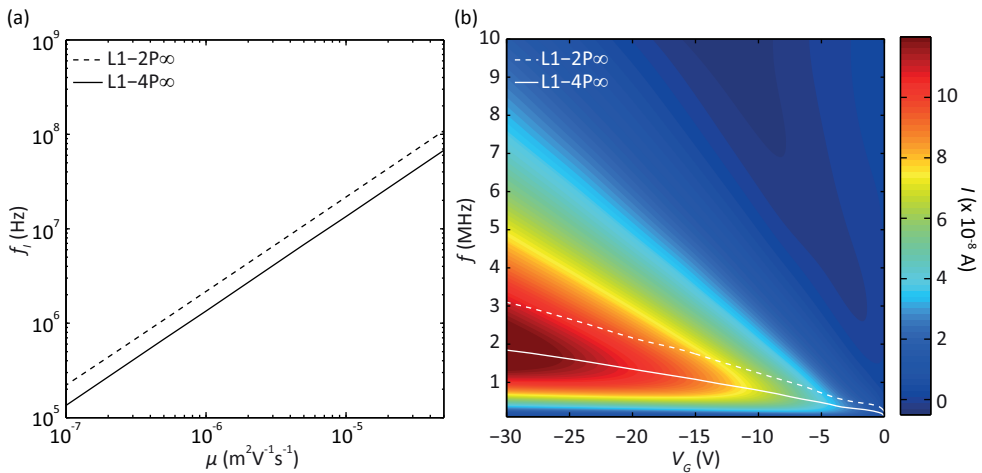
Figure 4.3 | (a) Modeled frequency at current maximum f_I versus mobility μ for an L1–2P∞ and L1–4P∞ ratchet. Modeling settings: $V_G = -20$ V, $V_O = -7$ V, $V_A = 8$ V. **(b)** Modeled contour plot for an L1–4P∞ ratchet for different frequencies f and gate voltages V_G. Modeling settings: $\mu = 10^{-6}$ m²/Vs, $V_A = 8$ V, $V_O = -7$ V. The color indicates the ratchet current I. The white lines show the frequency at which a maximum current is reached for the corresponding gate voltage values for an L1–2P∞ and L1–4P∞ ratchet.

4.3 Finite ratchet devices

So far, the modeling results indicate that the frequency at current maximum is independent of the applied amplitude and that $f_I \sim \mu V_G$ for infinite devices. In the coming paragraphs finite devices as shown in Figure 4.1b are investigated experimentally. In Figure 4.4, a measured current contour plot for an L1–4P4 ratchet for different frequencies and amplitudes V_A is shown. The white line shows for which frequency a maximum current value is reached for the corresponding amplitude values V_A. The result shows that the frequency for maximum current is basically independent of the amplitude, which is in agreement with the modeling results.
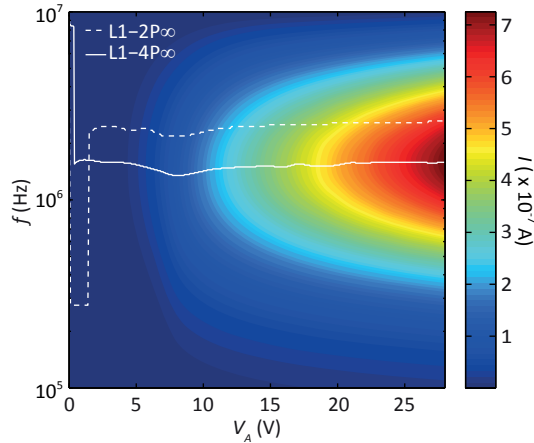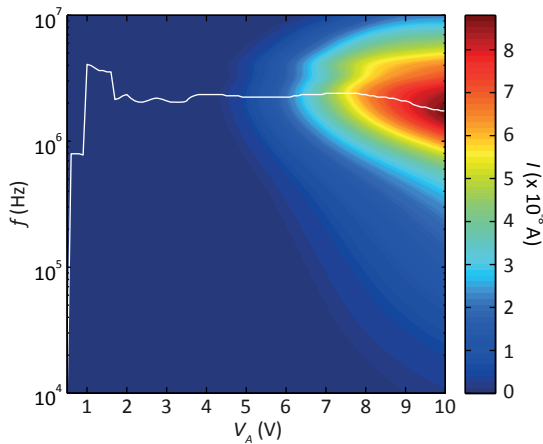

Figure 4.4 | Measured contour plot for an L1–4P4 ratchet for different frequencies f and amplitudes V_A. The color indicates the ratchet current. The white line shows the frequency at which a maximum current is reached for the corresponding amplitude values. Measurement settings: $V_O = -7$ V, $V_G - V_{TH} = -20$ V, with V_{TH} the threshold voltage.

The influence of the gate voltage for an L1–4P8 ratchet is displayed in Figure 4.5. The contour plot in Figure 4.5a shows the current values for different frequencies and gate voltages. The white line indicates the frequency values at which the current reaches a maximum. In contrast to the modeling result in Figure 4.3b the relationship between frequency and gate voltage is not linear. This can be understood as follows. In the model a constant mobility is assumed. In reality, the pentacene mobility is density dependent and/or field dependent [9]. As the density depends on the gate voltage the data from Figure 4.5a need to be corrected for this. In Figure 4.5b the measured mobility as a function of the gate voltage is depicted for the L1–4P8 ratchet. Next, for each gate voltage the measured frequency at maximum current (panel a) is divided by the corresponding normalized mobility μ_N (i.e. $\mu_N(V_G) = \mu(V_G)/\mu_M$, with μ_M the
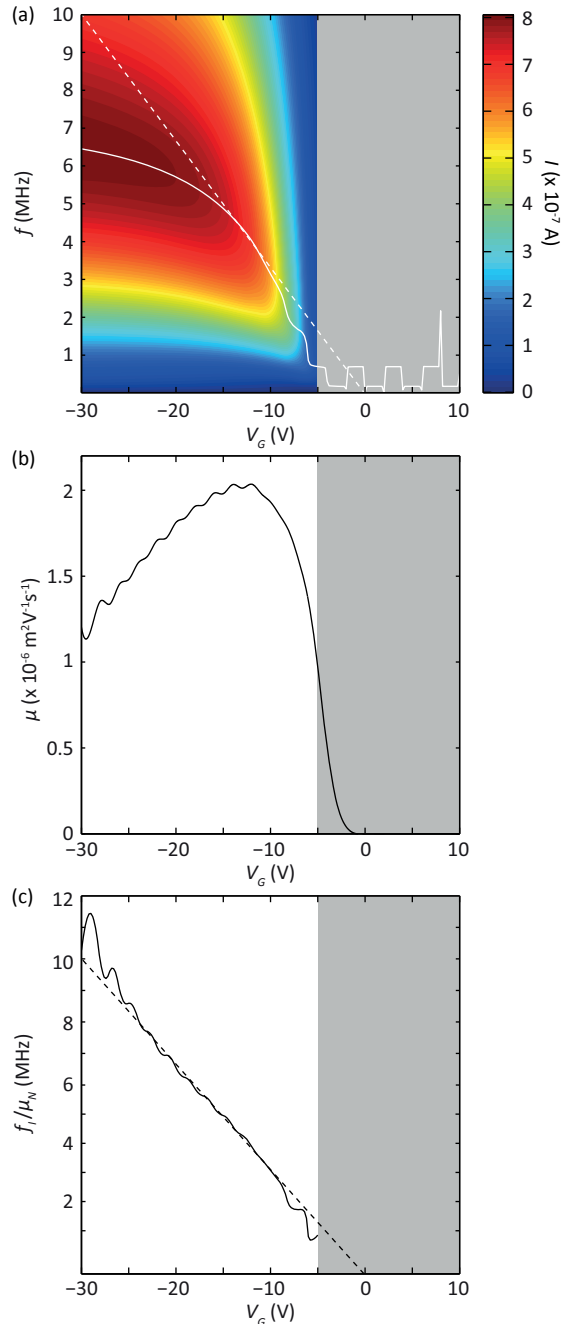
Figure 4.5 | (a) Measured current contour plot for an L1–4P8 ratchet for different frequencies f and gate voltages V_G. The color indicates the ratchet current I. The white line shows the frequency at which a maximum current is reached for the corresponding gate values. Measurement settings: V_A = 8 V, V_O = −7 V. **(b)** Measured mobility μ versus gate voltage V_G for an L1–4P8 ratchet. **(c)** Frequency at maximum current f_I of (a) divided by the normalized mobility μ_N of (b) versus the gate voltage V_G. The dashed lines in (a) and (c) show a linear fit to the corrected measurement results in panel (c).

maximum mobility), giving a linear relationship as shown in panel c. This is a typical result which is found for ratchets with different asymmetries and finger electrode pairs and is in agreement with the modeling (Figure 4.3b).

4.4   Amplitude and gate potential

The present modeling and measurement results both indicate that $f_I \sim \mu V_G$. For a single particle in a flashing ratchet the optimal on–time was previously found to be $t_{on} = \gamma (1 - \alpha)^2 L^2 / U$, with γ the drag coefficient which is inversely proportional to the mobility μ, $(1 - \alpha)$ a constant reflecting the asymmetry of the ratchet (see also Chapter 1), U the barrier height, and L the total length of one asymmetric unit [8]. Comparing this relationship to the scaling of our many–particle ratchet suggests that the role of the barrier height U is taken over by the gate potential V_G. Again, this would be a rather counterintuitive finding, as the gate voltage (or charge density) has no straightforward relation to the transit time, which the barrier height does. We therefore look at how the amplitude of the channel potential (ΔV_{CH}) (Figure 4.6a) changes with changing V_G or V_A. Figure 4.6a shows two snap shots of the channel potential at different times for two different gate potentials: –10 V (solid line) and –50 V (dashed line). The snap shots show the channel potential when it reaches its maximum and minimum values during one on–off sequence. When decreasing the gate potential, the amplitude of the channel potential increases. In Figure 4.6c, ΔV_{CH} is shown as a function of V_G for both times. A linear relationship is found, which might indicate that the relationship $f_I \sim \mu V_G$ for the many–particle ratchet is complementary with $f_I \sim \mu V_A$ found for the single particle ratchet. However, the role of V_A on ΔV_{CH} is still unclear. Actually V_A is the most likely parameter in the present system to play the role of the barrier height U. On the other hand, both simulations and experiments showed a clear independence of the frequency at maximum current on V_A. In Figure 4.6b, two snap shots of the channel potential are plotted versus the position x for two different amplitudes: 5 V (solid line) and 25 V (dashed line). One of the snap shots shows a drastic decrease in channel potential with increasing amplitude in the region of AF1. Due to the offset and amplitude value, the accumulation layer located above AF1 is forced into depletion for an increasing amount of time during the on–off sequence. It should be noted that, when the channel for a period of time is forced into depletion, this does not actually mean that the channel is depleted in the sense of void of carriers. Due to the high frequency of the oscillating potentials, the charge carriers do not always have enough time to move away. In either

case, increasing V_A increases ΔV_{CH} as is shown in Figure 4.6d. The curves for the two times start to deviate for amplitude values of approximately 7 V, as the channel located above AF1 is forced into depletion. Summarizing, both V_G and V_A have a considerable influence on the channel potential and the 'barrier height' ΔV_{CH}, indicating that the relationship $f_I \sim \mu V_G$ for the many–particle ratchet is not complementary with the relationship $f_I \sim \mu V_A$ for the single particle ratchet.
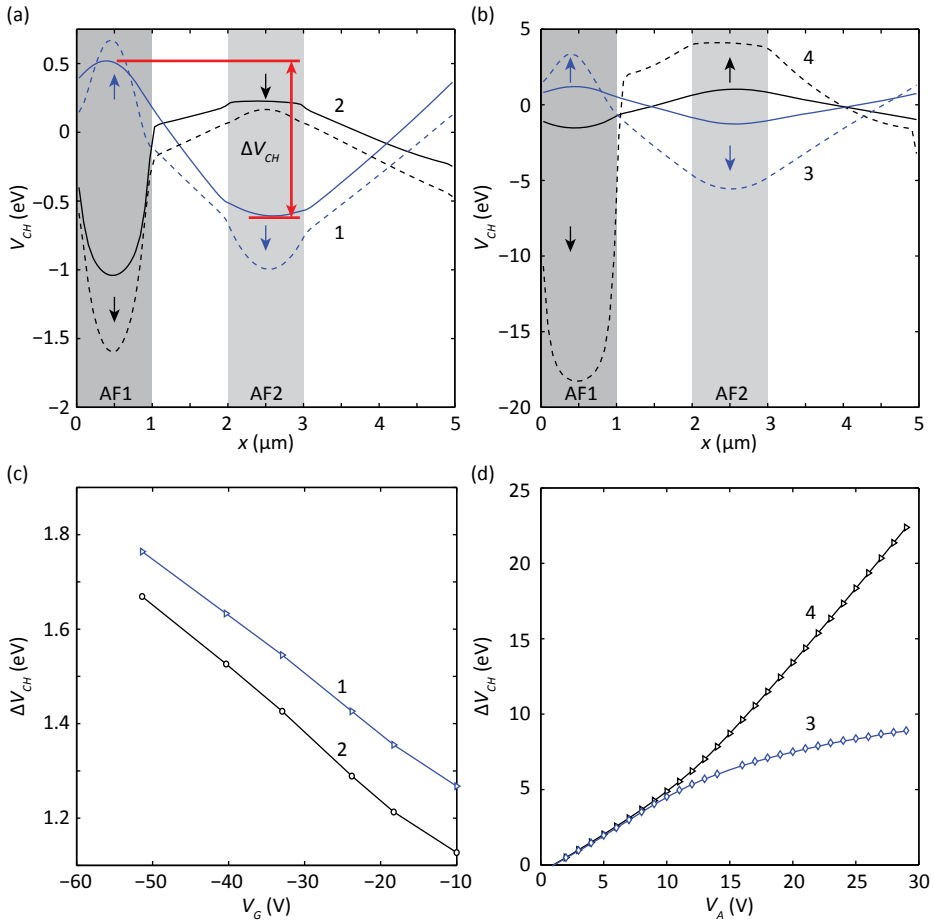
Figure 4.6 | (a) Modeled channel potential V_{CH} versus position x for two different gate potentials, $V_G = -10$ V (solid line) and $V_G = -50$ V (dashed line). Two extreme cases of the channel potential occurring during one on–off sequence are shown. **(b)** Modeled channel potential versus position for two different amplitudes, $V_A = 5$ V (solid line) and $V_A = 25$ V (dashed line). Two extreme cases of the channel potential occurring during one on–off sequence are shown. In panel **(c)** and **(d)** the change between maximum and minimum channel potential ΔV_{CH} versus the applied gate voltage V_G and amplitude V_A is shown respectively. The grey background in (a) and (b) shows the location of the finger electrodes AF1 (dark grey) and AF2 (light grey).

Investigating the RC–time —a typical response time— might give some new clues. The RC–time is taken as the channel resistance R multiplied by the gate capacitance C. The charge density in a part of the channel is given by $qp = V_G C / d_{PEN} W L$, with W and L the width and length of the channel part, respectively and d_{PEN} the thickness of the pentacene layer. The conductivity is given by $\sigma = qp\mu$ and the conductance by $S = \sigma \cdot d_{pen} W / L$. Combining these equations gives $S = V_G C \mu / L^2$. The RC–time is then found to be $RC = L^2 / V_G \mu$, where we used $R = S^{-1}$. The inverse of the RC–time shows the same relationship for the mobility and gate voltage as found for f_I. This is the same relationship as found for the upper limit of the cut–off frequency of a field effect transistor: at $V_G = V_{SD}$ this is given by $f_0 \leq \mu V_G / 2\pi L^2$, with L the channel length [10]. In both cases the charge density in the channel is linearly dependent on the gate voltage. It should be noted that the (local) charge density is also dependent on the amplitude. However, the average charge density in the channel is independent of amplitude as long as $V_A \leq V_O$. At present it is unclear why the amplitude has negligible effect on the frequency at current maximum when $V_A > V_O$ even though the average charge density does change with amplitude.

4.5 Characteristic length scales

The frequency at current maximum for the single particle ratchet is depending on L^{-2}, with L the length of one asymmetric unit [8]. In this section, it is investigated if this relationship also holds for the organic electronic ratchets. In Figure 4.7a, modeled and measured frequencies f_I are depicted versus L^{-2}. Two ratchet series are modeled; L1–yP∞ and L0.5–yP∞ ratchets, where the short distance between two finger electrodes is respectively 1 and 0.5 μm. Both L and the asymmetry change with variable long inter–finger spacing y. The curve indicates that going to larger asymmetries (i.e. smaller L^{-2} values), a minimum in frequency is reached after which a slight increase in frequency is observed. This same trend is also visible for the measurement results on L1–yPa ratchets. The quantitative difference in frequency between modeled and measured ratchets is mainly due to differences in mobility.

The optimal on–time for a flashing ratchet depends on the length L but also on the asymmetry. The asymmetry dependence can be removed by investigating ratchets with different periodicity but constant asymmetry. The results are shown in Figure 4.7b. A linear relationship is found between the optimum frequency f_I and L^{-2}. From Figures 4.7a–b it becomes clear that $f_I \sim \left(\mu V_G / L^2 \right) \cdot g_{as}$, with g_{as} an unknown function of the asymmetry.
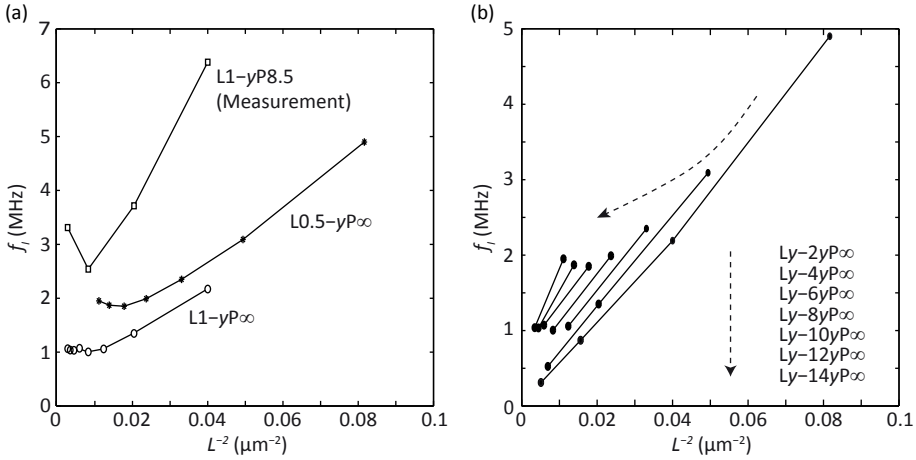
Figure 4.7 | (a) Modeled frequency at current maximum f_I versus L^{-2} for ratchets with a fixed short distance x of 1 μm and 0.5 μm. Measurement results are also shown in the figure. A similar trend as in the modeling results is visible. **(b)** Frequency at current maximum f_I versus L^{-2} for ratchets with various, fixed asymmetry ratios. Modeling settings (a): $\mu = 10^{-6}$ m²/Vs, $V_G = -20$ V, $V_O = -7$ V, $V_A = 8$ V. L1–yP∞: y ranges from 2 to 16 μm with steps of 2 μm, L0.5–yP∞: y ranges from 1 to 7 μm with steps of 1 μm. Measurement settings (a): $V_O = -6$ V, $V_A = 8$ V, $V_G - V_{TH} = -20$ V. L1–yP∞ (measurement): y is 2, 4, 8 and 16 μm. Modeling settings (b): $\mu = 10^{-6}$ m²/Vs, $V_G = -20$ V, $V_O = -7$ V, $V_A = 8$ V, y values of 0.5, 1, 2 and 4 μm are used.

After the above discussion, the scaling of the frequency at maximum current with key device parameters is largely established but full quantitative understanding hinges on understanding the origin of g_{as}.

This discussion is finished with a brief inspection of the scaling of the frequency at maximum charge per cycle f_Q, instead of at maximum current. At this frequency the charge displacement efficiency almost reaches its maximum (Chapter 5) [6]. The charge displacement efficiency is defined as the net amount of charge moved in one oscillation period over the total amount of moved charge, with 'moved charge' taken as (drift and diffusion) current divided by frequency. In Figure 4.8 f_Q is shown as a function of μ/L^2. Surprisingly, f_Q is not only proportional to L^{-2} for fixed asymmetry, like f_I, but for all modeled asymmetries: the numerical data points all coincide on a single curve, indicating that f_Q is not influenced by the asymmetry of the ratchet potential. In the experiments a similar trend seems to be present as shown by the dashed line in Figure 4.8. Another difference between the scaling properties of f_Q and f_I is the fact that f_I does (Figure 4.3b) and f_Q does not scale with V_G. Modeling results for f_Q show significant deviations from a linear scaling with V_G (not shown). The causes underlying these intriguing differences are presently unclear.
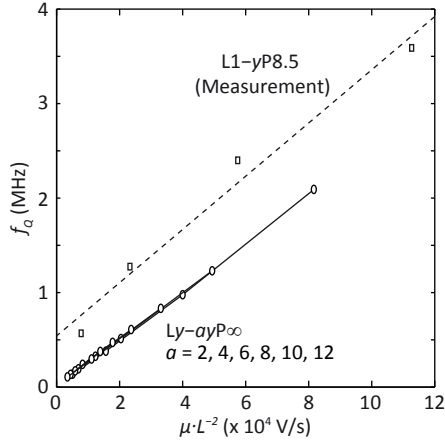
Figure 4.8 | Modeled frequency at charge maximum f_Q versus $\mu \cdot L^{-2}$ for ratchets with various, fixed asymmetry ratios. The measurement (L1–yP8.5 (Measurement)) results are obtained for ratchets with a fixed short distance y of 1 μm. Modeling settings: $\mu = 10^{-6}$ m²/Vs, $V_G = -20$ V, $V_O = -7$ V, $V_A = 8$ V. Measurement settings: $V_O = -6$ V, $V_A = 8$ V, $V_G - V_{TH} = -20$ V.

4.6   Summary

The organic electronic ratchets presented in this chapter work by the grace of charge–charge interactions and behave fundamentally different from single particle ratchets. In the interesting regime for current transport (10^5–10^7 Hz, where diffusion is negligible) modeling and measurement results show that the amplitude of the applied ratchet potential has a negligible influence on the frequency at which maximum current is reached, f_I. This distincts from single particle systems reported previously, where the frequency at current maximum was linearly dependent on the amplitude. It is furthermore found that $f_I \sim \left(\mu V_G / L^2 \right) \cdot g_{as}$, which is, apart from the asymmetry term g_{as}, the RC–time for one asymmetric ratchet unit. In marked contrast, the frequency at maximum charge transport efficiency is not depending on the asymmetry of the ratchet and scales as $f_Q \sim \mu / L^2$.

Apart from their fundamental interest, the presented scaling rules allow the prediction of the optimum frequency for charge and current transport for electronic ratchets. This can contribute to the rational design of ratchets for use in actual applications.

4.7   References

[1]   Hänggi, P. & Marchesoni, F. Artificial Brownian motors: Controlling transport on the nanoscale. *Rev Mod Phys* **81**, 387–442, (2009).

[2]   Reimann, P. Brownian motors: noisy transport far from equilibrium. *Physics Reports–Review Section of Physics Letters* **361**, 57–265, (2002).

[3]   Linke, H. *et al.* Experimental tunneling ratchets. *Science* **286**, 2314–2317, (1999).

[4]   Khrapai, V. S., Ludwig, S., Kotthaus, J. P., Tranitz, H. P. & Wegscheider, W. Double–Dot Quantum Ratchet Driven by an Independently Biased Quantum Point Contact. *Phys Rev Lett* **97**, 176803, (2006).

[5]   Majer, J. B., Peguiron, J., Grifoni, M., Tusveld, M. & Mooij, J. E. Quantum ratchet effect for vortices. *Phys Rev Lett* **90**, 056802, (2003).

[6]   Roeling, E. M. *et al.* Organic electronic ratchets doing work. *Nat Mater* **10**, 51–55, (2011).

[7]   Hänggi, P. Organic electronics: Harvesting randomness. *Nat Mater* **10**, 6–7, (2011).

[8]   Linke, H., Downton, M. T. & Zuckermann, M. J. Performance characteristics of Brownian motors. *Chaos* **15**, 026111, (2005).

[9]   Coehoorn, R., Pasveer, W. F., Bobbert, P. A. & Michels, M. A. J. Charge–carrier concentration dependence of the hopping mobility in organic materials with Gaussian disorder. *Phys Rev B* **72**, 155206, (2005).

[10]   Scheinert, S. & Paasch, G. Fabrication and analysis of polymer field–effect transistors. *Phys Status Solidi A* **201**, 1263–1301, (2004).

Chapter 5

Performance of organic electronic ratchets

In this chapter the performance characteristics —i.e. current, charge per cycle, open circuit voltage, power efficiency and charge displacement efficiency— of organic electronic ratchets are investigated using numerical modeling and measurements. It is shown how the characteristic parameters of the time–varying asymmetric potential like length scales and amplitude, as well as the charge carrier density and mobility influence the performance characteristics.

For ratchets with a constant asymmetry but changing length, the current increases when going to smaller length scales while the net charge displaced per cycle, as well as the power and charge displacement efficiencies decrease. To optimize the power efficiency for a given geometry, (voltage) settings need to be chosen such that the charge displaced per oscillation cycle reaches a maximum, rather than near the current maximum.

When all settings are brought close to optimum, a ratchet with a predicted charge displacement efficiency of over 49% and a power efficiency of approximately 6.9% is obtained.

5.1 Introduction

In the previous chapters we have introduced organic electronic ratchets that generate currents close to 1 µA and voltages of approximately 8 V at room temperature. These high current and voltage values are obtained as these ratchets work by the grace of charge–charge interactions, in contrast to other ratchet systems [1]. As shown in Chapter 3, enough work can be extracted from these ratchets to drive simple logic circuitry. Results from drift–diffusion simulations presented therein indicate that the power efficiency can be as high as 1.5% for an L1–8P∞ ratchet. Using numerical modeling and measurements, the role of system parameters (e.g. asymmetry and gate voltage) on the characteristic frequencies of the ratchets has been addressed in Chapter 4. Hence, a view on how the performance of this particular type of ratchet can be optimized is still lacking. In this chapter, the influence of system parameters (e.g. asymmetry, applied gate voltage) on the performance characteristics of these organic electronic ratchets, in particular the current, charge displaced per cycle, open circuit voltage, power efficiency, and charge displacement efficiency, is addressed. The drift–diffusion model introduced in Chapter 2 is used to investigate these performance parameters. Measurement results are used to support the results obtained from the model.

In Figure 5.1 a cross section of a typical organic electronic ratchet is shown. The oscillating potentials applied on the finger electrodes are $V_{AF1}(t) = V_O + (V_A/2)(1 + \sin(\omega t))$ and $V_{AF2}(t) = V_O - (V_A/2)(1 - \sin(\omega t + \phi))$. Here V_O is a central offset voltage, V_A is the amplitude of the ratchet potential (i.e. the peak–peak voltage of each individual potential), ω the angular frequency, t the time and ϕ is the phase difference between V_{AF1} and V_{AF2}. In previous chapters, the phase difference between V_{AF1} and V_{AF2} was always 180° (Figure 5.1). In this chapter, the influence of the phase difference ϕ on current and charge transport is explicitly addressed.

The efficiency of ratchet systems is widely studied [2–4]. The commonly used definition for a Brownian motor connected to a load is:

$$\eta_p = \langle \dot{x} \rangle A_0 / \langle P \rangle_{in} , \tag{5.1}$$

with $\langle \dot{x} \rangle A_0$ the average mechanical work done per unit of time against an applied load A_0, and $\langle P \rangle_{in}$ the average net power pumped into the system. This same definition is used for the power efficiency of organic electronic ratchets:

$$\eta_p = \langle P_{out} \rangle / \langle P_{in} \rangle . \tag{5.2}$$

The output power $\langle P_{out} \rangle$ is the time averaged (DC) source–drain current I_{SD} multiplied by the source–drain bias V_{SD}, normally taken at the maximum power point. The input
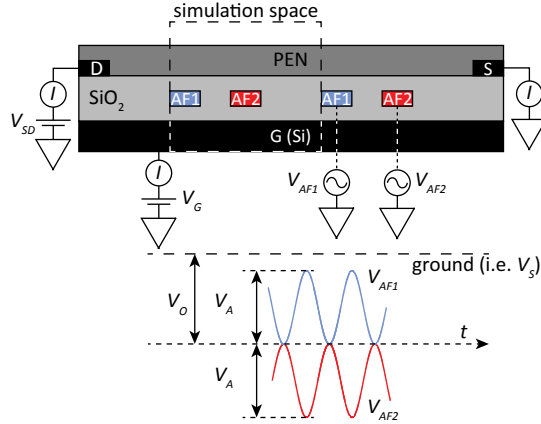
Figure 5.1 | Cross section of an L1–2P2 electronic ratchet. Visible are the source (S) and drain (D) contacts, which are separated from the silicon (Si) gate (G) contact by the silicon dioxide (SiO$_2$) gate dielectric. Asymmetrically spaced interdigitated finger electrodes denoted by AF1 and AF2 are placed inside the gate dielectric. Note the color coding of the finger electrodes; fingers with the same color are electrically connected. Pentacene (PEN) is used as a semiconductor. Note that the potentials V_{AF1} and V_{AF2} as a function of time are shown in anti–phase, which is not necessarily the case.

power $\langle P_{in} \rangle$ is the total amount of energy put into the system via the finger electrodes, averaged over one on–off sequence $t = 2\pi/\omega$ (see also Chapter 2). In the numerical modeling a single period of an infinitely long device is considered, as indicated by the dashed box in Figure 5.1. Hence, there are no contacts present and the source–drain bias V_{SD} is replaced with the tilt potential V_{tilt}, which is the applied potential over one asymmetric repeat unit.

When no load is applied, the power efficiency is zero by definition. In order to make quantitative statements on how efficient a certain operation is performed under zero load, a generalized efficiency has been introduced for microscopic engines [5]. It is defined as $\eta = E_{in}^{min}/E_{in}$, with E_{in}^{min} the minimum energy input required to perform the same task as the engine, like moving through a viscous medium at constant temperature. Using this expression the operation of molecular motors in various situations can be compared [5]. For the same purpose, i.e. to compare electronic ratchets under zero load, the charge displacement efficiency η_q is introduced. In contrast to the just mentioned generalized efficiency, the charge displacement efficiency is not an energy efficiency. It is defined as the net amount of charges moved into one direction divided by the total amount of moved charges [1]:

$$\eta_q = \int I_{SD}(t)\,dt \Big/ \int \left| I_{SD}(t) \right| dt \,, \tag{5.3}$$

where the integrals run over one oscillation cycle.

A different number for how well these ratchets can move charges is the fraction of particles γ_t that can be transferred from one asymmetric potential unit to a neighboring unit. It is found by dividing the net moved charge through the total amount of charge that is located in one asymmetric repeat unit. For a flashing ratchet γ_t can theoretically be as high as 16% as is shown in Section 1.2 [4]. It must be emphasized that γ_t is not the same as η_q. For the electronic ratchets discussed in this thesis the charge displacement efficiency η_q is a more meaningful number than the fraction of moved charges γ_t as it only takes into account those charges that participate in the charge transport and with that dissipate or deliver energy. In other words, static charges are not accounted for in η_q but are so in γ_t. Therefore γ_t is not further investigated. However, at the end of this chapter, γ_t is calculated for an optimized ratchet and compared with the 16% found for the flashing ratchet from Section 1.2.

The rest of this chapter is organized as follows. First, the influence of the geometrical parameters, i.e. length scales and asymmetry, on the device performance will be addressed. Then the electrical parameters, i.e. charge carrier density and mobility, and the amplitude, offset, phase, and frequency of the oscillating biases on the finger electrodes are discussed in relation to performance. This cumulates into an estimate for the maximum efficiency that realistically can be reached with this type of ratchet device.

5.2 Length scale influences

In Figure 5.2a, the modeled source–drain current I_{SD} is plotted versus the tilt potential V_{tilt} for different asymmetries. The frequencies $f\left(=\omega/2\pi\right)$ used in the numerical modeling are the frequencies at which a maximum current value is reached $\left(f = f_I\right)$. Figure 5.2a shows that for the infinitely long ratchets the simulations reveal a linear relationship between I_{SD} and V_{tilt}, in agreement with previously reported results [2]. The inset in Figure 5.2a shows the measured source–drain current versus source–drain bias for an L1–2P4 ratchet. This experimental result shows that in real devices a slightly non–linear relationship is present, which will be discussed in more detail in Chapter 6.

Figure 5.2b displays the modeled average channel resistance R of one asymmetric period versus the repeat unit length L, which is the inverse slope of the I–V curves shown in Figure 5.2a. Ratchets with constant (Ly–2yP∞ and Ly–4yP∞) and varying asymmetry (L0.5–yP∞) are modeled at $f = f_I$ and $f = f_Q$. The latter is the frequency at which the maximum charge per cycle is reached. The charge per cycle is the net amount of charges
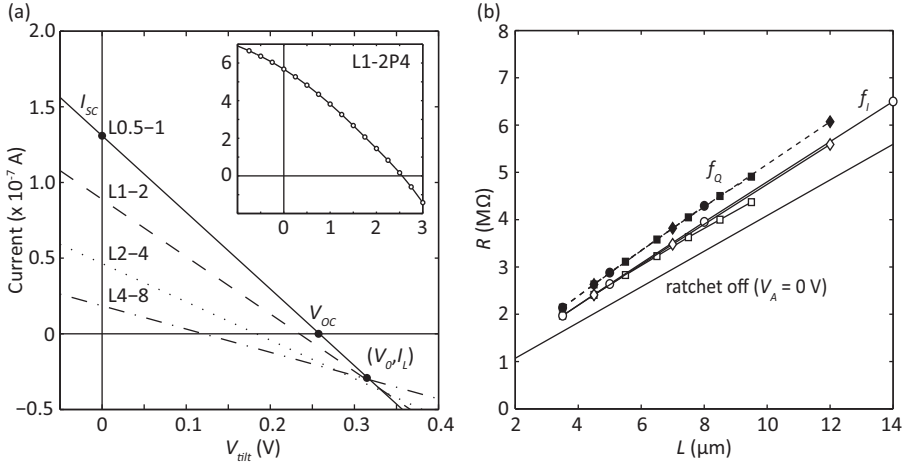
Figure 5.2 | (a) Modeled current I_{SD} versus tilt potential V_{tilt} for several Ly–2yP∞ ratchets (constant asymmetry, L0.5–1P∞, L1–2P∞, L2–4P∞, and L1–4P∞) at f_I. The inset shows a measurement result of the current versus source–drain bias V_{SD} for an L1–2P4 ratchet. **(b)** Modeled channel resistance R versus characteristic length L for ratchets with constant (Ly–2yP∞, Ly–4yP∞) and varying (L0.5–yP∞) asymmetry at f_I and f_Q. The solid line shows the channel resistance for a structure where the ratchet is turned off (i.e. V_A = 0 V). Modeling settings are: $\mu = 10^{-6}$ m^2/Vs, V_G = −20 V, V_A = 8 V, V_O = −7 V, ϕ = 180° and V_{SD} = 0 V. For the Ly–2yP∞ series, y = 0.5, 1, 2, and 4 (only f_I). For the Ly–4yP∞ series, y = 0.5, 1, and 2. For the L0.5–yP∞ series, y ranges from 1 to 7.

moved during one sequence and is obtained by dividing I_{SD} by the ratchet frequency f. At charge maximum, i.e. $f = f_Q$, a linear relationship is found between the channel resistance and length scale for different asymmetries, indicating that the asymmetry is not important for devices operating at f_Q. In Chapter 4 it was already shown that f_Q is only depending on L and not on the asymmetry of the ratchet. Also when comparing ratchets with a constant asymmetry operating at f_I, an (almost) linear dependence between the average channel resistance R and the repeat unit length L is found. For comparison, the bottom solid line in Figure 5.2b shows the channel resistance without the ratchet mechanism turned on (i.e. V_A is set to 0 V in the model). An increase in channel resistance is observed when moving from 'ratchet off' to f_I to f_Q.

The data in Figures 5.2(a) and (b) can phenomenologically be described as $I - I_L = (V_0 - V)/R$ where (V_0, I_L) is the intersection point of the I–V curves in panel (a) and $R = \alpha L + R_L$ is the channel resistance consisting of a part that is linear in repeat unit length L and an almost constant offset term R_L. Unfortunately, the physical meaning of the parameters I_L and R_L is not very transparent. Clearly, they do represent a performance loss over an idealized device, but their associated power losses (≈70–95%) grossly underestimate the actual losses that will be discussed below. Nevertheless, the
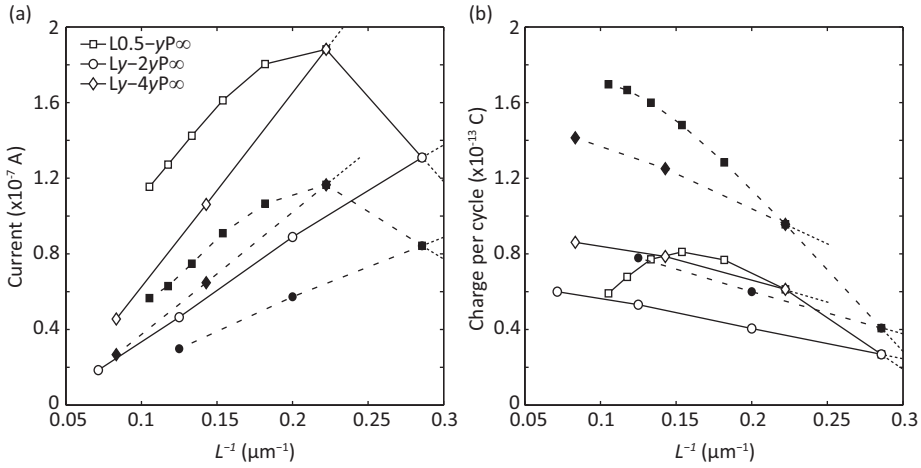
Figure 5.3 | Calculated source–drain current **(a)** and charge per cycle **(b)** versus L^{-1} for ratchets with constant (Ly–2yP∞, Ly–4yP∞) and varying asymmetry (L0.5–yP∞) at f_I (solid lines) and f_Q (dashed lines). Modeling settings are: $\mu = 10^{-6}$ m²/Vs, $V_G = -20$ V, $V_A = 8$ V, $V_O = -7$ V, $\phi = 180°$ and $V_{SD} = 0$ V.
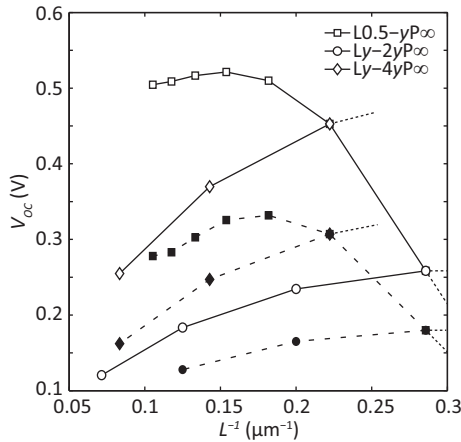
Figure 5.4 | Calculated open circuit voltage V_{OC} versus L^{-1} for ratchets with constant (Ly–2yP∞, Ly–4yP∞) and varying (L0.5–yP∞) asymmetry at f_I (solid lines) and f_Q (dashed lines). Modeling settings are: $\mu = 10^{-6}$ m²/Vs, $V_G = -20$ V, $V_A = 8$ V, $V_O = -7$ V, and $\phi = 180°$.

fact that I_L and R_L are nonzero shows that the system can only in crude approximation be treated as a linear superposition of an ideal charge pump (the ratchet) and an internal load (the channel resistance). On the other hand, given the highly non–linear nature of ratchets in general, the relatively small values of I_L and R_L may be considered surprising.

The modeled short circuit current I_{SC} (i.e. the ratchet generated current at $V_{tilt} = 0$ V) versus L^{-1} at f_I (solid lines) and f_Q (dashed lines) is displayed in Figure 5.3a. Results are shown for ratchets with constant asymmetry (Ly–2yP∞ and Ly–4yP∞) and varying

asymmetries (L0.5–yP∞). A linear relationship is found between I_{SC} and L^{-1} for ratchets with constant asymmetry. Decreasing the characteristic ratchet length scale L leads to an increase in current. In Figure 5.3b, the charge per cycle Q at f_I and f_Q is plotted versus L^{-1}. Opposite to the current, the charge per cycle decreases with decreasing length L for all three ratchet series.

The open circuit voltage V_{OC}, which may be considered the stall load of the device [2], versus L^{-1} is displayed in Figure 5.4 for ratchets with constant and varying asymmetries at f_I (solid lines) and f_Q (dashed lines). For ratchets with constant asymmetry a sub–linear increase in V_{OC} is observed. Ratchets with changing asymmetry show a maximum in V_{OC} of approximately 0.5 V for the L0.5–4P∞ ratchet. It should be pointed out that the data in Figures 5.2(a) and (b), 5.3(a) and 5.4 are not independent.

The open circuit voltage remains constant when the mobility is changed, just like the charge per cycle. This is a direct consequence of the fact that the mobility sets the time scale at which carrier motion takes place, but has no effect when the other time scales in the system —in this case the driving frequency f— are scaled accordingly [4]. Another consequence of this scaling of time scales with mobility is that the charge per cycle versus frequency curve $Q(f)$ shifts linearly with mobility, but doesn't change shape or height. In Chapter 4 it was already shown that $f_I \sim \mu$. Hence, the current $I_{SD} = Q(f)f$ scales linearly with mobility. Modeling results (not shown) confirm that indeed $I_{SD} \sim \mu$ [2,6].

The charge displacement efficiency and power efficiency at f_I (solid lines) and f_Q (dashed lines) versus L^{-1} corresponding to the devices in Figures 5.2–4 are displayed in Figure 5.5. For ratchets with constant asymmetry, the charge displacement (a) and power efficiencies (b) at f_I show a small increase for increasing L. When looking at ratchets with varying asymmetry (L0.5–yP∞) a maximum in charge displacement efficiency is reached for the L0.5–5P∞ ratchet and in power efficiency for the L0.5–4P∞ ratchet. The charge displacement and power efficiencies for ratchets operating at f_Q are larger than those at f_I and show a sharper increase with increasing repeat unit length. These particular devices show respectable efficiencies as charge pumps, i.e. 3 to 17% of all charge motion is directed. Unfortunately, the associated power efficiencies lay below 0.5%. The relation between charge displacement and power efficiency will be discussed below. At the end of this chapter it will be shown that in particular the power efficiency can be significantly enhanced.
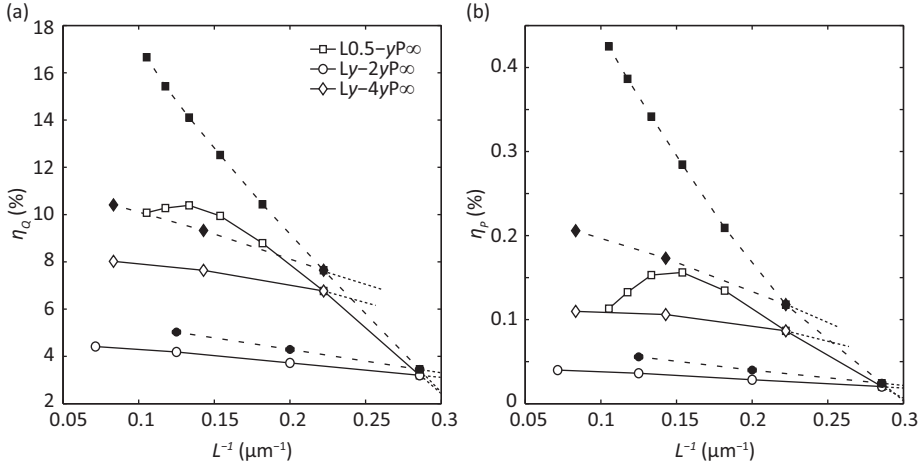
Figure 5.5 | Calculated charge displacement efficiency η_Q **(a)** and power efficiency η_p **(b)** versus L^{-1} for ratchets with constant (Ly–2yP∞, Ly–4yP∞) and varying (L0.5–yP∞) asymmetry at f_I (solid lines) and f_Q (dashed lines). Modeling settings are: $\mu = 10^{-6}$ m^2/Vs, $V_G = -20$ V, $V_A = 8$ V, $V_O = -7$ V, $\phi = 180°$, $V_{SD} = 0$ V (only for (a)).

Combining the data from Figures 5.2–5 shows in general an increase in current for smaller ratchets at the cost of a decrease in the charge displacement and power efficiencies. In order to achieve higher currents without losing efficiency the mobility should therefore be increased, which comes at the cost of an increased operating frequency. In practice this requires the use of higher mobility materials than the pentacene used here. This scaling relies, as discussed above, on the fact that the charge per cycle versus frequency curve only shifts with mobility without changing shape. Implicitly, we have also made use of the fact that the frequency at which the charge per cycle maximum is reached is almost equal to the frequency at the maximum in charge displacement efficiency.

When all parameters are optimized and the charge displacement efficiency at $V_{tilt} = 0$ V is known, the power efficiency can be estimated quite accurately. The power efficiency is defined as $\eta_p = \langle P_{out} \rangle / \langle P_{in} \rangle$, which equals $\eta_p = I_{DC}^2 R / \langle I_{AC}^2 R' \rangle$. The latter term $\langle I_{AC}^2 R' \rangle$ consists of local time–varying currents I_{AC} and local time–varying resistances R', summed over space and time. The current I_{DC} is the current at the maximum power point. For the infinitely long ratchets that are modeled this is half the current at short circuit (Figure 5.2a). Substituting $I = Q / \Delta t$, the power efficiency becomes $\eta_p = Q_{SC}^2 R / 4 \langle Q_{AC}^2 R' \rangle$.

When it is assumed that the channel resistance is constant and homogeneously distributed over the channel, $R' = R$ and $\eta_p = Q_{SC}^2 / 4 \langle Q_{AC}^2 \rangle = \eta_q^2 / 4$. This back–of–the–envelope

estimation turns out to be correct within a factor 2 for the modeling results of the charge displacement and power efficiencies shown in Figure 5.5. However, when all parameters —i.e. V_G, V_A, V_O, f, ϕ — are optimized the estimate is correct within a few percent.

5.3   Amplitude–offset

The influence of amplitude V_A and offset V_O on the current is investigated in Figure 5.6, where a calculated current contour plot for an L1–4P∞ ratchet (a) is compared to the same plot as measured for an L1–4P2 ratchet (b). As the frequency is kept constant in these plots, the current contour plots also resemble the shape of the charge per cycle contour plot. The modeled and measured plots are very similar in shape. For both plots, no (change in) current is observed for $V_O \geq V_{TH}$. In this offset region (I), DC currents are blocked since the accumulation layer is locally depleted, as the applied potential on AF1 is continuously higher than the threshold voltage V_{TH}. Note that for the model the threshold voltage is 0 V.

The region of significant current transport (II) has a triangular shape, and is enclosed by the lines $V_O = V_{TH}$ and $V_A = |V_O - V_{TH}|$. In region (II) the channel above the asymmetric finger electrodes AF1 is temporarily forced into depletion during the oscillation period,

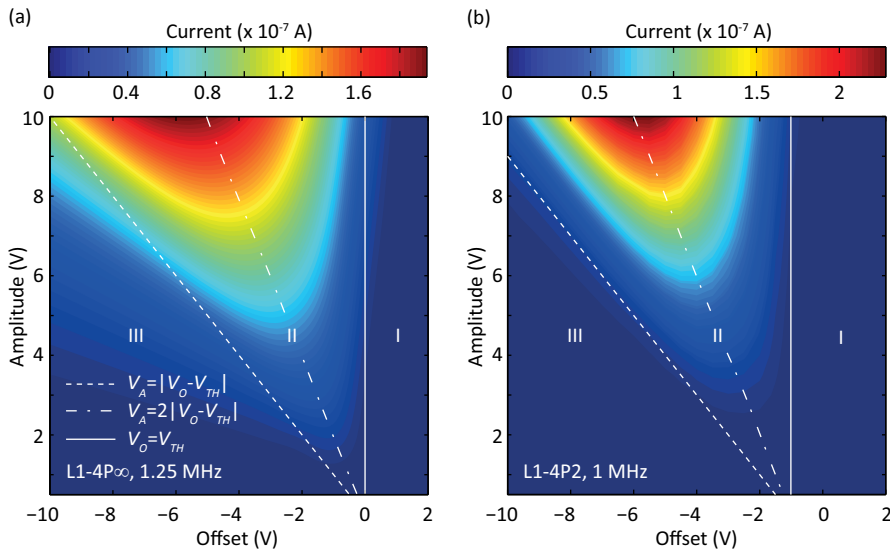**Figure 5.6 |** Contour plot of current as a function of the applied amplitude V_A and offset V_O for a modeled L1–4P∞ ratchet **(a)** and a measured L1–4P2 ratchet **(b)**. Modeling settings for (a) are: $\mu = 10^{-6}$ m²/Vs, $V_G = -20$ V, $f = 1.25$ MHz, $\phi = 180°$, and $V_{SD} = 0$ V. Measurement settings for (b) are: $V_G - V_{TH} = -20$ V, $f = 1$ MHz, $\phi = 180°$, and $V_{SD} = 0$ V.

which increases the current drastically for unknown reasons. The panels in Figure 5.6 are typical results for ratchets with an integer number of finger pairs (Lx–yPa with a an integer) and for the modeled infinitely long ratchets for different asymmetries and frequencies. As a rule of thumb the optimum offset–amplitude ratio for current transport for these ratchets is 1:2, indicated by the dashed–dotted lines.

In region (III) (where $V_A \leq |V_O - V_{TH}|$) the current transport seems negligible. However, in this region the non–linear behavior of these ratchets becomes clear once more. When the current as a function of amplitude for constant offset values is modeled, current reversals appear in the region where $V_A < |V_O - V_{TH}|$ as shown in Figure A2.1. The modeled current changes linearly with the amplitude in the region where $V_A > |V_O - V_{TH}|$ (Figure A2.1). These current reversals cannot be seen in the measured current contour plots due to the used amplitude step size (0.5 V) and the low current values which are in the order of the background noise. Ratchets with a non–integer number of finger pairs (Lx–yPa.5) do show rather different current–offset–amplitude relations, shown in Chapter 3, including current reversals that are not reproduced in the simulations of infinite ratchets. These current reversals are attributed to the presence of the source–drain contacts and the associated additional asymmetries, and will be further discussed in Chapter 6.

5.4   Gate voltage–frequency

In Figure 5.7a, the calculated charge per cycle as a function of the gate potential and frequency is shown for an L1–4P∞ ratchet. A maximum in the charge per cycle is obtained for $V_G \approx -4$ V, in contrast to the current maximum (see Figure 4.3 and 4.5). Measurement results also indicate that the maximum charge per cycle is reached for relatively low gate voltages. In Figure 5.7b, a measurement result is shown for an L1–4P8 ratchet. The shape of the figure is in qualitative agreement with the modeling results. The frequency for which the maximum charge per cycle is reached differs by about a factor 5 between the measurement and modeling results, which is due to a difference in mobility of about a factor 5. The scaling of the frequency at which the current reaches a maximum with gate voltage is discussed in Chapter 4. Note that the (red) region of high charge per cycle in the left–bottom corner of panel (b) is due to the presence of contacts as will be shown in Chapter 6.
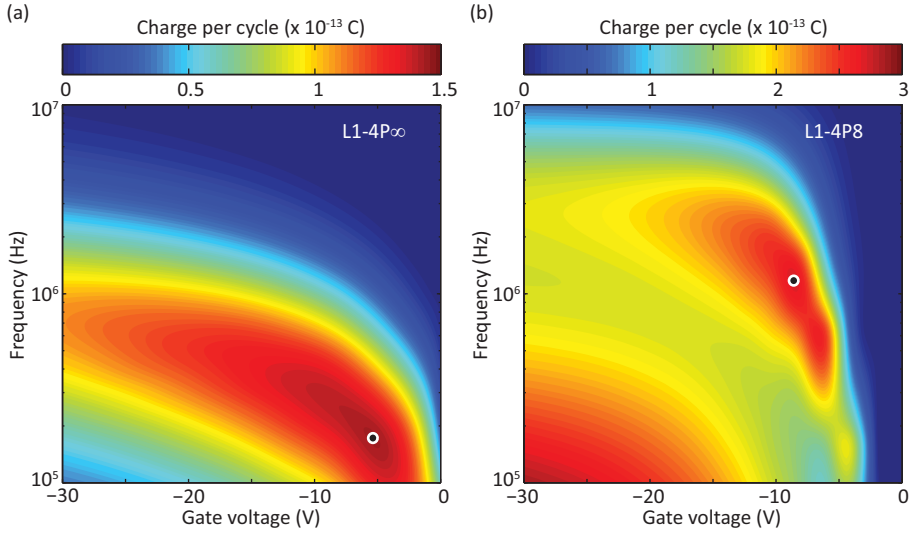
Figure 5.7 | Contour plot of charge per cycle as a function of frequency f and gate voltage V_G for a modeled L1–4P∞ ratchet **(a)** and a measured L1–4P8 ratchet **(b)**. Modeling settings for (a) are: $\mu = 10^{-6}$ m²/Vs, $V_A = 8$ V, $V_O = -7$ V, $\phi = 180°$, and $V_{SD} = 0$ V. Measurement settings for (b) are: $V_A = 8$ V, $V_O = -7$ V, $\phi = 180°$, and $V_{SD} = 0$ V.

5.5   Phase–frequency

All measurements and simulations discussed so far were performed with the applied potentials V_{AF1} and V_{AF2} in anti–phase with each other. In this section it is shown how the current changes for different frequency f and phase ϕ. In Figure 5.8 a contour plot of the current as a function of frequency and phase is shown for an L1–8P∞ ratchet (a) and an L1–8P8 ratchet (b). Again the modeling and measurement results are very similar; the apparent shift along the frequency axis is due to the mobility difference mentioned in the previous paragraph. When the phase is varied between 0° and 360° two current reversals occur as anticipated. However, both in experiment and model, the current minimum is smaller in magnitude than the current maximum, and occurs at a lower frequency. Also the phase difference between the current minimum and maximum is approximately, but not exactly 180°. These effects are direct consequences of the fact that changing the phase by 180° does not completely invert the potential; this requires the additional transformation $V_A \rightarrow -V_A$. Changing both $V_A \rightarrow -V_A$ and $\phi \rightarrow \phi + 180°$ also completely inverts the experimental Lx–yPa ratchets; an Lx–yPa.5 ratchet cannot be inverted.

The optimum phase difference for current transport is approximately 215°, i.e. 35° higher than the standard 180° we used.
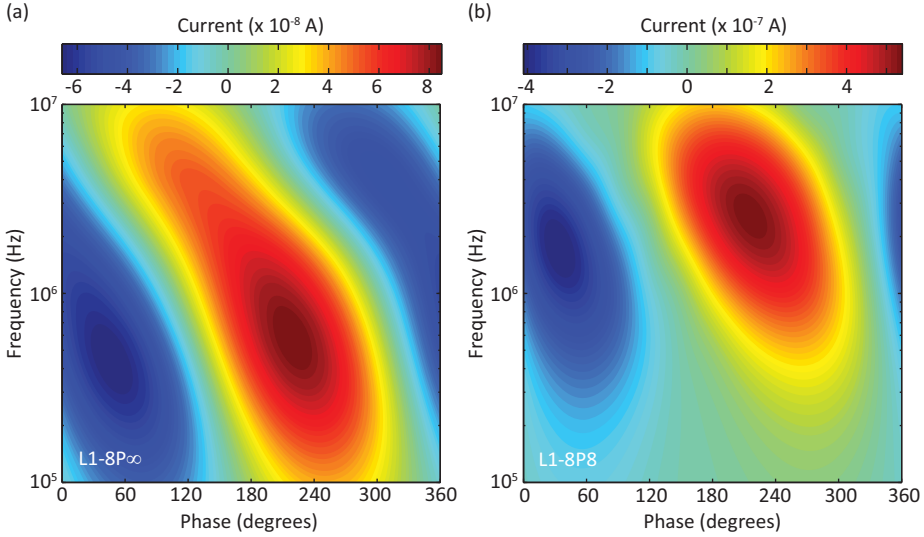
Figure 5.8 | Contour plot of the current as a function of frequency f and phase ϕ for a modeled L1–8P∞ ratchet **(a)** and a measured L1–8P8 ratchet **(b)**. Modeling settings for (a) are: $\mu = 10^{-6}$ m²/Vs, $V_G = -20$ V, $V_A = 8$ V, $V_O = -7$ V, and $V_{SD} = 0$ V. Measurement settings for (b) are: $V_G - V_{TH} = -20$ V, $V_A = 8$ V, $V_O = -7$ V, and $V_{SD} = 0$ V.

5.6 Optimization of the charge displacement and power efficiencies

So far, the influence of length scale L, mobility μ, amplitude V_A, offset V_O, gate voltage V_G, and phase ϕ on the current transport and on the charge displacement and power efficiencies were investigated and, where possible, rationalized. In this section all results are combined to optimize the efficiency of the ratchets. An L1–8P∞ ratchet is chosen since the 1:8 ratio gives the optimal power efficiency, as shown in Figure 5.5b. A realistic amplitude of 10 V is chosen with, according to the rule of thumb introduced in the discussion of Figure 5.6, a matching offset of –5 V. A gate voltage of –4 V is applied, close to the charge per cycle maximum (Figure 5.7). In Figure 5.9, contour plots of the charge per cycle (a) and charge displacement efficiency (b) are shown as a function of frequency and phase. For the chosen parameters a charge displacement efficiency of more than 49% is obtained. The maximum power efficiency when a load is applied to the ratchet is calculated to be 6.9%. The fraction of moved particles γ_t is calculated at about 11% for this optimized ratchet. There is a large gap with the charge displacement efficiency of 49% which indicates that a large fraction of charges does not contribute to the charge transport. Nevertheless, there is only a 5 percentage points difference with the 16% estimated for the flashing ratchet [4]. The latter value is an estimate for the fraction
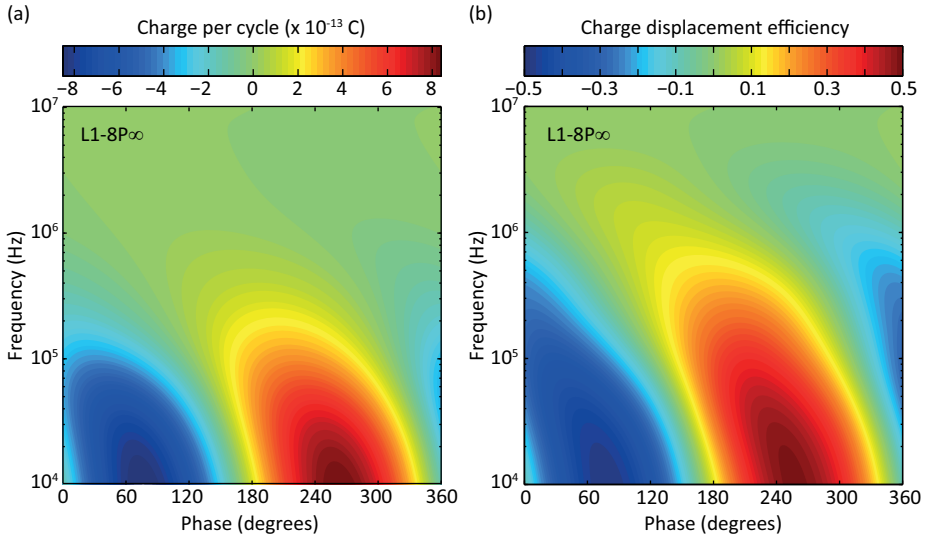
Figure 5.9 | Calculated contour plots of charge per cycle **(a)** and charge displacement efficiency η_Q **(b)** as a function of frequency f and phase ϕ for an L1–8P∞ ratchet. Modeling settings are: $\mu = 10^{-6}$ m^2/Vs, $V_G = -4$ V, $V_A = 10$ V, $V_O = -5$ V, and $V_{SD} = 0$ V.

of moved non–interacting particles in an optimized device. Also, the organic electronic ratchets are operated in a quasi–flashing mode, applying a sinusoidal potential to the finger electrodes instead of turning a potential on and off.

It must be noted that the definition of the power efficiency comes close to the actual system efficiency which is the output power divided by the power put into the system by charging the finger electrodes. Currently incorporated in the power efficiency calculation is the energy transfer between the finger electrodes and the accumulation layer. However, the coupling of the finger electrodes to the bottom gate contact is currently ignored. Although no quantitative estimate of the losses associated with this coupling has been made, they might be substantial in the current ratchet design due to the large carrier mobility of the highly p–doped silicon gate substrate. These losses are however of technical nature; changing the design of the structures could highly reduce these losses, e.g. in ratchets with bottom gate, top finger electrode configuration the accumulation layer screens the oscillating finger potentials from the gate, decoupling the gate and finger electrodes. The calculated power efficiency is than (almost) equal to the actual system efficiency.

5.7   Summary

The performance of electronic ratchets is investigated by numerical modeling and measurements results. It is shown how the characteristic parameters of the time–varying asymmetric potential like length scales and amplitude, as well as the charge carrier density and mobility influence the performance. For ratchets with a constant asymmetry but changing length, the current increases when going to smaller length scales but the net charge displaced per cycle, as well as the power and charge displacement efficiencies decrease. To optimize the power efficiency for a given geometry, (voltage) settings need to be chosen such that the charge displaced per oscillation cycle reaches a maximum, rather than near the current maximum. To increase the current while preserving the power efficiency, the mobility of the semiconductor must be increased. Accordingly, the operating frequency must be increased proportionally. When all settings are brought close to optimum a ratchet with a charge displacement efficiency of over 49% is found and with a power efficiency of approximately 6.9%.

It should be noted that when the typical length scale L of the ratchets is reduced to the sub–micrometer regime, diffusion of particles will start to play an important role. Extension of the above results to these length scales is not straightforward. At even smaller length scales also quantum effects will become important [2,7].

5.8   References

[1]   Roeling, E. M. *et al.* Organic electronic ratchets doing work. *Nat Mater* **10**, 51–55, (2011).

[2]   Reimann, P. Brownian motors: noisy transport far from equilibrium. *Physics Reports–Review Section of Physics Letters* **361**, 57–265, (2002).

[3]   Hänggi, P. & Marchesoni, F. Artificial Brownian motors: Controlling transport on the nanoscale. *Rev Mod Phys* **81**, 387–442, (2009).

[4]   Linke, H., Downton, M. T. & Zuckermann, M. J. Performance characteristics of Brownian motors. *Chaos* **15**, 026111, (2005).

[5]   Derenyi, I., Bier, M. & Astumian, R. D. Generalized efficiency and its application to microscopic engines. *Phys Rev Lett* **83**, 903–906, (1999).

[6]   Scheinert, S. & Paasch, G. Fabrication and analysis of polymer field–effect transistors. *Phys Status Solidi A* **201**, 1263–1301, (2004).

[7]   Linke, H. *et al.* Experimental tunneling ratchets. *Science* **286**, 2314–2317, (1999).

Chapter 6

Finite size effects on organic electronic ratchets

Random motion of particles can be rectified by ratchet potentials which are asymmetric potentials repeated in space. In this chapter, the effects of the finite size of the ratchets on the performance of organic electronic ratchets are investigated. These ratchets are modified organic field effect transistors, where inside the gate dielectric asymmetrically spaced interdigitated finger electrodes are placed. Oscillating potentials applied to these finger electrodes drive the system out of equilibrium, resulting in a current flowing between source and drain contacts, even with zero source–drain bias. Measurements show that the presence of source–drain contacts alters the ratchet behavior. Hence, not only the length and asymmetry of the repeat unit of the ratchet potential, but also the way it is terminated by the contacts and the total system length are of crucial importance. These effects are further investigated using drift–(diffusion) models in which source and drain contacts are explicitly included to account for finite size effects. It is shown that the open circuit voltage saturates with increasing device length due to the contacts. Calculations univocally confirm that the measured current reversals in ratchets with a non–integer number of electrode pairs are related to the reduced symmetry of these devices. These reversals are related to diffusive transport. Furthermore, the influence of the dimensionality of charge transport, the density dependent mobility and the balance between drift and diffusion are investigated and mainly found to quantitatively affect the behavior at (lower) frequencies where diffusion is important.

6.1   Introduction

Uncorrelated motion of particles can be rectified by the use of so–called ratchets, where particles are subjected to an asymmetric potential which is repeated in space. Operating out of equilibrium where the second law of thermodynamics no longer applies, these systems are known for intriguing effects such as current reversals [1–3]. In Figure 6.1a the flashing ratchet, which is closely related to the system investigated further on in this work, is explained. Particles are trapped inside an asymmetric potential well. When the potential is turned off, particles spread due to diffusion and, in the case of charged particles, due to drift. Turning the potential on again traps particles in the in energy nearest potential minimum. Since this is not necessarily the spatially nearest minimum, a net particle displacement may result.

Ratchets have been intensively studied in theory [2]. Experimentally, the ratchet concept has been realized in a variety of systems [1], such as granular media [4], bipedal motors [5], liquid cells [6], Leidenfrost droplets [7], and motile cells [8]. So far, ratchet driven charge transport has been studied in tunneling ratchets [9–11] and in the organic electronic ratchets introduced in this thesis [3,12]. Here, we focus on ratchets transporting electronic charges. An interesting characteristic of this category of ratchet devices is that in order to probe their functionality, almost unavoidably, electrical contacts have to be introduced to the system. Hence, in order to probe the system, it has to be changed. In particular, it must have a finite size and the periodicity has to be terminated, which can be done in various ways. In this work we address these finite–size effects on the functionality of organic electronic ratchets that have been introduced in the preceding chapters. We will show that periodicity and symmetry breaking lead to non–trivial deviations from the behavior of an infinite device. Moreover, the differences in characteristics of systems in which charges can move in one and two dimensions will be addressed. Finally, the influence of 'particularities' related to the disordered organic semiconductor that is used is addressed and shown to be large at low frequencies where diffusion is important.

The investigated organic electronic ratchets were shown before to generate enough power to drive even low–end logic circuitry and to function by the grace of particle–particle interactions [3]. The system may therefore be regarded as a relevant step towards application of ratchets in actual devices. It consists of a modified organic field effect transistor (OFET) where source (S) and drain (D) contacts are separated from the silicon (Si) gate contact by the silicon dioxide (SiO_2) gate dielectric. Inside the gate dielectric asymmetrically spaced interdigitated finger electrodes are placed, denoted by AF1 and AF2 (Figure 6.1b). The width of these electrodes is 1 μm. Alternating potentials placed

on the finger electrodes AF1 and AF2 mimic the principle of the flashing ratchet. In these devices, a current can flow between the source and drain contact with zero source–drain bias $(V_{SD} = 0 \text{ V})$ [3]. The applied potentials in so–called forward drive are described by $V_{AF1}(t) = V_O + (V_A/2)(1 + \sin(\omega t))$ and $V_{AF2}(t) = V_O - (V_A/2)(1 + \sin(\omega t))$. In reverse drive the potentials applied on AF1 and AF2 are exchanged. V_O is a central offset voltage and V_A is the peak–peak amplitude of each signal. Both are set with respect to the grounded source contact. Furthermore, ω is the angular frequency with the frequency f given by $(f = \omega/2\pi)$ and t is the time.

The ratchets differ in length and asymmetry, which is reflected in the notation. An Lx–yPa ratchet has an asymmetry of x to y, where x and y are respectively the short and long distance in micrometers between the interdigitated finger electrodes from AF1 and AF2. Pa is the number of pairs of finger electrodes that is present in the device. Note that in the notation, L stands for length and P stands for pairs. In some cases there is a non–integer number of pairs of finger electrodes, in which case AF1 has one extra finger as compared to AF2; e.g. Figure 6.1b depicts an L1–2P2.5 ratchet.

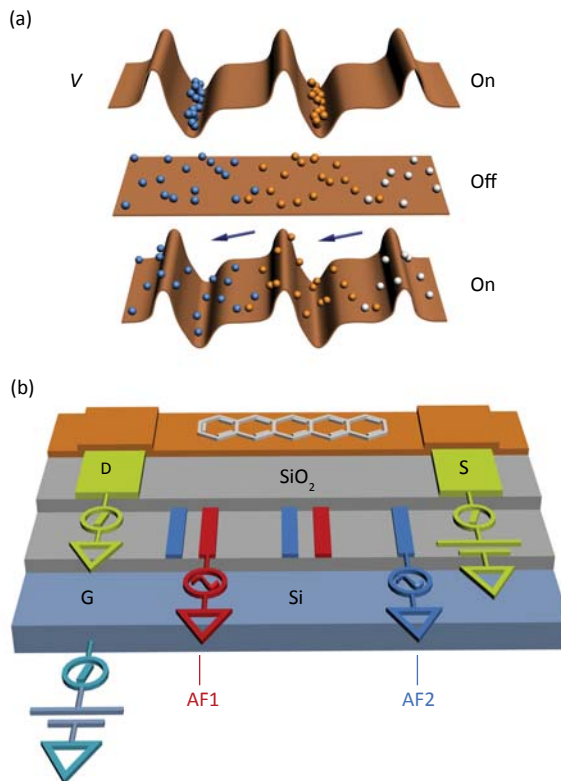**Figure 6.1 | (a)** Flashing ratchet mechanism. **(b)** Drawing of an L1–2P2.5 organic electronic ratchet. The source (S) and drain (D) contacts are separated from the silicon (Si) gate (G) contact by the silicon dioxide (SiO$_2$) gate dielectric. Asymmetrically spaced interdigitated finger electrodes AF1 and AF2 are placed half way the gate dielectric. Pentacene is used as a semiconductor (layer with structural formula on top).

Throughout this thesis experimental results are combined with calculations to unravel the properties of organic electronic ratchets. So far, in the calculations infinitely long ratchets have been simulated in a transistor–like geometry that is similar to the device shown in Figure 6.1b. Current transport has been treated as purely one–dimensional (1D). This choice is motivated by the fact that in OFETs charge transport takes place in a thin accumulation layer right above the dielectric–semiconductor interface [13–14], although the actual semiconducting layer is 50 nm thick. Furthermore, effects related to the disorder–broadened density of states of the organic semiconductor are disregarded from the model. Despite these simplifications the numerical model describes the behavior of the actual ratchet devices strikingly well in the high frequency regime (10^5–10^7 Hz), as was shown in Chapters 3–5. However, in its current state the model lacks the ability to describe effects which are observed in the experiments and that can be related to the presence of the source and drain contacts. For instance, ratchets with a non–integer number of electrode pairs show current reversals which are absent in ratchets with an integer number of pairs [3]. These effects are often, but not always, occurring at lower frequencies than modeled so far.

In the following sections the influence of source and drain contacts on the charge transport is investigated by comparing modeling results with experimental results. The drift–diffusion model used in Chapters 3–5 is extended to include ohmic contacts and 2D charge transport, see also Chapter 2. Due to computational constraints the grid cells in the horizontal direction are taken to be 250 nm long instead of 62.5 nm used when modeling infinitely long 1D ratchet devices.

6.2   Contact role in electronic ratchets

In Figure 6.2a the modeled current as a function of frequency is shown for an L1–2P2 and L1–2P2.5 ratchet operated in forward (F) and reversed (R) drive, together with the modeling result obtained for an L1–2P∞ ratchet. The color indicates the current sign, with red meaning positive and blue meaning negative currents. The modeling results for the infinitely long ratchet show an increase in current with increasing frequency, reaching a maximum around 2.2 MHz after which the current decreases again. This same trend is observed for the L1–2P2 ratchet in forward drive, where a maximum in current is reached at slightly higher frequency (2.7 MHz). The currents are however higher and the increase in current with increasing frequency is less steep. Note that as the finger pattern of the L1–2P2 ratchet is mirror symmetric, the simulation result for

the ratchet operating in reversed drive is identical to the forward drive except for a sign change in current.

The modeling results obtained for the L1–2P2.5 ratchet operated in forward drive are similar as for the L1–2P2 ratchet, albeit that the current is lower. Interestingly, current reversals appear when the L1–2P2.5 ratchet is operated in reversed drive. With the applied modeling settings, the current changes sign twice in the frequency range between 10^4 and 10^7 Hz. A global (negative) maximum is reached at 3.6 MHz, the same frequency as where the maximum current is reached when operating the ratchet in forward drive. These modeling results show that the presence of source and drain contacts qualitatively alter the charge transport behavior which is in agreement with experimental results.

In Figure 6.2b the experimental current as a function of frequency is shown for the L1–2P2 and L1–2P2.5 ratchets operated in forward drive. Like in the simulations, current reversals are present in the current–frequency curve of the L1–2P2.5 device and absent in that of the L1–2P2 device. However, when simulating the L1–2P2.5 ratchets the current reversals are observed in reversed drive, whereas they are experimentally observed in forward drive (see also Figure 3.4).

Also shown in Figure 6.2b is the measured current as a function of frequency for an L1–2P32 ratchet, which is the ratchet configuration that matches most closely with the infinitely long L1–2P∞ ratchet shown in Figure 6.2a because of the large number of pairs of finger electrodes. The measured current versus frequency curve of the L1–2P32 ratchet is very similar to those found for both the experimental and the modeled L1–2P2 ratchet and to the modeled L1–2P∞ ratchet. This can be explained by the symmetry of these asymmetric devices; the finger pattern of ratchets with an integer number of electrode pairs like the L1–2P2 and L1–2P32 ratchets is mirror symmetric, like that of the (modeled) infinitely long ratchets. Differences between experiment and calculation can however be found. These differences are especially visible at lower frequencies (10^4–10^5 Hz) in the charge per cycle–frequency relationship. Below, they will be shown to be caused by the presence of source and drain contacts. The charge per cycle is the net amount of charge moved in $t = f^{-1}$ s, and is found by dividing the current $I(f)$ by the corresponding frequency f. In Figure 6.2 the modeled (c) and measured (d) charge per cycle are shown as a function of frequency for the L1–2P2, L1–2P2.5, L1–2P∞ (c–only) and L1–2P32 (d–only) ratchets. For all modeled ratchets a global maximum in the

absolute charge per cycle is observed at frequencies around 1 MHz. When decreasing the frequency, a reduction in charge per cycle is observed. The measurement results show a local maximum in the absolute charge per cycle at these high frequencies and the measured charge per cycle stays rather constant or even increases for decreasing frequency (see also Figure 3.4).
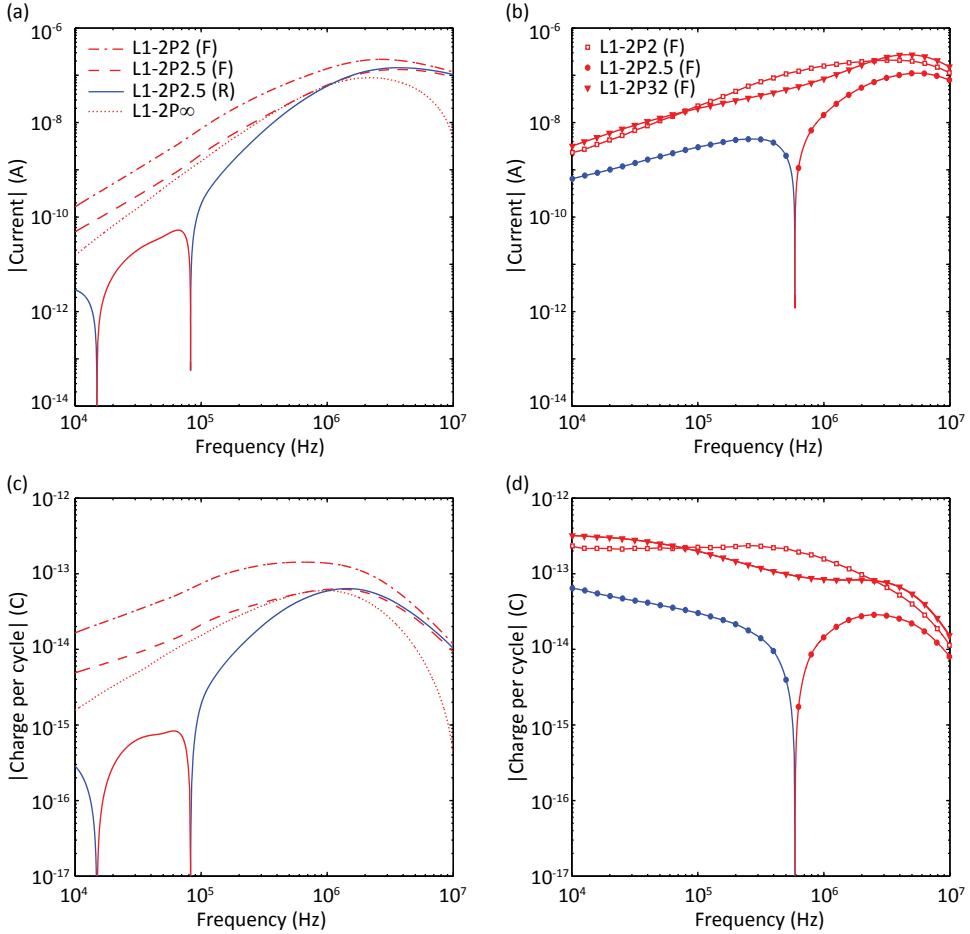
Figure 6.2 | Modeled current **(a)** and charge per cycle **(c)** versus frequency for an L1–2P2 and an L1–2P2.5 ratchet in forward (F) and reversed (R) drive and for an L1–2P∞ ratchet. 1D charge transport is assumed. Further modeling settings are: $V_O = -7$ V, $V_A = 8$ V, $V_G = -20$ V and $\mu = 10^{-6}$ m²/Vs, with V_G the gate voltage and μ the mobility. The measured current and charge per cycle for an L1–2P2, L1–2P2.5 and L1–2P32 ratchet operated in forward drive are shown in panels **(b)** and **(d)**, respectively. Measurement settings are: $V_O = -7$ V, $V_A = 8$ V and $V_G - V_{TH} = -20$ V, with V_{TH} the threshold voltage. The color indicates the current sign; red is positive and blue is negative.

In general, measurement results from ratchets with different asymmetry and channel length all show the behavior described in the previous paragraphs as is shown in Appendix III. Ratchets with an integer number of electrode pairs show two maxima in contour plots of the charge per cycle versus offset and frequency; a high–frequency maximum around 1 MHz, and a maximum at frequencies around and below 100 kHz. Ratchets with a non–integer number of electrode pairs show regions of positive and negative charge per cycle, with a (positive) maximum found at approximately the same location as the high–frequency maximum found for ratchets with an integer number of pairs of finger electrodes.

From the measurement results shown in Appendix III it can be concluded that the charge per cycle maximum (and current maximum) observed in the high–frequency region ($\sim 10^6$ Hz) is related to the asymmetry and length L of the repeat unit of the ratchet potential: its position is virtually independent of the number of repeat units and the gap b between the source and drain electrodes and the nearest finger (Figure 2.1). In contrast, it does critically depend on L. The latter observation is consistent with the analysis of the scaling of the position of the high–frequency maximum with L as presented in Figure 4.7. For the maximum at lower frequencies the reverse holds: it shifts to lower frequencies with increasing number of repeat units and with increasing b, see Figure A3.4. These observations indicate that the low–frequency maximum is related to overall length of the device cl (i.e. the channel length). However, its position also depends on the asymmetry of the repeat unit, and no monotonic relation between cl and its position exists. Therefore, the low frequency maximum reflects an interplay between the asymmetric ratchet repeat unit and the termination of the periodicity by the contacts.

The occurrence of positive and negative (local) maxima in the charge per cycle versus frequency curves is related to the way the contacts break the spatial periodicity. As long as the geometric finger electrode pattern remains mirror symmetric, i.e. for L1–yPa ratchets, no current reversals are found as a function of frequency. In absence of mirror symmetry, i.e. for L1–yPa.5 ratchets, current reversals occur and do so in the (lower) frequency regime that is affected by both the short and long characteristic length scales of the device.

Although current reversals are observed in the modeling results, they are found at the opposite drive (i.e. reversed instead of forward). The modeling results furthermore show

no local maximum in charge per cycle at lower frequency for the L1–2P2 ratchet. So far, several characteristics from the experimental devices were omitted from the drift–diffusion model: the two–dimensional charge transport in the semiconducting layer, and two effects related to the disorder–broadened density of states, namely the density dependence of the mobility and the larger role of diffusion than expected from the classical Einstein relation. Furthermore, the role of drift and of diffusion in the finite ratchet modeling results was not yet addressed. In the next sections these effects are investigated.

6.2.1 Drift and diffusion influence

In Chapter 3 it was shown that the role of diffusion is negligible at high frequencies, i.e. where the maximum in current is reached. In Figure 6.3, modeling results are shown for current and charge per cycle for the L1–2P2 and L1–2P2.5 ratchet. The color again indicates the current sign, with red meaning positive and blue meaning negative currents. The L1–2P2 ratchet is operated in forward drive (a–b) and the L1–2P2.5 ratchet is operated in forward (c–d) and reversed (e–f) drive. When comparing the (1D) drift–only results (dotted lines, obtained by omitting the diffusion term in Equation 2.1) with the (1D) drift–diffusion (solid lines) results it becomes clear that the role of diffusion is no longer negligible, especially for the L1–2P2.5 ratchet operated in reversed drive. The current reversals observed in the drift–diffusion calculation are no longer present in the drift–only calculation. Furthermore an increase in charge per cycle is observed at lower frequencies. For the L1–2P2 and L1–2P2.5 ratchets operated in forward drive the differences between drift–only and drift–diffusion calculations are mainly quantitative, but still with higher current and charge per cycle values at lower frequencies for the drift–only calculations. Hence, the current reversals must be related to an interplay between diffusion and drift of particles in which the broken symmetry at the contacts plays a role. The exact mechanism is unknown.

6.2.2 Two–dimensional charge transport

Until now, charge transport in the organic semiconducting layer was assumed to be 1D. Charge movement in the normal direction was neglected, as charge is accumulated in a thin layer right above the semiconductor–gate dielectric interface. In the actual devices the pentacene layer is 50 nm thick. The potentials applied to the asymmetric finger electrodes vary in time, continuously moving charge from or to the finger electrodes, and might do so in both the longitudinal and normal directions. Charge transport in the vertical direction might therefore play a bigger role than assumed so far.
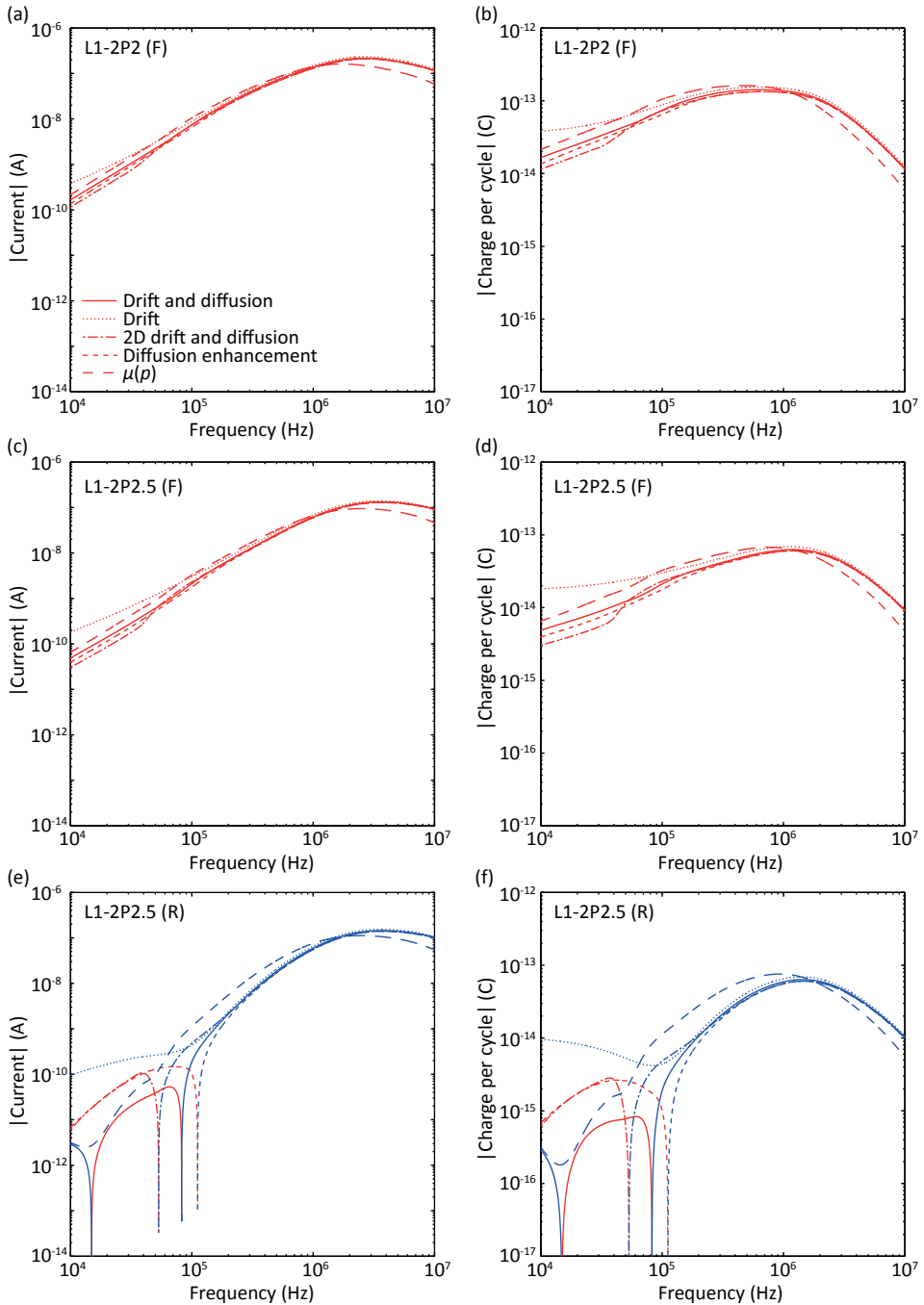
Figure 6.3 | Respectively, the modeled current and charge per cycle for an L1–2P2 ratchet operated in forward drive **(a)** and **(b)**, an L1–2P2.5 ratchet operated in forward drive **(c)** and **(d)**, and an L1–2P2.5 ratchet operated in reversed drive **(e)** and **(f)**. Modeling results are shown for a variety of simulations, i.e. 1D drift and diffusion, 1D drift–only, 2D drift and diffusion, 1D drift and diffusion with density dependent mobility $\mu(p)$, and 1D drift and diffusion with diffusion enhancement. The color indicates the current sign, with red indicating positive and blue indicating negative currents. General modeling settings are: $V_O = -7$ V, $V_A = 8$ V, $V_G = -20$ V and $\mu = 10^{-6}$ m²/Vs (except for $\mu(p)$).

Like in the preceding section, source and drain contacts are included in the calculation as are drift and diffusion. The semiconducting layer in the model is 50 nm thick, divided over 6 grid cells with thicknesses of 3, 5, 7, 10, 10 and 15 nm, starting at the gate dielectric. In previous 1D calculations the semiconducting layer was always assumed to be 3 nm thick. The 2D calculation results are shown in Figure 6.3 as dash–dotted lines. They agree qualitatively with the results obtained with 1D charge transport, again showing current reversals for ratchets with a non–integer number of electrode pairs and none for integer numbers of pairs. Quantitative differences are found at frequencies below 200 kHz. The location of the current reversals is shifted to lower frequencies (c–d). For frequencies between 10 kHz and 200 kHz the modeled current values for the 2D L1–2P2.5 and L1–2P2 ratchets show respectively an increase (c–d) and decrease (a–b) as compared to 1D charge transport. At frequencies above 200 kHz no quantitative differences are observed when comparing 1D and 2D charge transport. Interestingly, these are also the frequencies at which diffusion starts to become relevant (See also Figure 3.2). In equilibrium, the vertical carrier distribution is the result of balanced drift and diffusion forces. Hence, it may be expected that the time scale at which this distribution can respond to a perturbation is set by the slowest of the two processes, i.e. diffusion. This is confirmed by a comparison of 1D and 2D drift–only calculations for an L1–2P2 ratchet which are indeed found to be identical (not shown).

6.2.3   Density dependent mobility

Also investigated is the influence of the density dependent mobility $\mu(p)$ that results from the disorder–broadened density of states. The results are shown in Figure 6.3 as long–dashed lines. The charge transport is again assumed to be 1D and both drift and diffusion are taken into account. Assuming an exponential density of states the mobility follows $\mu(p) \sim \delta^{T_0/T-1}$, with δ the carrier occupation, T the temperature of the system and T_0 a parameter indicating the width of the exponential distribution [15]. In the model, the factor $T_0/T - 1$ is set at 0.5, which is reasonable for pentacene [15]. Qualitative differences are found for the L1–2P2.5 ratchet operated in reversed drive (c–d). Surprisingly, the current reversals found in the (1D) drift–diffusion simulation with a constant mobility vanish when including the density dependence. The underlying cause for the disappearance of the current reversal is unclear, also because the balance between drift and diffusion is not altered by the density dependent mobility as the Einstein relation is maintained —see also the next section. For the L1–2P2 (a–b) and L1–2P2.5 (c–d) ratchets operated in forward drive only quantitative differences are observed.

6.2.4   Diffusion enhancement

The shape of the density of states of the organic semiconductor also influences the balance between drift and diffusion [16]. For an exponential density of states in the low density regime, diffusion is enhanced by a factor T_0/T over the value obtained from the conventional Einstein relation (Equation 2.5) [17]. In Figure 6.3 results are shown for 1D calculations in which the diffusion coefficient is enlarged by a factor 1.5, see short–dashed lines. A constant mobility is assumed. For the L1–2P2 (a–b) and L1–2P2.5 (c–d) ratchets operated in forward drive the current is decreased. However for the L1–2P2.5 (e–f) ratchet operated in reversed drive an increase in current is observed at lower frequencies. Furthermore the location of the current reversal is shifted to a higher frequency. Apparently there is no clear cut relation between the balance between drift and diffusion and the magnitude of the net current, as might have been expected from the fact that the current in the drift–only calculations systematically lays above the current in the drift–diffusion calculations in which the conventional Einstein relation is used —see above.

6.2.5   Complete 2D calculation

In Figure 6.4 modeling results are shown for an L1–2P2 and L1–2P2.5 ratchet, taking into account all the above described effects. Charge transport is regarded as 2D. A density dependent mobility is taken into account and diffusion is enhanced by a factor 1.5. Although no current reversals were observed when only taking into account the density dependence of the mobility, a current reversal is still observed when taking into account all effects (L1–2P2.5 (R)). No major differences are observed for the L1–2P2 and L1–2P2.5 ratchet operated in forward drive compared to previous calculation results.

Summarizing the above, it has become clear that the organic electronic ratchets in this thesis may be regarded as Brownian motors when operated at frequencies below, roughly, 100 kHz. Interestingly these are also the frequencies at which the devices reach their maximum efficiency, see also chapter 5. Also, the current reversals observed in the finite devices of the lowest symmetry are inherently related to the interplay between the various asymmetries, drift and diffusion, but their occurrence is not particularly sensitive to the details of the calculation.

The major —quantitative— difference between the measurement results (Figure 6.2) and the calculations of Figure 6.4 is that the former show a second maximum in the charge
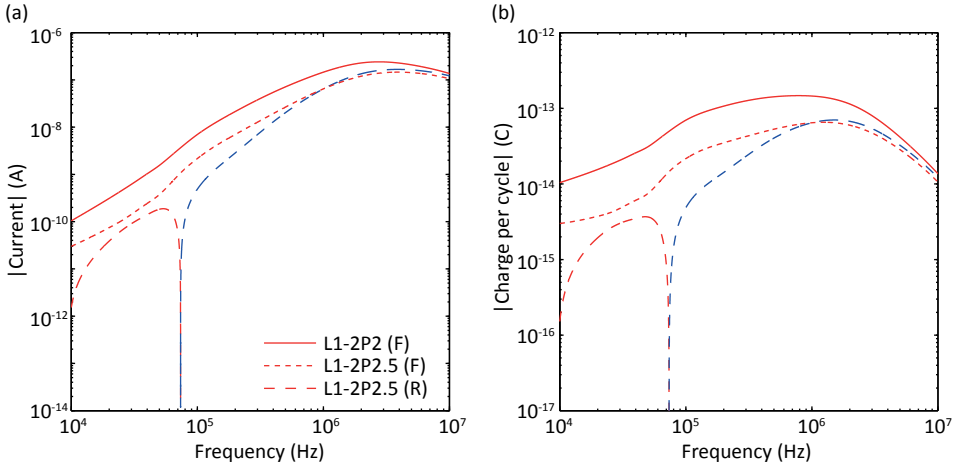
Figure 6.4 | The modeled current **(a)** and charge per cycle **(b)** for the L1–2P2 and L1–2P2.5 ratchets operated in forward drive and the L1–2P2.5 ratchet operated in reversed drive. The density dependent mobility, 2D charge transport and diffusion enhancement is taken into account in the drift–diffusion calculations. General modeling settings are: $V_O = -7$ V, $V_A = 8$ V, $V_G = -20$ V.

per cycle at lower frequencies. Having included 2D charge transport and the effects of the disorder–broadened density of states, this maximum likely falls beyond the type of drift–diffusion calculations used in this thesis. It seems unlikely that using a significantly finer mesh, which is problematic from a computational perspective, would boost the low frequency current. The use of the complete generalized Einstein relation, that would include the full Fermi statistics and at the present densities might lead to modifications in the drift–diffusion balance of the order unity [16], is neither expected to make major differences. More likely, the assumption of local thermal equilibrium, underlying the use of the (generalized) Einstein relation, breaks down. It is known that this relation no longer holds when far from equilibrium [2,18], and diffusion may be boosted under such conditions. Since diffusive effects are mostly relevant for the low frequency regime such a scenario might explain the present discrepancy between experiment and model.

6.3   Open circuit voltage

A linear relationship is found when modeling the current as a function of tilt bias V_{tilt} for infinitely long ratchets [2] as shown in Figure 5.2. Experimentally a curved relation is found, as shown in the inset of the same figure, that was attributed to the presence of source and drain contacts. In this section it is investigated how the tilting curve, and in particular the short circuit current I_{SC} and the open circuit voltage V_{OC} are influenced by
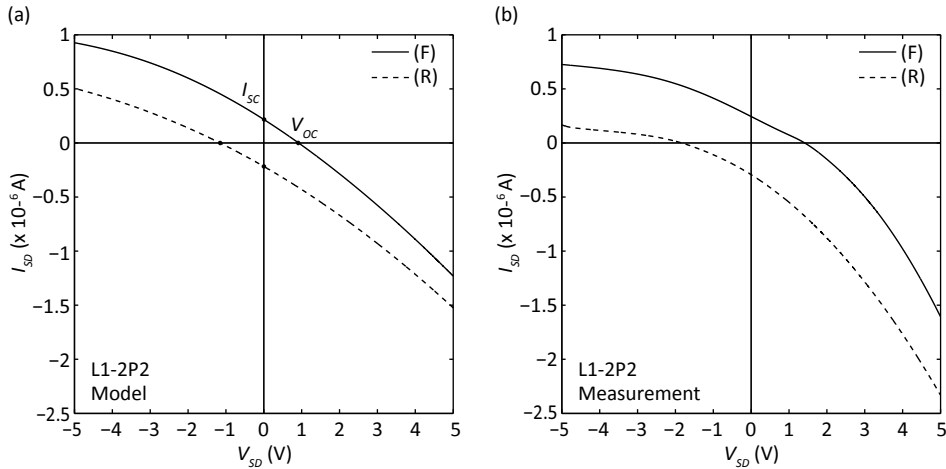
Figure 6.5 | Modeled **(a)** and measured **(b)** source–drain current I_{SD} as a function of source–drain bias V_{SD} for an L1–2P2 ratchet operated in forward (F) and reversed (R) drive. Modeling settings are: $V_O = -7$ V, $V_A = 8$ V, $V_G = -20$ V and $\mu = 10^{-6}$ m²/Vs. Measurement settings are: $V_O = -7$ V, $V_A = 8$ V, and $V_G - V_{TH} = -20$ V.

the presence of the source and drain contacts. For all simulations, the charge transport is assumed to be 1D.

In Figure 6.5, the modeled (a) and measured (b) current in forward and reversed drive is shown as a function of the source–drain bias for the L1–2P2 ratchet. The measured and modeled curves show very similar behavior. Although the ratchet itself is symmetric, the shape and absolute values of the currents in forward and reversed drive differ. In Figure 6.5a and b, the absolute value of the current in reversed drive at $V_{SD} = 0$ V is equal to the current in forward drive as should be due to mirror symmetry. At nonzero source–drain bias the electric field breaks the mirror symmetry of the device, resulting in different behavior for the forward and reversed drive. In terms of device operation, the ratchet and the applied field counteract (amplify) each other for forward (reversed) drive at positive biases, and vice versa for negative biases.

In Figure 6.6a and b respectively the measured short circuit current and open circuit voltage as a function of number of electrode pairs is shown for ratchets with different asymmetries. The dashed lines are trend lines drawn by hand. All measurements are conducted with the same offset V_O, amplitude V_A and effective gate voltage $(V_G - V_{TH})$. The frequency f used is the frequency at current maximum f_I which is different for each ratchet. Modeling results for L1–2Pa (a = 2, 4, 8, 16, and 32) ratchets are also displayed, together with the results for an L1–2P∞ ratchet. Due to computational constraints the
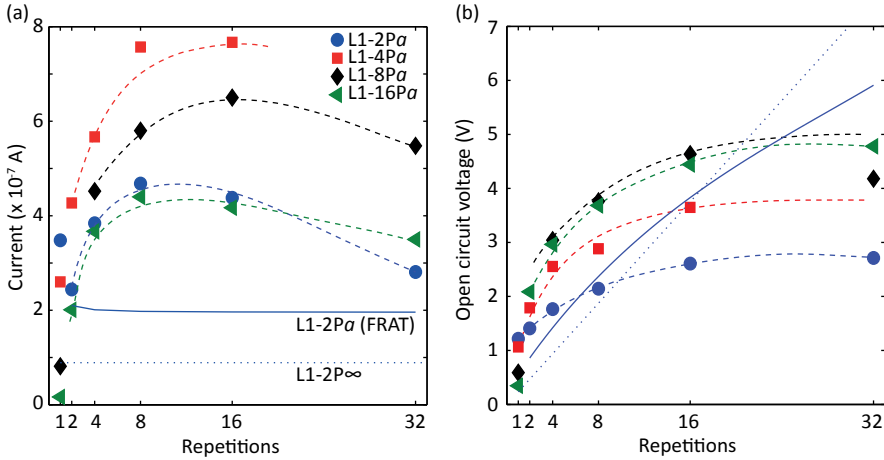
Figure 6.6 | Short circuit current **(a)** and open circuit voltage **(b)** as a function of the number of asymmetric repeat units a for L1–2, L1–4, L1–8 and L1–16 ratchets. Also shown is the modeled current for an L1–2Pa and an L1–2P∞ ratchet. The color shows the current sign (red positive, blue negative). The dashed lines are guidelines drawn by hand. Modeling settings are: $V_O = -7$ V, $V_A = 8$ V, $V_G = -20$ V and $\mu = 10^{-6}$ m²/Vs. Measurement settings are: $V_O = -7$ V, $V_A = 8$ V, and $V_G - V_{TH} = -20$ V. For each mesurement point the frequency at current maximum f_I is used.

fast ratchet analysis tool (FRAT, see Chapter 2) had to be used to obtain the results for the L1–2Pa ratchets, instead of the full drift–diffusion model. In FRAT, the ratchet is represented as an RC network, using the gradual channel approximation [19]. It is verified for ratchets with a low number of pairs of finger electrodes that around f_I identical results are obtained as with the drift–diffusion model with source–drain contacts.

Naively one would expect that the current is independent of the number of repeat units; each asymmetric stage transports the same amount of charge and has the same stall force. Doubling the number of repeat units should then lead to a doubling in open circuit voltage and a constant current. These expectations underlay the dotted lines in Figure 6.6, which are based on the calculations for the L1–2P∞ ratchet. In contrast, measurement results show an increase in short circuit current with increasing number of repetitions, reaching a maximum between the 8 and 16 pairs, after which a (slight) decrease in current is observed. The modeling results obtained with FRAT (solid line) show a constant current, as expected. This difference might partially be caused by contact resistance. The s–shaped curve in the current–drain bias plots in Figure 6.5b and Figure 3.7a point to the presence of a significant contact resistance [20]. In organic field effect transistors, the relative influence of contact resistance on the source–drain current is larger for shorter channel lengths which might explain the increase in current with

increasing number of finger electrodes [21]. The subsequent decrease in current might be related to the constant offset V_O used during the measurements. In Appendix III it is shown that for unknown reasons the ideal offset shifts to lower values when the number of repeat units is increased.

Measured and modeled open circuit voltage as a function of number of repetitions is shown in Figure 6.6b. Measurement results show indeed that for a small number of pairs (2–4) the open circuit voltage increases linearly by approximation. However the increase levels off fast. Increasing the number of pairs from 16 to 32 barely changes the open circuit voltage.

In Figure 6.6b the modeled open circuit voltage is depicted for an L1–2Pa ratchet. In spite of the constant current (Figure 6.6a), the calculation for the open circuit voltage is in qualitative agreement with the measurements although the open circuit voltage levels off less dramatically. This behavior may be understood as follows. When a bias is applied, the local offset–amplitude combination changes as compared to the situation with V_{SD} = 0 V. In Figure 5.6 it is shown that as a rule of thumb the offset V_O should be half the amplitude V_A for maximum charge pumping efficiency. For short channel lengths, i.e. small V_{OC}, this condition is roughly fulfilled throughout the channel. For longer channels the effective (local) offset increases significantly due to the increasing channel potential while the gate voltage remains constant. This decreases the pumping efficiency, and therefore the added voltage of successive repeat units. This is further illustrated in Figure A3.5, where a snap shot of the channel potential as a function of position is mapped on top of the open circuit voltage as a function of number of repetitions. The open circuit voltage corresponds one–on–one to the local channel potential. The same effect is also visible in Figure 6.5a and b, where for high negative drain voltages the channel gets pinched off [19] due to the shift in effective local offset, resulting in the observed saturation of the current. Depending on the chosen settings, the channel might off course also be pinched off due to the drain voltage become more negative than the gate voltage which is the common cause for current saturation in OFETs [19]. For increasing positive drain voltages the ratchet effect will at some moment become of negligible influence, which must result in coinciding curves for the forward and reversed drive.

6.4   Summary

The source and drain contacts —necessarily present in actual electronic ratchet devices— have a large influence on the characteristic properties of these devices. In modeling as well as in experiments, current reversals are found for ratchets with a non–integer number of pairs of finger electrodes. For ratchets with an integer number of finger pairs these reversals are absent. Diffusive transport of particles plays a major role in the current reversals as was shown by results from drift–only calculations; the organic electronic ratchets in this thesis may thus be regarded as Brownian motors when operated at frequencies below, roughly, 100 kHz. The high–frequency (~1 MHz) behavior —where diffusion contributions are negligible— can completely be attributed to the asymmetry and length of the repeat unit, and is unaffected by the presence of contacts.

The major —quantitative— difference found between the measurement results and the calculations is that the former show a second maximum in the charge per cycle at lower frequencies. Having included 2D charge transport and the effects of the disorder–broadened density of states, reproduction of this maximum likely is beyond the type of drift–diffusion calculations used in this thesis. In the model local thermal equilibrium is assumed, underlying the use of the (generalized) Einstein relation. When operating far from equilibrium, the Einstein relation no longer holds and diffusion might be accelerated. Since diffusive effects are mostly relevant for the low frequency regime such a scenario might explain the present discrepancy between experiment and model.

The source–drain contacts also influence the open circuit voltage. For infinitely long ratchets a linear relationship is found between the ratchet–generated current and the tilt bias, whereas for finite ratchets a non–linear relationship is found. The open circuit voltage saturates with increasing number of repeat units due a shift in the effective locally applied potentials, which is also visible when sweeping the source–drain bias.

6.5   References

[1]   Hänggi, P. & Marchesoni, F. Artificial Brownian motors: Controlling transport on the nanoscale. *Rev Mod Phys* **81**, 387–442, (2009).

[2]   Reimann, P. Brownian motors: noisy transport far from equilibrium. *Physics Reports–Review Section of Physics Letters* **361**, 57–265, (2002).

[3]   Roeling, E. M. *et al*. Organic electronic ratchets doing work. *Nat Mater* **10**, 51–55, (2011).

[4]   Eshuis, P., van der Weele, K., Lohse, D. & van der Meer, D. Experimental Realization of a Rotational Ratchet in a Granular Gas. *Phys Rev Lett* **104**, 248001, (2010).

[5]   Svoboda, K., Schmidt, C. F., Schnapp, B. J. & Block, S. M. Direct Observation of Kinesin Stepping by Optical Trapping Interferometry. *Nature* **365,** 721–727, (1993).

[6]   Loutherback, K., Puchalla, J., Austin, R. H. & Sturm, J. C. Deterministic Microfluidic Ratchet. *Phys Rev Lett* **102**, 045301, (2009).

[7]   Linke, H. *et al.* Self–propelled Leidenfrost droplets. *Phys Rev Lett* **96**, 154502, (2006).

[8]   Mahmud, G. *et al.* Directing cell motions on micropatterned ratchets. *Nature Physics* **5**, 606–612, (2009).

[9]   Linke, H. *et al.* Experimental tunneling ratchets. *Science* **286**, 2314–2317, (1999).

[10]   Linke, H. *et al.* Asymmetric nonlinear conductance of quantum dots with broken inversion symmetry. *Phys Rev B* **61**, 15914–15926, (2000).

[11]   Khrapai, V. S., Ludwig, S., Kotthaus, J. P., Tranitz, H. P. & Wegscheider, W. Double–Dot Quantum Ratchet Driven by an Independently Biased Quantum Point Contact. *Phys Rev Lett* **97**, 176803, (2006).

[12]   Hänggi, P. Organic Electronics Harvesting Randomness. *Nat Mater* **10**, 6–7, (2011).

[13]   Horowitz, G., Hajlaoui, R. & Delannoy, P. Temperature–Dependence of the Field–Effect Mobility of Sexithiophene – Determination of the Density of Traps. *J Phys III* **5**, 355–371, (1995).

[14]   Horowitz, G., Hajlaoui, R., Bouchriha, H., Bourguiga, R. & Hajlaoui, M. The concept of "threshold voltage" in organic field–effect transistors. *Adv Mater* **10**, 923–927, (1998).

[15]   Vissenberg, M. C. J. M. & Matters, M. Theory of the field–effect mobility in amorphous organic transistors. *Phys Rev B* **57**, 12964–12967, (1998).

[16]   Roichman, Y. & Tessler, N. Generalized Einstein relation for disordered semiconductors – Implications for device performance. *Appl Phys Lett* **80**, 1948–1950, (2002).

[17]   Nguyen, T. H. & O'Leary, S. K. Generalized Einstein relation for disordered semiconductors with exponential distributions of tail states and square–root distributions of band states. *Appl Phys Lett* **83**, 1998–2000, (2003).

[18]   Reimann, P. *et al.* Giant acceleration of free diffusion by use of tilted periodic potentials. *Phys Rev Lett* **87**, 010602, (2001).

[15]   Sze, S. M. & Ng, K. K. *Physics of semiconductor devices.* 3rd edn, (Wiley–Interscience, 2007).

[16]   Wu, Y. L., Li, Y. N. & Ong, B. S. Printed silver ohmic contacts for high–mobility organic thin–film transistors. *J Am Chem Soc* **128**, 4202–4203, (2006).

[17]   Horowitz, G., Lang, P., Mottaghi, M. & Aubin, H. Extracting parameters from the current–voltage characteristics of field–effect transistors. *Adv Funct Mater* **14**, 1069–1074, (2004).

Summary

Organic electronic ratchets

A *Gedankenexperiment* conceived by Marian Smoluchowski and extended by Richard Feynman showed how asymmetry can be used to rectify the undirected (Brownian) motion of particles in a device called a ratchet. Ratchets are intriguing and counterintuitive devices. Experimentally, ratchets have been realized in a variety of systems, e.g. granular media, Leidenfrost droplets, motile cells and electronic ratchets. Although electronic ratchets have been of scientific interest, so far the electronic ratchets reported in literature were of limited practical use due to the low currents and voltages that were generated and the need for cryogenic temperatures. In this thesis organic electronic ratchets were studied. These ratchets are of a conceptually new design, deliver currents and voltages that are orders of magnitude higher then previously reported electronic ratchets and operate at room temperature. Furthermore they display the rich non–linear behavior that is typical for ratchets. Using measurement results from ratchets that differ in length scale and asymmetry and modeling results from numerical device models, the functioning and performance of these organic electronic ratchets were investigated.

Using the example of the flashing ratchet —where an asymmetric time–dependent potential was used to direct particles— the subject of ratchets and more specifically organic electronic ratchets was introduced. The main building block of these ratchets was a bottom–contact bottom–gate organic field effect transistor. Pentacene, an organic semiconductor, was deposited on top, in contact with source and drain electrodes and separated from the gate contact by a silicon dioxide gate dielectric. Inside the gate dielectric, asymmetrically spaced interdigitated electrodes were placed. For operation, a gate bias was applied to accumulate charges right above the pentacene–silicon dioxide interface. By applying specific time–varying potentials on the interdigitated finger electrodes a (quasi–flashing) ratchet effect was induced; a net charge moves between source and drain contacts at zero source–drain bias.

Design and fabrication of the ratchets was discussed in Chapter 2. The ratchets were fabricated on top of a highly doped silicon wafer serving as the gate contact. Standard cleanroom techniques, i.e. ultra–violet contact photolithography and lift–off processes, were used to fabricate the finger electrodes and source–drain contacts. It was shown that patterning of the organic semiconductor is crucial for the fabrication of functioning ratchets.

Also introduced in Chapter 2 were the device models used throughout this thesis. The standard model was a quasi two–dimensional model in which the drift–diffusion equation was solved for infinitely long ratchet devices by forward integration in time. In the model, the Coulomb interaction between particles was taken into account via Poisson´s equation. Assuming local thermal equilibrium, the Einstein relation was used to couple the mobility to the diffusion constant. An extended version of this model was used at the end of this thesis. It incorporates the source and drain contacts from the actual devices, giving a full device description. Due to computational time constraints, this model could only be used for short channel devices. Therefore a second model was used describing the ratchet as a resistance–capacitor (RC) network, which can be used for frequencies where diffusion has a negligible influence on the charge transport.

The proof of principle of the electronic ratchets was given in Chapter 3. Measurement results showed ratchet operation up to radio frequencies. The possibility to extract work from these ratchet devices was shown by driving low–end logic. Moreover, characteristic reversals in the time–averaged current were observed in a multidimensional parameter space formed by the (a)symmetry, frequency, amplitude and offset of the driving ratchet potential. Drift–diffusion simulations showed that inter–particle interactions play a major role.

Scaling of the characteristic frequencies for organic electronic ratchets operating in a flashing mode was examined in Chapter 4. Measurements and numerical simulations showed that the frequency at current maximum is linearly dependent on the applied DC gate potential and the mobility and is inversely proportional to the squared length of one ratchet period, which can be related to the RC–time of one asymmetric unit. It was furthermore shown that the frequency at current maximum depends on the asymmetry of the ratchet potential. The frequency at maximum charge displacement was also investigated and surprisingly turned out not to depend on the asymmetry of the ratchet potential but only on the length of the asymmetric unit.

In Chapter 5 the performance indicators —i.e. current, charge per cycle, open circuit voltage, power efficiency and charge displacement efficiency— of organic electronic ratchets were studied. It was shown how the characteristic parameters of the time–varying asymmetric potential like length scales and amplitude, as well as the charge carrier density and mobility influence the performance characteristics. For ratchets with a constant asymmetry but changing length, the current increases when going to smaller length scales while the net charge displaced per cycle, as well as the power and charge displacement efficiencies decrease. To optimize the power efficiency for a given geometry, (voltage) settings need to be chosen such that the charge displaced per oscillation cycle reaches a maximum, rather than near the current maximum. When all settings were brought close to optimum, a ratchet with a predicted charge displacement efficiency of over 49% and a power efficiency of approximately 6.9% was obtained.

The effect on the characteristics of organic electronic ratchets of dimensionality and finite size was investigated in Chapter 6. Measurement results showed that the presence of source–drain contacts qualitatively alters the ratchet behavior. Not only the length and asymmetry of the repeat unit of the ratchet potential, but also the way it is terminated by the contacts and the total system length are of crucial importance. Measurement results were combined with modeling results from drift–(diffusion) models to study these effects. It was shown that the open circuit voltage saturates with increasing device length due to the presence of contacts. Calculations reproduced the current reversals at low frequency for devices with a non–integer number of finger pairs, showing the importance of the symmetry loss upon termination of the ratchet potential by contacts. These current reversals disappeared in drift–only calculations, showing the influence of diffusion on the ratchet behavior. At low frequencies the ratchet turned out to be a genuine Brownian motor. Finally, two–dimensional charge transport and the effects of the disorder–broadened density of states were investigated. Mainly quantitative differences in modeling results were observed.

All in all, major steps were made in the development and subsequent understanding of organic electronic ratchets. However, questions concerning the mechanism behind the contact influence on charge transport remain and are interesting subjects for further research. Being able to control the location of the characteristic current reversals can for instance lead to interesting new applications. Also interesting to investigate would be the possibility of wirelessly powering these devices, using an external oscillating electric

field. Feasibility of this idea can be investigated by operating these ratchets in a rocking mode, i.e. superimposing a linear potential across the channel, oscillating between two extremes of opposite sign, on top of a constant asymmetric potential. In the organic electronic ratchets this oscillating potential can be applied using the source and drain contacts, albeit experimental difficulties might arise.

To summarize, several contributions were made to the rich and diverse research field on (Brownian) ratchets. As was shown the charge transport mechanism differs from previously reported ratchets as the devices function by the grace of the Coulomb interactions between charges. Generated currents and voltages were orders of magnitude larger than previously reported in literature, bringing implementation of electronic ratchets in actual devices closer by. This was emphasized by the implementation of a ratchet as a power source in an electronic circuit. For functional electronic ratchet–devices contacts are necessary. These contacts break the spatial periodicity of the ratchet potential leading to major differences in charge transport, adding an extra dimension to the already complex behavior of ratchets.

Samenvatting

Organische elektronische ratchets

Een vraag die wetenschappers altijd geïntrigeerd heeft is of het mogelijk is om energie te halen uit 'het niets'. Is het mogelijk om thermische energie van deeltjes —gemanifesteerd door de ongerichte Brownse beweging— om te zetten in bruikbare energie? In een *Gedankenexperiment* uit 1912 beschreef Marian Smoluchowski een apparaat waarmee dit op het eerste gezicht mogelijk zou moeten zijn. Het systeem, de Feynman–Smoluchowski ratchet, is weergegeven in Figuur 1. Het systeem is erg klein zodat de thermische energie van deeltjes (moleculen) die bij botsingen overgedragen wordt het systeem kunnen beïnvloeden. De draairichting van het ratchet– (letterlijk vertaald: ratel–) vormige wiel wordt gecontroleerd door een dunne en flexibele pal. Vanwege de vorm van het wiel en
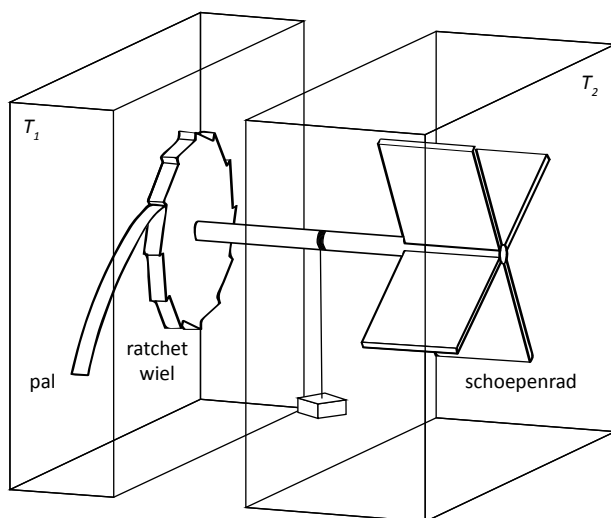
Figuur 1 | Feynman–Smoluchowski ratchet. Te zien is een schoepenrad dat via een as verbonden is met een ratchetvormig wiel. De draairichting wordt gecontroleerd via een pal. In het geval van de Feynman–Smoluchowski ratchet is T_1 gelijk aan T_2. In Feynmans gedachte–experiment (Feynman ratchet) zijn T_1 en T_2 niet langer aan elkaar gelijk.

de pal kan het systeem maar één kant op draaien. Aan het wiel zit verder een dunne as met daaraan een schoepenrad. Deeltjes die tegen het schoepenrad botsen brengen het systeem in beweging, wat vanwege de aanwezigheid van de pal slechts één kant op kan. Tot zover lijkt niets de werking van dit apparaat te stoppen en zou de vraag die aan het begin gesteld is met ja beantwoord kunnen worden. Het gedachte–experiment is echter een wetenschappelijke rariteit, het daagt de tweede hoofdwet van de thermodynamica uit. Volgens deze wet kan dit apparaat niet functioneren; het is een perpetuum mobile van de tweede soort wat betekent dat je energie onttrekt uit een systeem in thermisch evenwicht. Smoluchowski liet uiteindelijk zien dat dit apparaat inderdaad niet werkt. Het palletje dat de draairichting van het wiel controleert wordt namelijk ook bloot-gesteld aan thermische botsingen. Doordat het palletje dun en flexibel moet zijn om het wiel überhaupt te kunnen laten draaien kan het door botsingen ook van zijn plaats komen waardoor het systeem opeens naar beide kanten kan draaien. Over langere tijd zal het systeem niet veranderd zijn ten opzichte van de begintoestand.

In 1963 werd het gedachte–experiment van Smoluchowski herhaald en uitgebreid door Richard Feynman. Feynman liet —in *The Feynman lectures on physics*— zien dat door het systeem uit thermisch evenwicht te halen het mogelijk is om de ongerichte beweging van deeltjes te gebruiken om energie over te dragen. Doordat het systeem uit thermisch evenwicht moet zijn om te werken moet er continu energie aan het systeem worden toegevoegd. Het systeem is daarmee ook niet langer een perpetuum mobile, maar een soort van energieomvormer geworden. Wetenschappelijke experimenten hebben de gedachte–experimenten van Smoluchowski en Feynman nagebootst en de uitkomsten daarvan bevestigd.

Begonnen als een wetenschappelijke rariteit, groeide na het gedachte–experiment van Richard Feynman het onderzoeksgebied naar (Brownian) ratchets of motors snel. Het mag dan wel niet mogelijk zijn om 'energie uit het niets' te halen, ratchets zijn zeer interessant. Normaal gesproken wordt de thermische beweging van deeltjes gezien als nadeel omdat het zorgt voor verliezen in systemen. Bij ratchets wordt juist geprobeerd deze thermische energie te gebruiken. Tot op de dag van vandaag blijft het experiment-ele onderzoek echter vaak steken bij het maken van ingenieuze wetenschappelijke gad-gets; apparaten die wetenschappelijk zeer interessant zijn maar ver van een mogelijke toepassing afstaan. Enkele voorbeelden van deze gadgets zijn waterdruppels (Leidenfrost druppels) die omhoog kunnen lopen op een gloeiende plaat met een wasbord patroon, levende cellen die selectief een bepaalde richting op bewegen in een ratchetvormig ge-

structureerd kanaal en elektronische ratchets waarmee lading wordt verplaatst via asymmetrische potentialen. Deze elektronische ratchets leken tot voor kort niet van praktisch nut vanwege de lage stromen en spanningen en vanwege de extreem lage temperaturen waarbij ze werken. In dit proefschrift worden organische elektronische ratchets bestudeerd. Deze ratchets zijn conceptueel nieuw in ontwerp, leveren stromen en spanningen die ordes van grootte hoger zijn dan eerder gerapporteerde elektronische ratchets en werken bij kamertemperatuur. Bovendien vertonen deze ratchets niet–lineair gedrag zoals stroomomkeringen; een effect dat later nog toegelicht wordt met een figuur. Meetresultaten verricht aan ratchets die verschillen in asymmetrie en lengteschalen zijn gecombineerd met numerieke simulaties om het functioneren te onderzoeken.

Het principe achter de organische elektronische ratchets kan het best uitgelegd worden aan de hand van de aan–uit ratchet (Figuur 2a). In dit type ratchet wordt een asymmetrische tijdsafhankelijke potentiaal gebruikt om de willekeurige beweging van deeltjes om te zetten in een beweging naar één kant. De eerste stap is dat ladingen opgesloten worden in een asymmetrische potentiaal. De ladingen zoeken steeds de locatie van de laagste potentiaal op omdat dat energetisch het gunstigst is. In de tweede stap wordt de potentiaal uitgeschakeld en de ladingen verspreiden zich gelijkmatig naar links en naar rechts door diffusie. Drift van ladingsdragers speelt echter een nog belangrijkere rol: ladingen stoten elkaar onderling af en versnellen daarmee het verspreidingsproces. Als de asymmetrische potentiaal opnieuw wordt aangezet zullen de ladingen weer opgesloten worden. Als dit op het juiste tijdstip gebeurd zullen vanwege de asymmetrie de ladingsdragers eerder geneigd zijn één bepaalde kant op te lopen. Door dit proces van aan– en uitzetten van de ratchetpotentiaal te herhalen zal er een continue stroom gaan lopen.

Het is eenvoudig voor te stellen dat de frequentie waarmee de asymmetrische potentiaal aan– en uitgezet wordt van belang is voor de hoeveelheid stroom die er gaat lopen. Bij een hoge aan–uit frequentie hebben de ladingen geen tijd meer om te reageren op het aan– en uitschakelen van de asymmetrische potentiaal. Het gevolg is dat er geen stroom gaat lopen. Wanneer het aan–uitschakelen met een zeer lage frequentie gebeurt, krijgen de ladingen alle tijd om zich gelijkmatig over de hele structuur te verdelen en er zal dan ook geen stroom gaan lopen. Het is dus van belang om uiteindelijk de juiste frequentie te kiezen om het transport van ladingen te optimaliseren.
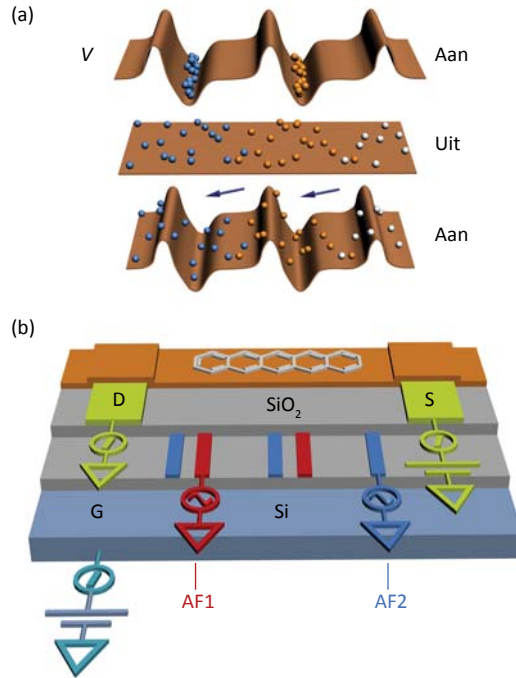
Figuur 2 | (a) Het principe van de aan–uit ratchet. Ladingen zitten opgesloten in een asymmetrische potentiaal (*V*). Door de potentiaal uit te zetten verspreiden de ladingen door drift– en diffusieprocessen. Wanneer de asymmetrische potentiaal weer wordt aangezet worden de ladingen opnieuw gevangen. Vanwege de asymmetrie verplaatsen ladingen zich van (in dit geval) rechts naar links. **(b)** Schematische weergave van een ratchet. Te zien zijn de source (S) en drain (D) contacten die gescheiden zijn van de gate (G) elektrode door een silicumdioxide (SiO_2) laag. Halverwege de SiO_2 laag zijn asymmetrische vingerelektrodes geplaatst (AF1 en AF2), weergegeven in rood en blauw. Vingerelektroden met dezelfde kleur zijn elektrisch met elkaar verbonden. Bovenop ligt een pentaceenlaag (laag met structuurformule). Door een specifieke tijdsafhankelijke spanning op de vingerelektroden te zetten kan er een stroom gegenereerd worden tussen source en drain contacten zonder dat daarvoor een spanningsverschil tussen source en drain contact nodig is.

De bouwsteen van de organische elektronische ratchets is de organische veldeffect–transistor. Met een veldeffect–transistor kan de stroom die loopt tussen de source en drain contacten gecontroleerd worden door de elektrische spanning op de gate elektrode. Transistors vormen zo de bouwstenen voor computers. Figuur 2b laat een organische elektronische ratchet zien. Pentaceen, een organische halfgeleider, wordt aangebracht bovenop de source en drain contacten en is gescheiden van de gate elektrode door een laag siliciumdioxide wat een zeer goede isolator is. Twee sets van asymmetrisch in elkaar grijpende vingerelektroden (AF1 en AF2) worden halverwege de siliciumdioxide laag geplaatst. Door een (negatief) gate voltage aan te leggen wordt (positieve) lading aangetrokken boven het grensvlak van de halfgeleider en de isolerende laag. Er ontstaat

een geleidend pad tussen de source en drain contacten wat mogelijk maakt dat er ook een stroom kan gaan lopen tussen de contacten. Bij een transistor is daar een spanningsverschil voor nodig tussen de contacten. Bij de organische elektronische ratchets is dat spanningsverschil niet nodig. Door het aanleggen van specifieke tijdsafhankelijke voltages op de sets van vingerelektrodes wordt een aan–uit ratcheteffect geïnduceerd, waardoor een stroom gaat lopen tussen source en drain contact.
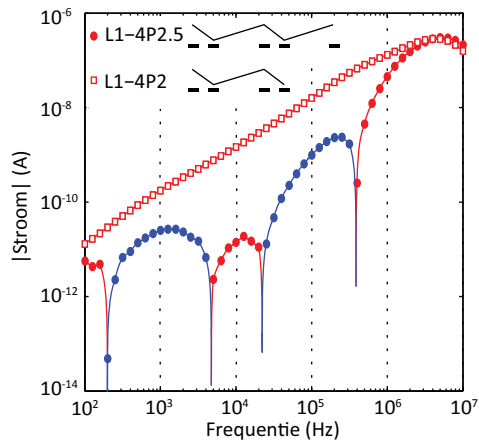
Figuur 3 | De source–drain stroom uitgezet tegen de frequentie waarmee de asymmetrische potentiaal oscilleert. De rode kleur geeft een positieve stroom weer terwijl de blauwe kleur een negatieve stroom weergeeft. De L1–4P2.5 ratchet is de ratchet zoals weergegeven in Figuur 2. De L1–4P2 ratchet heeft twee 'blauwe' en twee 'rode' vingerelektroden. Eén 'blauwe' vingerelektrode minder dan de L1–4P2.5 ratchet. De grafiek laat zien dat een kleine wijziging in het ratchetontwerp grote veranderingen in het uiteindelijke gedrag veroorzaakt.

Het verrassende resultaat van een experiment is te zien in Figuur 3. Er zijn twee soorten ratchets gemaakt. In Figuur 2b is een ratchet te zien waarbij er 3 'blauwe' en twee 'rode' vingerelektrodes zijn. Er zijn ook ratchets gemaakt waarbij het aantal 'blauwe' en 'rode' vingerelektrodes gelijk is. In Figuur 3 staat de gemeten stroom uitgezet tegen de frequentie. Wanneer gekeken wordt naar een ratchet met een gelijk aantal 'blauwe' en 'rode' vingerelektrodes neemt bij stijgende frequentie de stroom toe totdat er een maximum is bereikt waarna de stroom snel daalt. Dit lijkt sterk op het eerder voorspelde gedrag van de aan–uit ratchet. Bij een ratchet met 3 'blauwe' en 2 'rode' vingers is het beeld totaal anders. Bij toenemende frequentie verandert de richting van de stroom steeds. Bij een kleine frequentieverandering draait de stroomrichting plotseling om —negatieve en positieve stromen zijn aangegeven met blauwe en rode lijnen, respectievelijk. Het is typisch voor ratchets dat kleine veranderingen kunnen leiden tot een totaal ander gedrag. Dit maakt ze moeilijk te doorgronden maar wetenschappelijk gezien worden ze daardoor een stuk interessanter en leuker.

Hieronder volgt nu een korte, zakelijke opsomming van wat er in elk hoofdstuk van dit proefschrift is beschreven. In de laatste twee paragrafen wordt het hele proefschrift in eenvoudigere bewoordingen samengevat.

Het ontwerp en de fabricage van de ratchetstructuren wordt behandeld in hoofdstuk 2. De ratchets zijn gefabriceerd bovenop een silicium wafer die dient als gate contact. Standaard cleanroom fabricage technieken zoals ultra–violette contact–fotolithografie en lift–off processen zijn gebruikt voor het fabriceren van de vingerelektrodes en de source en drain contacten. Meetresultaten laten zien dat het patroneren van de organische halfgeleider cruciaal is voor de fabricage van de ratchets.

De in dit proefschrift gebruikte simulatiemodellen worden ook geïntroduceerd in hoofdstuk 2. Het standaardmodel is een quasi–tweedimensionaal model waarbij de drift–diffusie vergelijking wordt opgelost voor oneindig lange ratchets via voorwaartse integratie in de tijd. In het model is de Coulomb interactie tussen ladingen meegenomen via de Poisson–vergelijking. Door lokaal thermisch evenwicht aan te nemen kon de Einstein relatie gebruikt worden om de mobiliteit van de ladingsdragers te koppelen aan de diffusieconstante. Een uitgebreidere versie van dit model is aan het einde van het proefschrift gebruikt. Hierin zijn source en drain contacten geïntroduceerd zoals aanwezig in de echte organische elektronische ratchets (Figuur 2b). Vanwege belemmeringen in de rekentijden kan dit model alleen gebruikt worden in het geval van kleine kanaallengtes. Daarom is een tweede model geïntroduceerd waarbij de ratchets als een weerstand–condensator (RC) netwerk worden voorgesteld. Dit model kan gebruikt worden voor (hoge) frequenties waarbij diffusie van ondergeschikt belang is voor het ladingstransport.

In hoofdstuk 3 wordt het proof–of–principle van de organische elektronische ratchets geleverd. Meetresultaten laten ratchet–geïnduceerd transport van ladingen zien tot frequenties in het radiogolfgebied. Het aansturen van een simpel logisch circuit laat de mogelijkheid zien om energie terug uit het systeem te halen. Meetresultaten laten voor ratchets karakteristieke omkeringen zien in de tijdsgemiddelde stroom, in een multidimensionale parameterruimte gevormd door de (a)symmetrie, frequentie, amplitude en offset van de ratchetpotentiaal. Drift–diffusie simulaties tonen aan dat interacties tussen ladingen onderling een grote rol spelen in het proces.

Het schalen van karakteristieke frequenties voor organische elektronische ratchets in een quasi aan–uit modus is bestudeerd in hoofdstuk 4. Metingen en numerieke simulaties laten zien dat de frequentie bij het stroommaximum lineair afhankelijk is van de aange-

legde DC gate potentiaal en de mobiliteit, en omgekeerd evenredig is met het kwadraat van de lengte van een asymmetrische potentiaal–eenheid. Verder is de frequentie bij het stoommaximum afhankelijk van de asymmetrie van de ratchetpotentiaal. De frequentie bij maximale ladingsverplaatsing is ook onderzocht. Verrassend genoeg blijkt deze niet afhankelijk te zijn van de asymmetrie van de ratchetpotentiaal.

In hoofdstuk 5 zijn de prestatie–indicatoren zoals stroom, verplaatste lading per cyclus, openklemspanning, vermogensefficiëntie en ladingsverplaatsingsefficiëntie onderzocht. We hebben laten zien dat de karakteristieke parameters van de in de tijd variërende asymmetrische potentiaal zoals lengteschaal en amplitude als ook de ladingsdichtheid en mobiliteit van invloed zijn op de prestatiekarakteristieken. Ratchets met een constante asymmetrie maar veranderende lengte laten een stroomtoename zien wanneer naar kleinere lengteschalen wordt gegaan. Dit gaat echter ten koste van de netto ladingsverplaatsing en de vermogens– en ladingsverplaatsingsefficiëntie die allemaal een afname laten zien. Om de vermogensefficiëntie voor een gegeven geometrie te optimaliseren moeten de spanningsinstellingen zo gekozen worden dat de ladingsverplaatsing per oscillatiecyclus, en niet de stroom, een maximum bereikt. Indien alle instellingen geoptimaliseerd worden, heeft de ratchet een berekende ladingsverplaatsingsefficiëntie van meer dan 49% en een vermogensefficiëntie van 6.9%.

Het effect van dimensionaliteit en eindige lengteschalen op de eigenschappen van organische elektronische ratchets is onderzocht in hoofdstuk 6. Meetresultaten laten zien dat de aanwezigheid van source en drain contacten het ratchetgedrag kwalitatief veranderen. Niet alleen de lengte en asymmetrie van een potentiaaleenheid, maar ook de manier waarop de potentiaal beëindigd wordt bij de contacten en de totale lengte van het systeem zijn van cruciaal belang. Meetresultaten zijn gecombineerd met drift–diffusie simulaties om deze effecten te bestuderen. We laten zien dat de openklemspanning satureert bij toenemende lengte vanwege de aanwezigheid van de contacten. Berekeningen reproduceren de stroomomkeringen bij lage frequenties voor ratchets met een niet–geheel aantal paren van vingerelektrodes. Dit toont de invloed aan van het doorbreken van de periodiciteit door de aanwezigheid van de source en drain contacten. Deze stroomomkeringen verdwijnen bij berekeningen waarbij alleen drift is meegenomen wat aantoont dat diffusie niet langer verwaarloosbaar is. Bij lage frequenties blijken deze ratchets zich te gedragen als authentieke Brownse motoren. Uiteindelijk zijn de invloed van tweedimensionaal ladingstransport en de effecten van een door wanorde verbreedde toestandsdichtheid onderzocht. Voornamelijk kwantitatieve verschillen tussen de verschillende simulatieresultaten zijn gevonden.

Al met al zijn er belangrijke stappen gezet in de ontwikkeling en het bijbehorende begrip van (organische) elektronische ratchets. Er blijven echter vragen bestaan met betrekking tot de invloed van de contacten op het ladingstransport welke interessant kunnen zijn voor vervolgonderzoek. Het kunnen controleren van de locaties van de stroomomkeringen kan leiden tot nieuwe toepassingen. Ook interessant om te onderzoeken is de mogelijkheid om de ratchets in te zetten als draadloze stroombron, waarbij een extern oscillerend elektrisch veld de ratchets van de benodigde energie voorziet. Haalbaarheid van dit idee kan onderzocht worden door de ratchets te opereren in zogenaamde rocking modus. Een lineair toenemende potentiaal wordt gesuperponeerd over de kanaalpotentiaal en oscilleert tussen twee extrema met tegengesteld teken terwijl de asymmetrische potentiaal constant gehouden wordt. In de organische elektronische ratchets kan deze oscillerende potentiaal worden aangelegd via de source en drain contacten, alhoewel dit experimenteel niet eenvoudig zal zijn.

Samenvattend zijn er diverse bijdragen geleverd aan het rijke en diverse onderzoeksveld van Brownse ratchets. Er is aangetoond dat het ladingstransportmechanisme verschilt van eerder gerapporteerde ratchets omdat ze functioneren door de Coulomb interactie tussen ladingen onderling. Gegenereerde stromen en spanningen zijn ordes van grootte hoger dan eerder gerapporteerde waarden wat de implementatie van elektronische ratchets in systemen dichterbij brengt. Dit is benadrukt door het aansturen van een simpel logisch circuit. Voor functionele elektronische ratchets zijn contacten noodzakelijk. Deze contacten verbreken de ruimtelijke periodiciteit van de ratchetpotentiaal wat leidt tot grote veranderingen in het ladingstransport. Dit voegt een extra dimensie toe aan het toch al complexe gedrag van ratchets.

Appendices

Appendix I | Sample fabrication

Appendix II | Current–amplitude relation

Appendix III | Finite size effects

Appendix I | Sample fabrication

Cleaning procedure

- Ultrasonic acetone bath, time: 15 minutes.
- Ultrasonic isopropanol bath, time: 15 minutes.
- Ultrapure water rinse, time: 10 minutes.
- O_2 plasma, 300 W, sample placed in Faraday cage, time: 10 minutes.

Asymmetric finger electrode fabrication

HMDS procedure[1]

- Ultrapure water rinse, time: 10 minutes.
- HMDS oven at 140 ˚C, N_2 environment, time: 3 minutes, 15 seconds.

Spincoating (Suss CT 62)

- MaN405 negative photoresist (MicroResist Technologies).
- Spincoating acceleration: 500 rpm/s.
- Spincoating speed: 3000 rpm.
- Time: 30 seconds, layer thickness: 200 nm.

Prebake procedure

- Hotplate at 95 ˚C, time: 1 minute, 30 seconds.

UV lithography (Suss MA6)

- Contact mode: vacuum, illumination time: 140 seconds.

Photoresist development

- MaD531s tetramethylammoniumhydroxide developer (MicroResist Technologies), time: 90 seconds.

Metal evaporation (Temescal FC2000 e−beam evaporator)

- 5 nm Ti/20 nm Au/5 nm Ti.

Lift−off procedure

- Acetone vapor, time: 1 hour.
- Acetone rinse.
- Ultrasonic acetone bath, time: ~10 minutes.
- Isopropanol rinse.
- Ultrapure water rinse, time: ~10 minutes.
- O_2 plasma, 300 W, sample in Faraday cage, time: 10 minutes.

---

[1] Prior to spincoating, a monolayer of HMDS is applied to the SiO_2 surface to promote adhesion of the photoresist layer.

Silicon dioxide deposition

Plasma Enhanced Chemical Vapor Deposition (Oxford Instruments)

- SiO_2 thickness: ~100 nm.
- Time: 1 minute, 55 seconds.
- Gas flow: SiH_4, 8.5 SCCM, N_2, 161.5 SCCM; N_2O, 710 SCCM.
- Pressure: 1000 mTorr.
- Temperature: 300 ˚C .
- Power: 20 Watt.

Source–drain contact fabrication

HMDS procedure

- Ultrapure water rinse, 10 minutes.
- HMDS oven at 140 ˚C, N_2 environment, time: 3 minutes, 15 seconds.

Spincoating (Suss CT 62)

- MaN415 negative photoresist (MicroResist Technologies).
- Spincoating acceleration: 500 rpm/s.
- Spincoating speed: 4000 rpm, time: 30 seconds.
- Layer thickness: ~600 nm.

Prebake procedure

- Hotplate at 95 ˚C, time: 2 minutes.

UV lithography (Suss MA6)

- Contact mode: vacuum, illumination time: 20 seconds.

Photoresist development

- MaD531s tetramethylammoniumhydroxide developer (MicroResist Technologies), time: 65 seconds.

Metal evaporation (Temescal FC2000 e–beam evaporator)

- 10 nm Ti/40 nm Au.

Lift–off procedure

- Acetone vapor, time: 1 hour.
- Acetone rinse.
- Ultrasonic acetone bath, time: ~10 minutes.
- Isopropanol rinse.
- Ultrapure water rinse, time: ~10 minutes.
- O_2 plasma, 300 W, sample in Faraday cage, time: 10 minutes.

Photoresist shadow mask for patterning

HMDS procedure

- Ultrapure water rinse, time: 10 minutes.
- HMDS oven at 140 ˚C, N_2 environment, time: 3 minutes, 15 seconds.

Spincoating (Suss CT 62)

- MaN440 negative photoresist (MicroResist Technologies).
- Spincoating acceleration: 500 rpm/s.
- Spincoating speed: 3000 rpm, time: 30 seconds.
- Layer thickness: ~2 µm.

Prebake procedure

- Hotplate at 95 ˚C, time: 5 minutes.

UV lithography (Suss MA6)

- Contact mode: vacuum, illumination time: 2 minutes, 10 seconds.

Photoresist development

- MaD531s tetramethylammoniumhydroxide developer (MicroResist Technologies), time: 150 seconds.

Pentacene evaporation

O2 plasma

- Power: 50 W, time: 5 minutes, gasflow: O_2 55 SCCM, sample placed in Faraday cage.

HMDS procedure

- Ultrapure water rinse, time: 10 minutes.
- HMDS at room temperatures, N_2 environment, time: 3 minutes, 15 seconds.

Pentacene evaporation

- Thermal evaporation.
- Layer thickness: ~50 nm.
- Sample temperature: room temperature.
- Evaporation speed: manually controlled at 0.4 Å/s.
- High vacuum evaporator located in an N_2 atmosphere.

Appendix II | Current–amplitude relation

The influence of the frequency, characteristic voltages and length scale on the ratchet–generated current is investigated in Chapter 5, where it is shown that the modeled charge displacement efficiency can be nearly 50%. In Figure 5.6 the ratchet–generated current is shown as a function of amplitude V_A and offset V_O. From a (charge displacement) efficiency perspective, the interesting region for current transport is found when $V_A >$ $|V_O|$ —assuming that the threshold voltage V_{TH} = 0 V. Low currents are obtained for $V_A <$ $|V_O|$. Interestingly enough, the current as a function of amplitude is highly nonlinear in this region, as indicated by the occurrence of —for ratchets familiar— current reversals.
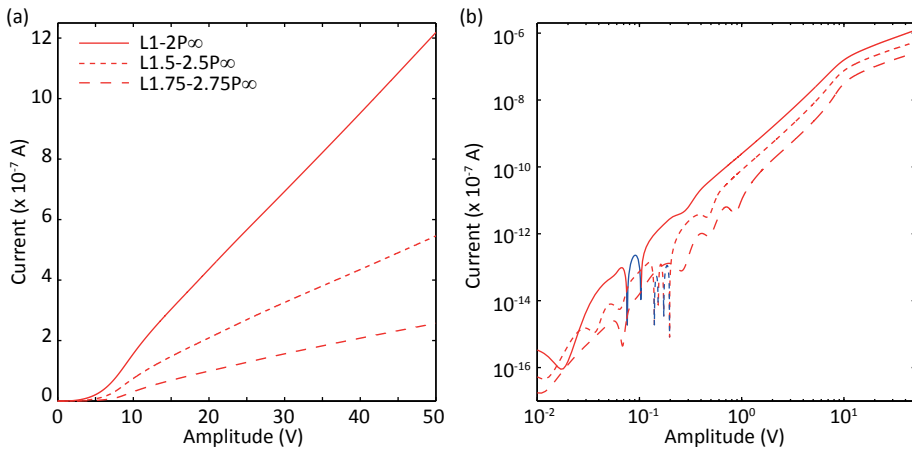

Figure A2.1 | Modeled current as a function of amplitude for an L1–2P∞, L1.5–2.5P∞ and L1.75–2.75P∞ ratchet on linear **(a)** and logarithmic **(b)** axis. The simulation settings are: L = 5 μm, f = 2.5 MHz, V_O = −7 V, μ = 10^{-6} m²/Vs, V_{SD} = 0 V and V_G = −20 V. Red is positive and blue is negative current. The width of the asymmetric finger electrodes for the L1–2P∞, L1.5–2.5P∞ and L1.75–2.75P∞ ratchets is respectively 1 μm, 0.5 μm and 0.25 μm.

In Figure A2.1 the simulated ratchet current is shown as a function of amplitude on linear (a) and logarithmic (b) axis. Infinitely long ratchets are modeled with the drift–diffusion model described in Chapter 2. The curve (labeled L1–2P∞) shows a current reversal for $V_A < |V_O|$ (V_O = −7 V). When $V_A > |V_O|$, a linear relationship between the current and amplitude is obtained. To investigate the influence of the finger width on the current transport, three different finger widths are modeled while the total length of one asymmetric unit L is kept constant: 1 μm (L1–2P∞), 0.5 μm (L1.5–2.5P∞) and 0.25 μm (L1.75–2.75P∞). Lower current values are obtained when decreasing the finger width as less charge can be moved. In spite of the decreasing current values, the three curves show a similar trend: non–linear behavior and current reversals for $V_A < |V_O|$ and linear behaviour for $V_A > |V_O|$.

Appendix III | Finite size effects

Contact influence

Throughout this thesis, modeling and measurement results are combined to unravel properties of the organic electronic ratchets. Using a drift–diffusion model with which infinitely long ratchet potentials are simulated, the influence of the source and drain contacts on charge transport is neglected. Nevertheless, good agreement between modeling and measurement results is obtained (e.g. Figure 3.2). The finiteness of the electronic ratchets is addressed in Chapter 6, where source and drain contacts are incorporated into the model. Simulation results show indeed qualitative differences between infinite and finite ratchets as well as between ratchets with an integer and non–integer number of pairs of finger electrodes. In this section measurement results are presented, showing that the maximum in charge per cycle observed at higher frequencies ($\sim10^6$–10^7 Hz) is indeed caused by the length L and asymmetry Lx–y of the asymmetric repeat unit, as was tacitly assumed in Chapters 3–5. It is, however, influenced by the presence of contacts in ratchets with shorter channel lengths and less pronounced asymmetries.

In Figure A3.1 the measured charge per cycle as a function of offset and frequency is shown for ratchets with different asymmetry having an integer number of repeat units. For the L1–2P8 ratchet one maximum in the charge per cycle is observed. When the asymmetry is increased (e.g. L1–16P8), not one but two maxima are found in the charge per cycle plot: one at lower and one at higher frequencies. Measurement results for the L1–16P2 ratchet show a global maximum at approximately $5 \cdot 10^5$ Hz, and a local maximum just above 1 MHz. Adding more repetitions shifts the first maximum to even lower frequencies, while the location of the second maximum is basically constant. This same behavior is found for ratchets with lower asymmetry (e.g. L1–8Pa and L1–4Pa), although the second, high–frequency maximum can be fully obscured by the proximity of the low–frequency maximum (e.g. L1–2Pa). The charge per cycle as a function of offset and frequency for ratchets with a non–integer number of repeat units is shown in Figure A3.2. There are large similarities between the ratchets with an integer and a non–integer number of repeat units. Also for the latter ones, a maximum in charge per cycle is found at higher frequencies. This maximum is clearly visible as the maximum found at lower frequencies is replaced with a (negative) minimum in charge per cycle.
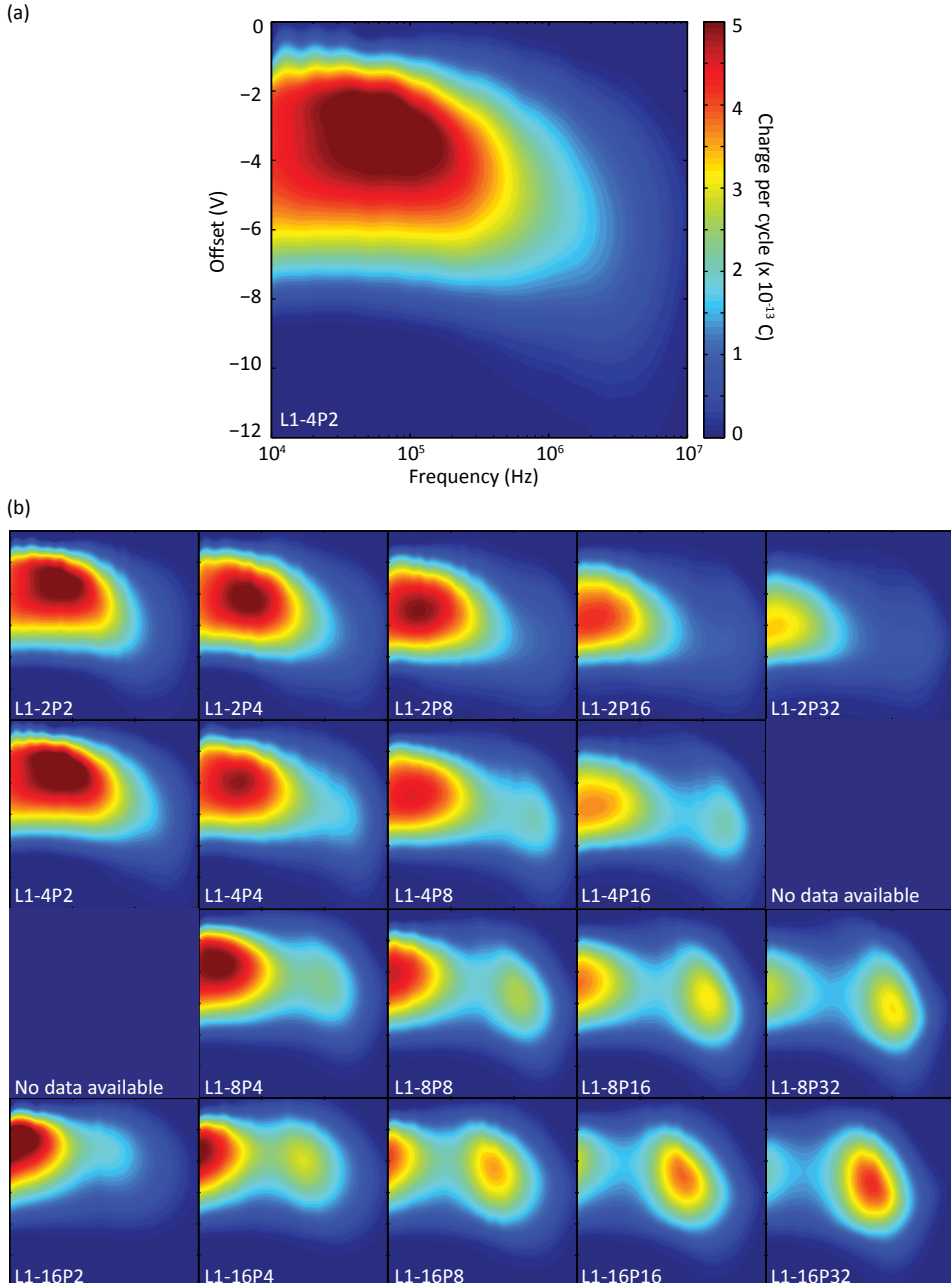
(a)

(b)

Figure A3.1 | (a) Measured charge per cycle–offset–frequency contour plot for an L1–4P2 ratchet (forward drive). **(b)** Charge per cycle contour plots for ratchets with different asymmetry and number of repeat units. The color scale is identical to (a). Note that the L1–4P2 ratchet is discussed in Figures 3.1 and 3.4. Measurement settings: V_A = 8 V, V_G–V_{TH} = −20 V, with V_G the gate voltage and the V_{TH} threshold voltage.
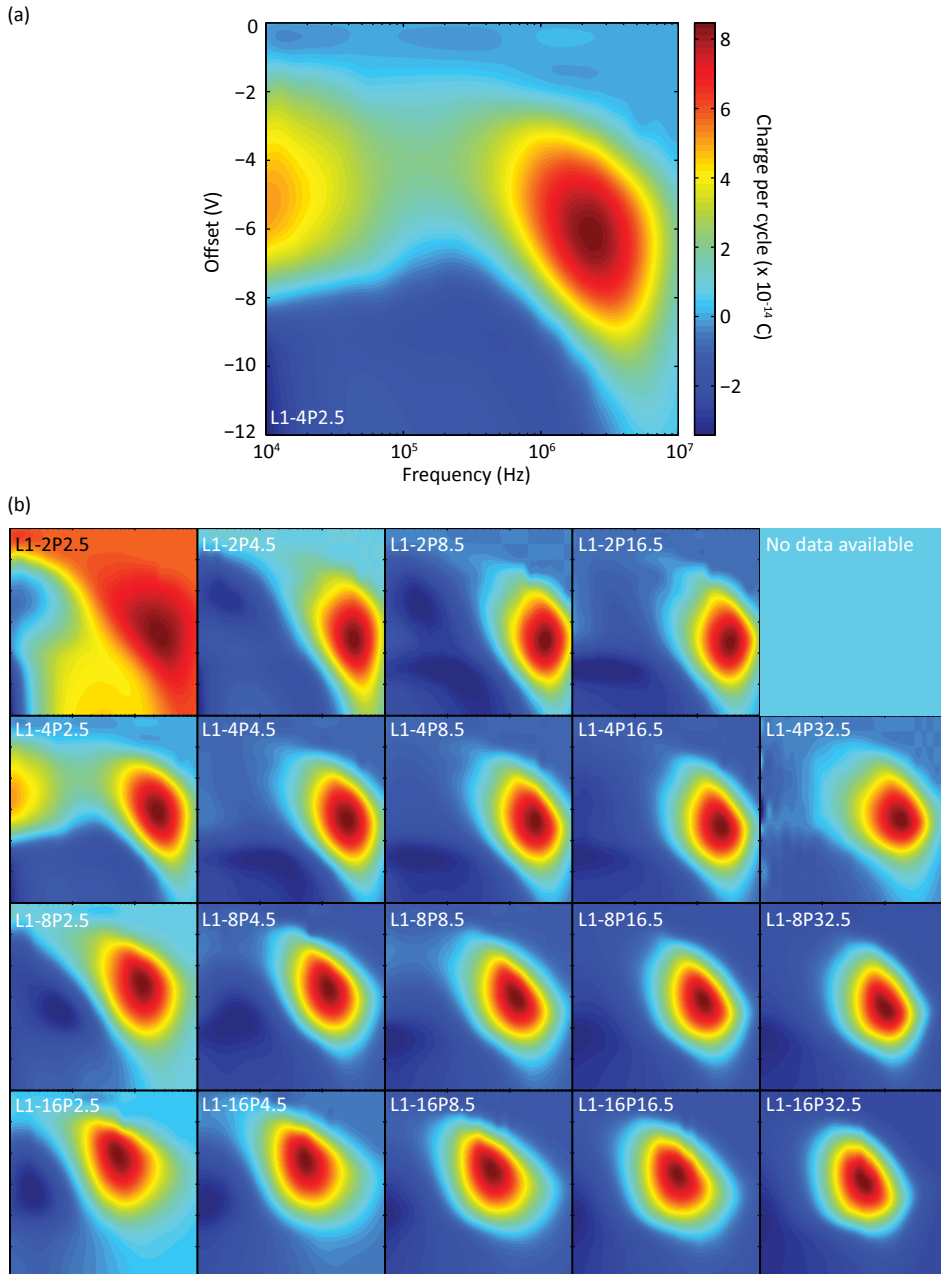
(a)

(b)

Figure A3.2 | (a) Measured charge per cycle–offset–frequency contour plot for an L1–4P2.5 ratchet (forward drive). **(b)** Charge per cycle contour plots for ratchets with different asymmetry and number of repeat units. Each panel has a different color scale to enhance the visibility of the minima in the charge per cycle. Note that the L1–4P2.5 ratchet is discussed in Figures 3.1 and 3.4. Measurement settings: V_A = 8 V, V_G–V_{TH} = −20 V.

In Figure A3.3 the frequency (a), charge per cycle (b) and offset (c) as a function of number of pairs of finger electrodes is shown for ratchets with different asymmetry. The frequency, charge per cycle and offset correspond to the high–frequency charge maxima found in Figures A3.1 and A3.2. For small asymmetries (e.g. L1–2 and L1–4) the optimum frequency depends on the number of pairs of finger electrodes. This dependence vanishes for L1–16P*a* and L1–16P*a*.5 ratchets, where for ratchets with an integer (closed symbols) and a non–integer (open symbols) number of pairs of finger electrodes the same value for the optimum frequency is found.

From the above described results, it can be concluded that the high–frequency maximum in charge per cycle ($\sim10^6$–10^7 Hz) is (predominantly) related to the length L and asymmetry Lx–y of the asymmetric repeat unit. This is corroborated by the fact that this maximum coincides with the maximum found in the drift–diffusion calculations used throughout this thesis, in which the ratchet potential is assumed to be infinitely long. The maxima and minima observed at lower frequencies for respectively ratchets with an integer and non–integer number of pairs of finger electrodes can therefore be attributed to the finiteness of the ratchets. Although they shift to lower frequencies for longer channels, no obvious relationship is found between the channel length (*cl*) and the location of these maxima and minima. This is illustrated in Figure A3.4 where charge per cycle contour plots are shown for L1–8P4 and L1–8P4.5 ratchets. The total channel length is varied by changing the distance b between the source and the drain contact and the nearest finger electrode. The low–frequency maximum (or minimum) shifts too fast to be consistent with an $f \sim cl^2$ relationship as was found for the high–frequency maximum in Chapter 4. This is not surprising as the calculation results show that diffusion plays a major role in the occurrence of the current reversals observed for ratchets with a non–integer number of pairs of finger electrodes, and the L^2 relationship was found for drift–based transport. Further research is necessary to study these low–frequency maxima and minima as currently no measurement data is available for frequencies below 10 kHz.

The charge per cycle as a function of number of repetitions saturates for larger numbers of repetitions as is shown in Figure A3.3b. Modeling results obtained with the fast ratchet analysis model (FRAT) (Figure 6.6) shows that the current is constant upon increasing the number of pairs of finger electrodes. The increase observed in the actual measurements is likely related to the decreasing influence of contact resistance with increasing channel length. The optimal offset decreases with increasing number of repetitions for all asymmetries (Figure A3.3c).
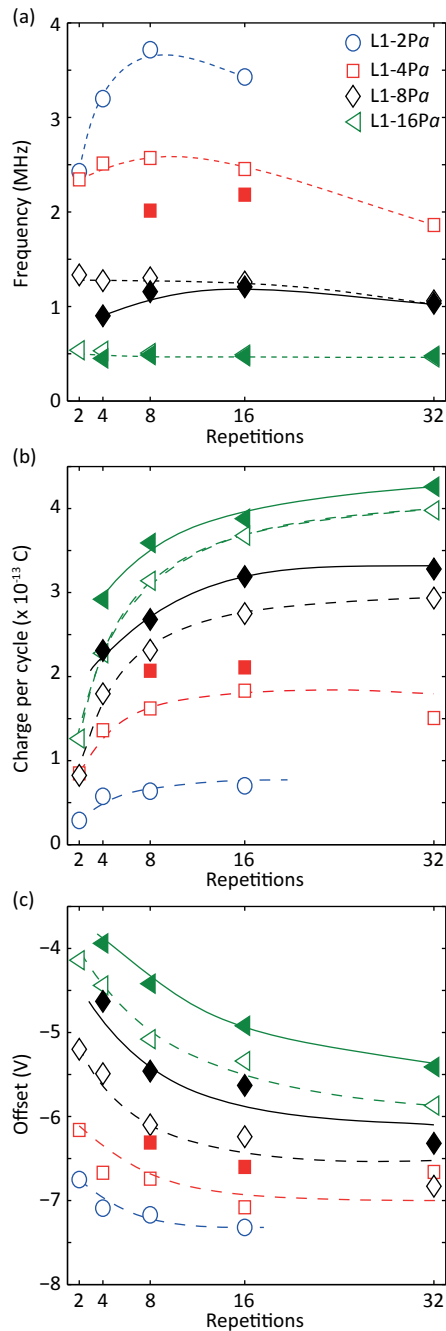
Figure A3.3 | Frequency **(a)**, charge per cycle **(b)** and offset **(c)** as a function of number of asymmetric repeat units *a* for ratchets with different asymmetry. The open and closed symbols are measurement results for ratchets with respectively a non–integer and an integer number of repeat units. The frequency, charge per cycle and offset correspond to the high–frequency charge maxima from Figures A3.1 and A3.2. The dashed lines are trend lines.
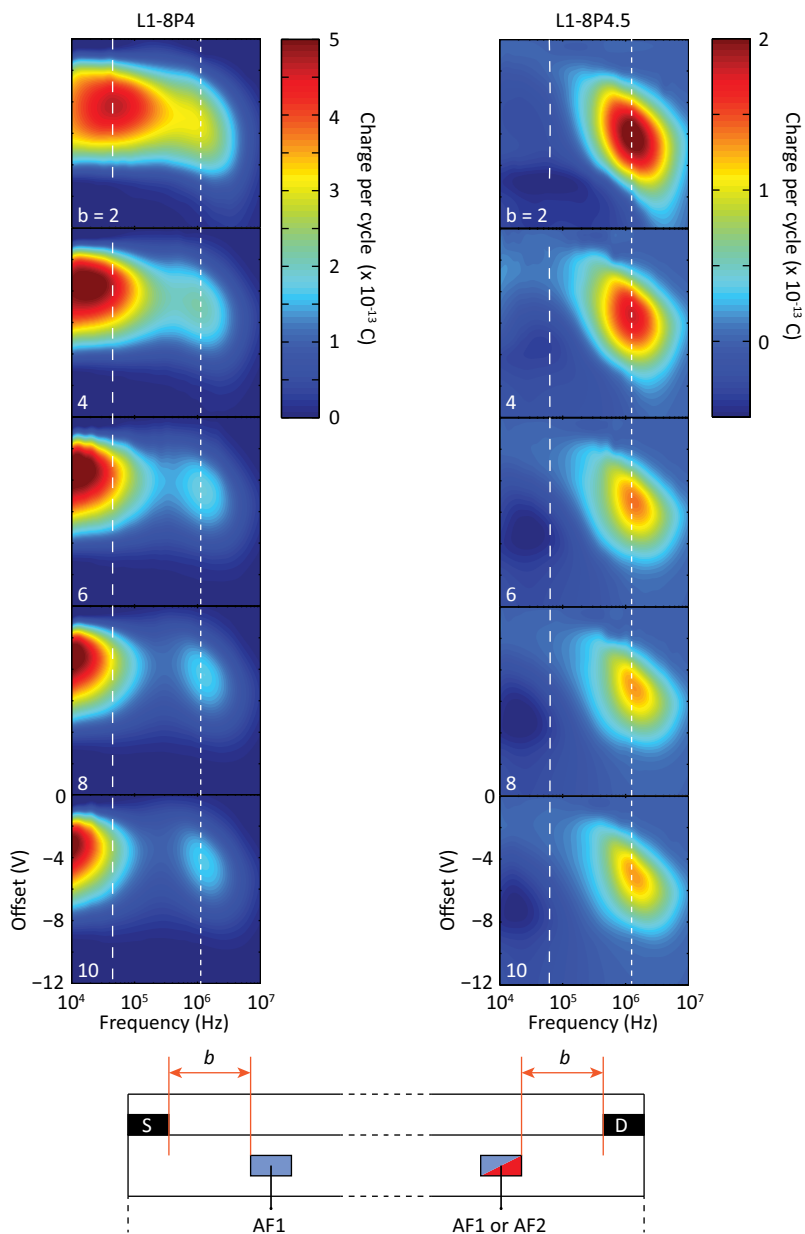
Figure A3.4 | Measured charge per cycle contour plots for an L1–8P4 and L1–8P4.5 ratchet (forward drive). The distance b between the source and drain contact and the nearest finger electrode is varied, ranging from 2 μm till 10 μm. The dashed lines show that the high–frequency maximum is independent of the channel length, while the low–frequency maximum (L1–8P4) or minimum (L1–8P4.5) is. Measurement settings: $V_A = 8$ V, $V_G - V_{TH} = -20$ V.

Open circuit voltage

In Figure A3.5 a snap shot of the channel potential as a function of position x is mapped on top of the open circuit voltage as a function of number of repetitions. Note that the number of asymmetric repetitions is translated to channel length. Both curves are simulation results obtained with FRAT. The open circuit voltage corresponds one–on–one to the local channel potential as the modeled current is independent of the number of repetitions (L1–2Pa ratchet (FRAT), Figure 6.6). The open circuit voltage saturates with increasing number of repeat units due to a shift of the effective local offset voltage. Moving along the channel, i.e. moving to devices with more repeat units and higher open circuit voltages, the offset–amplitude combination moves away from the optimum: in Figure 5.6 it is shown that as a rule of thumb the offset should be half the amplitude for maximum pumping efficiency. At small x in Figure A3.5 this condition is roughly fulfilled, but for larger x the effective offset increases due to the increasing channel potential (the gate voltage remains constant), decreasing the pumping efficiency, and therefore the added voltage, of successive repeat units.
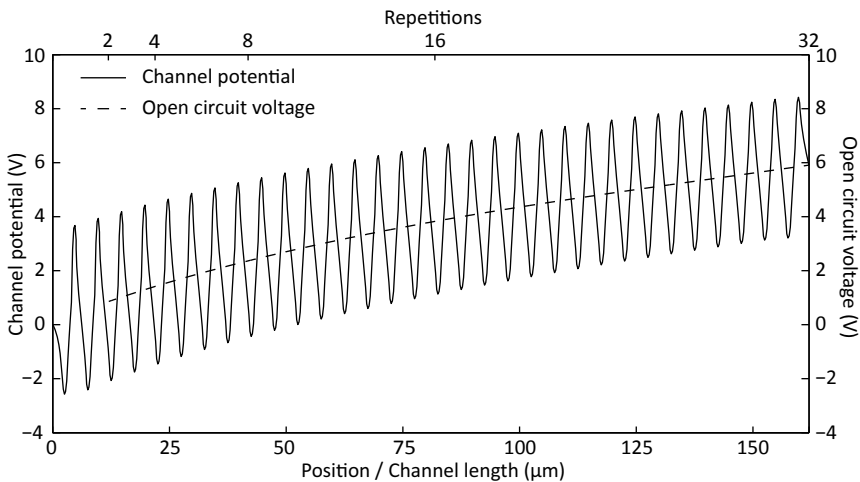

Figure A3.5 | Modeled snap shot of the channel potential as a function of position x in the channel (L1–2P32 ratchet), mapped onto the open circuit voltage as a function of channel length or number of repetitions a (L1–2Pa ratchets, with a = 2, 4, 8, 16, 32). Modeling settings: μ = 10^6 m^2/Vs, V_O = −7 V, V_A = 8 V, V_G = −20 V, f = 3.5 MHz.

List of publications

Published papers

1. Erik M. Roeling, Wijnand Chr. Germs, Barry Smalbrugge, Erik Jan Geluk, Tjibbe de Vries, René A. J. Janssen and Martijn Kemerink, Organic electronic ratchets doing work. *Nature Materials* **10**, 51–55, (2011).

Manuscripts in preparation

1. Erik M. Roeling, Wijnand Chr. Germs, Barry Smalbrugge, Erik Jan Geluk, Tjibbe de Vries, René A. J. Janssen and Martijn Kemerink, Scaling of characteristic frequencies of organic electronic ratchets.

2. Erik M. Roeling, Wijnand Chr. Germs, Barry Smalbrugge, Erik Jan Geluk, Tjibbe de Vries, René A. J. Janssen and Martijn Kemerink, Performance of organic electronic ratchets.

3. Erik M. Roeling, Wijnand Chr. Germs, Barry Smalbrugge, Erik Jan Geluk, Tjibbe de Vries, René A. J. Janssen and Martijn Kemerink, Finite size effects on organic electronic ratchets.

About the author

Erik Roeling was born on August 28, 1980 in Ammerzoden, the Netherlands. In 1997, he obtained his Higher General Secundary Education at the "Jeroen Bosch College" in 's–Hertogenbosch after which he started his study in Applied Physics at the Fontys Hogeschool in Eindhoven. After obtaining his propaedeutic degree in 1998 he started his study in Applied Physics at the Eindhoven University of Technology (TU/e). In 2004 he went for four months to the Lawrence Berkeley National Laboratory in Berkeley CA (United States of America) to perform an internship. His masters thesis project was performed in the Photonics and Semiconductor Nanophysics group at the TU/e under supervision of prof.dr. Huub Salemink and dr.ir. Rob van der Heijden. The subject of the project was gallium nitride photonic crystals. In April 2007 he obtained his engineering degree in Applied Physics. From April 2007 to May 2011, he performed his PhD study on organic electronic ratchets at the Molecular Materials and Nanosystems group of prof.dr.ir. René Janssen (TU/e). The project was performed on a VIDI–grant which was won by his copromotor dr.ir. Martijn Kemerink. The results of this work are presented in this thesis. Results are published in a refereed journal and presented at international conferences in San Francisco CA and Boston MA in the USA.

Dankwoord/Expression of gratitude

Aan het einde gekomen van mijn promotietraject en daarmee ook het schrijven van dit proefschrift, zijn er veel personen met wie ik heb samengewerkt die ik graag wil bedanken.

René, hartelijk dank dat je mijn promotor wilt zijn. Je enthousiasme voor de wetenschap en werklust zijn aanstekelijk en ik bewonder je vermogen om ook ver buiten je eigen expertise gebied de juiste vragen te stellen die een onderzoeker verder helpen. Ik heb de afgelopen jaren met veel plezier in een vooraanstaande groep gewerkt. Martijn, wij zijn elkaar lang geleden al eens tegengekomen bij de (toenmalige) groep halfgeleiderfysica. Tijdens één van mijn fietstochten naar de TU/e kwamen we elkaar in die periode tegen bij het Dommeltunneltje en probeerde je mij alvast te strikken voor een promotieonderzoek. Ondanks mijn beleefde antwoord in de trant van: "ik zal eraan denken," dacht ik in werkelijkheid: "hell no" (dat was niets persoonlijks trouwens). De werkelijkheid is anders gebleken. Hartelijk dank dat ik aan jouw inventieve VIDI–project heb mogen meewerken en dat jij mijn copromotor bent. Ik heb met veel plezier met je samengewerkt. Ik wil graag nog opmerken dat de eerste succesvolle ratchetmeting plaats heeft gevonden op 16 juli 2008 om 17:04 uur. Een ruime 15.5 maand na de start van mijn promotie…

I would like to thank the people from the thesis reading committee: prof.dr. Reinder Coehoorn, prof.dr. Patrick Wagner and prof.dr. Heiner Linke. Reinder, we have seen each other almost every Friday morning during the weekly groupmeeting. During my presentations you always asked questions which helped me in my research. Patrick, about twice a year we met during the pleasant STW project committee meetings in which you showed a genuine interest in the work that we performed. You also arranged a visit for us to the Hasselt University which was great. Heiner, thank you for your comments. We appreciate it that you —having a background in ratchets— were willing to

participate in the reading committee. Prof.dr. Dago de Leeuw, thank you for participating in my PhD defense. The last few years we have met several times which was always pleasant. You also provided the inverter samples for our experiments and were willing to help us together with Paul van Hal and Eugenio Cantatore with our sample design. It was a pity that the technologies didn't match in the end, but we are still thankful for the efforts that you, Paul and Eugenio made.

Ik wil graag Leo Korstanje, Albert van Breemen, John van Haare, Leo IJzendoorn, Menno Prins en Patrick Wagner bedanken voor hun bijdragen tijdens de bijeenkomsten van de STW gebruikerscommissie.

Iemand met wie ik de afgelopen jaren veel heb samengewerkt is Wijnand Germs. Naast uitvoerige discussies hebben we ook veel plezier gehad op ons kantoor en in het lab. Dank voor de fantastische tijd. Ver was ik niet gekomen in mijn onderzoek zonder de kennis en kunde van de cleanroomtechnici: Barry Smalbrugge, Erik Jan Geluk en Tjibbe de Vries. Jullie ervaring heeft ons vaak geholpen in het zoeken naar de juiste fabricagetechnieken. Fouad Karouta heeft ons geholpen met het delen van zijn kennis over siliciumdioxide depositie. Siang Oei en Huub Ambrosius hebben de mogelijkheid geboden om apparatuur te gebruiken in de cleanroom. Gerard Wijers, Wijnand Dijkstra en Marco van der Sluis —de technici in de M2N groep— hebben cruciaal werk voor het project verricht. Zonder jullie zouden veel meetopstellingen snel buiten gebruik zijn. Martijn Wienk heeft mij regelmatig geholpen met de organische opdamper in het device lab bij scheikunde. Ik heb twee stagiaires mogen begeleiden: Lars Peters en Pim van Nispen. Bedankt voor jullie bijdragen aan het onderzoek.

Ik wil graag mijn overige M2N collega's bij natuurkunde en scheikunde bedanken. Bij natuurkunde waren dit onder andere: Kevin 'Nobel' van de Ruit, Erwin Rossen, Ron Willems, Rik van Laarhoven, Joris Hagelaar, Jiří Červenka, Nick Podaru, Stephan 'dit is geen waardeoordeel' van Reenen, Christian Roelofs, Richard Vanraes, Kees Flipse, Zuhal Tasdemir, Siebe van Mensfoort, Marco Carvelli en Rein de Vries. I travelled with several people from the M2N group —Martijn, Johan Bijleveld, Jan Gilot, Bram Karsten, Stefan Oosterhout, Wijnand, Stephan, Dimitri Charrier, Klara Maturova, Simon Mathijssen, Daniele Di Nuzzo, Marie–France Falzon and Arjan Zoombelt— to Norrköping, San Francisco and Boston MA. That was great! Andrzej Dzwilewski, thank you for the enjoyable time in the labs and cleanroom. Klara, I enjoyed the time we spent together in Spectrum 1.83, the trips and the climbing events we had with Michael and Elise. I am sorry for almost but indirectly killing you with my enthusiasm for climbing. Dimitri, thank you for the nice time we had in our office and during our trips. Simon,

bedankt voor de gezelligheid en de discussies over organische stuff. Alex Nardes, it was really nice seeing you again last December in Boston. Toon, bedankt voor de onderhoudende gesprekken tijdens je avondronde. Salomon, ook jij bedankt voor de gesprekken tijdens je middagronde.

Bill, I would like to thank you and your wife for the brilliant time that Elise and I had in Aspres–sur–Buëch. We hope that your back is healing fine. Teresa and Dan, I enjoyed seeing you again in Napa valley. Maartje bedankt voor de gezelligheid de afgelopen jaren (sneeuwschoenwandelen in de Vogezen, Boogie's Challenge). Mijn mede–organisatoren van de MST–retreat 2009: Sascha, Marko, Veronique en Maartje: het was super! Harm en Wiebe bedankt voor de boulderuurtjes in het sportcentrum. De afgelopen jaren hebben Elise en ik heerlijke wandelingen en weekenden gehad met Igor en Marleen. Deze dagen zorgden voor de nodige ontspanning. Veel succes en plezier in New York samen met Wessel. Igor, Frank en Steven, de bivakweekenden zijn altijd legendarisch. Slapen met –15 ^{0}C in een tentje in de uiterwaarden van de Waal, Kung Fu eten met een watertekort, wie wil dat nou niet? Volgende stop de Appalachian trail. Jelle en Marian met jullie hebben wij de afgelopen jaren de nodige avonden doorgebracht. Ik vond het super om samen met Manja (nog bedankt voor de samenwerking!) de ceremoniemeesters bij jullie bruiloft te zijn. Vincent, we hebben elkaar afgelopen jaren niet zo heel vaak gezien maar het was wel altijd als vanouds. Het dieptepunt in de afgelopen vier jaar was het overlijden van mijn oud–huisgenote Hélène met wie ik zes jaar met veel plezier in het studentenhuis heb gewoond. Ik herinner haar als een leuk, gezellig, warm en ondernemend persoon.

Simone, Joop, Jeroen en Yvonne bedankt voor de gezelligheid, bijvoorbeeld tijdens de skivakantie en de week in de Ardennen. Ik wil graag mijn ouders, zussen en aanhang bedanken voor de afgelopen jaren —Peter en Greet—Monika, Erik–Jan, Suzanne en Lars—Annemieke, Raphaël en Wido—Ineke en Martin. Ondanks dat ik zelden in details iets over mijn promotietraject heb verteld waren jullie wel altijd geïnteresseerd.

Elise, met jou heb ik een heerlijke tijd. Mountainbiken, rotsklimmen, racefietsen, je doet het allemaal. Je bent een fantastische doorzetter en ik ben trots op wat je de afgelopen jaren allemaal hebt gedaan. Bedankt voor je ondersteuning, zeker bij het afronden van mijn promotie. Ik kijk alweer uit naar de dingen die we de komende jaren samen gaan ondernemen.

—Erik, Eindhoven, March 2011.

□